

UCSF

UC San Francisco Electronic Theses and Dissertations

Title

Coordination of Cotranslational Protein Targeting to the Membrane

Permalink

<https://escholarship.org/uc/item/0v02j3w7>

Author

Bradshaw, Niels Raab

Publication Date

2009

Peer reviewed|Thesis/dissertation

Coordination of Cotranslational Protein Targeting to the Membrane

by

Niels Raab Bradshaw

DISSERTATION

Submitted in partial satisfaction of the requirements for the degree of

DOCTOR OF PHILOSOPHY

in

Biochemistry

in the

GRADUATE DIVISION

of the

UNIVERSITY OF CALIFORNIA, SAN FRANCISCO

This dissertation is dedicated to my mother, Betty Lou Raab Bradshaw
who has dedicated so much to my education.

Acknowledgements:

One of the greatest pleasures I have enjoyed at UCSF has been working in an environment with generous and engaging people. Of these people, I would first like to single out my advisor, Peter Walter, whose enthusiasm and compassion permeates the UCSF community. My thesis committee, Carol Gross, Christine Guthrie, and David Agard, have been supportive, while challenging me to think more broadly and precisely. I am particularly grateful for their encouragement at the most difficult times. Bob Farese and Marc Shuman have also been important mentors and friends to me. The members of the Walter lab have been highly spirited and engaged, and I am very thankful for this. In particular working closely with Saskia Neher made science more exciting and fun. I am also grateful to many friends who have shared learning and adventuring with me during graduate school.

I would like to thank my parents and brother who have shared a joy for learning with me. I wish that my father could have been here to share this celebration with us. The time we spent together while I was at UCSF is one of my most treasured memories, and I feel his presence in many parts of this thesis. Finally, I thank Julia Kardon, who has been my constant support and compassionate companion. I am thrilled that we will start our next adventure together.

Chapter 1

The text of this chapter is a reprint of the material as it appears in *Molecular Biology of the Cell* (citation below).

Bradshaw, N. & Walter, P. (2007) The SRP RNA links conformational changes in the SRP to protein targeting. *Mol Biol Cell*. 18: 2728-2734.

Chapter 2

The text of this chapter is a reprint of the material as it appears in *Science* (citation below). N.B., S.B.N., and D.S.B. prepared reagents and performed the experiments; N.B., S.B.N., and P.W. wrote the article.

Bradshaw N, Neher SB, Booth DS, and Walter P. (2009) Signal sequences activate the catalytic switch of SRP RNA. *Science*. 323(5910): 127-30.

Chapter 3

The text of this chapter is a reprint of the material as it appears in *Nature Structural and Molecular Biology* (citation below). S.B.N and N.B prepared reagents and performed Ffh-FtsY association and dissociation assays; N.B. carried out GTPase experiments; N.B., S.N.F., and J.D.G. designed, executed and interpreted the NMR experiments; S.B.N. performed partial proteolysis assays; S.B.N., N.B., and P.W. wrote the article.

Neher, S.B., **Bradshaw, N.**, Floor, S.N., Gross, J.D., & Walter, P. (2008) SRP RNA controls a conformational switch regulating the SRP-SRP receptor interaction. *Nature Structural & Molecular Biology*. 15(9): 916-923.

Abstract

Secretory and transmembrane proteins are delivered to the ER membrane or eukaryotic cells or the plasma membrane of prokaryotic cells cotranslationally by the interaction of the signal recognition particle (SRP) with its membrane associated receptor (SR). SRP recognizes hydrophobic signal sequences in proteins as they are translated and delivers the ribosome nascent chain to the membrane by associating with SR. The ribosome is then transferred to the translocation channel, and synthesis of the protein continues through the membrane. Homologous GTPase domains of SRP and SR mediate their interaction cycle: SRP-SR association reciprocally stimulates their GTPase activities, and GTP hydrolysis disassembles the complex. How this cycle of GTP hydrolysis is coupled to productive targeting was unknown. Additionally, SRP requires an RNA subunit that catalyzes the SRP-SR interaction, accelerating both on and off rates by over 100 fold. The mechanism of SRP RNA catalysis and its role in protein targeting were also mysteries.

The first chapter describes the identification of mutations in the SRP protein that abrogate the activity of SRP RNA. This demonstrated a link between conformational changes in the SPR protein and the activity of SRP RNA. Furthermore, these studies suggested that SRP RNA activity might be controlled by signal sequence binding to SRP. The second chapter describes the discovery that the activity of SRP RNA to accelerate SRP-SR association requires that SRP be bound to a signal sequence. This effect was previously not observed because it was masked by a small amount of detergent included in the reaction buffer that acted as a signal sequence mimic. This couples the SRP-SR

interaction with cargo recruitment by SRP and ensures that GTP hydrolysis is productive. The third chapter describes the discovery that the structurally and evolutionarily related N-terminal helices of SRP and SR are autoinhibitory to complex formation in the absence of SRP RNA and that SRP RNA relieves this autoinhibition. Using NMR spectroscopy and enzymatic assays, we found that truncation of the N-terminal helix of SR allows it to adopt its SRP bound conformation. These studies demonstrate that SRP RNA controls a conformational switch in the SRP and SR to coordinate SRP-SR interaction with cargo recruitment by SRP.

Table of Contents

Preface:	Title Page	i
	Dedication	iii
	Acknowledgements	iv
	Abstract	vi
	Table of Contents	viii
	List of Tables	x
	List of Figures	xi
Introduction		1
Chapter 1:	The signal recognition particle (SRP) RNA links conformational changes in the SRP to protein targeting.	10
Chapter 2:	Signal sequences activate the catalytic switch of SRP RNA.	51
Chapter 3:	SRP RNA controls a conformational switch regulating the SRP-SRP receptor interaction.	80
Epilogue		130
Appendix A:	Using FRET to monitor SRP-SR interaction.	139

Appendix B: The interaction of SRP with signal peptides.	151
Appendix C: The interaction of SRP with ribosomes.	163
Publishing Agreement	179

List of Tables

Chapter 1	Table 1: GTP hydrolysis rates for Ffh variants.	36
	Table 2: Association and dissociation rate constants for Ffh variants binding to FtsY.	36
Chapter 2	Table 1: Association and dissociation rate constants for Ffh/FtsY binding.	63
Chapter 3	Table 1: Association and dissociation rate constants of Ffh/FtsY binding for Ffh and FtsY variants.	105

List of Figures

Chapter 1	Figure 1: Removal of the M-domain does not alter the interaction kinetics of Ffh and FtsY in the absence of 4.5S RNA.	39
	Figure 2: Binding to 4.5S RNA and basal GTPase activity is not affected by mutations L301P, L303D, L350D, and L354D	41
	Figure 3: Ffh mutations of L303D, L350D, and L354D abrogate the activity of the 4.5S RNA to catalyze association of Ffh and FtsY.	43
	Figure 4: Mutations L301P and L303D abrogate 4.5S RNA enhancement of the stimulated GTPase activity of SRP and FtsY.	45
	Figure 5: Ffh mutations L301P, L303D, L350D, and L354D lead to membrane protein integration defects in vivo.	47
	Figure 6: Mutations in Ffh that lead to defects in 4.5S RNA activity map to conformationally dynamic regions.	49

Chapter 2	Figure 1: Detergent activates 4.5S RNA to catalyze the Ffh-FtsY interaction.	65
	Figure 2: Concentration dependence of C12E8 activation of 4.5S RNA.	67
	Figure 3: Δ EspP binds SRP with micromolar affinity and stimulates 4.5S RNA catalysis of Ffh-FtsY interaction.	69
	Figure 4: Addition of peptide does not induce aggregation of SRP under the assay conditions used.	71
	Figure 5: The GTP hydrolysis-driven disassembly of the Ffh•FtsY complex is insensitive to 4.5S RNA activation.	73
	Figure 6: Mutations in Δ EspP that impair SRP-mediated targeting show decreased binding to SRP and decreased stimulation of 4.5S RNA.	75
	Figure 7: Concentration dependence of Δ EspP(F12A, L15T) activation of 4.5S RNA.	77
	Figure 8: Model for the role of 4.5S RNA in cotranslational protein targeting.	79

Chapter 3	Figure 1: Structural and schematic representations of the FtsY and Ffh constructs used in this study.	107
	Figure 2: Helix N1 is present in structures of uncomplexed FtsY.	109
	Figure 3: Truncation of the entire Ffh helix N1 (amino acids 1-20) is functionally equivalent to truncation of the first 8 amino acids.	111
	Figure 4: The N-terminal helices of Ffh and FtsY inhibit Ffh-FtsY association in the absence of 4.5S RNA.	113
	Figure 5: The N-terminal helices of Ffh and FtsY stimulate Ffh-FtsY complex dissociation in the presence of 4.5S RNA.	115
	Figure 6: The N-terminal helix of FtsY represses its basal GTPase activity.	117
	Figure 7: NMR analysis of FtsY-204 and FtsY Δ N1.	119
	Figure 8: FtsY Δ N1 but not FtsY-204 undergoes a GppNHp dependent conformational change.	121

Figure 9: FtsY Δ N1 assumes an 'Ffh bound' conformation in the presence of GppNHp.	123
Figure 10: Binding of Ffh to FtsY exposes the N-terminal helix of FtsY.	125
Figure 11: Model for Ffh-FtsY structural rearrangement upon complex formation.	127
Figure 12: Thermodynamic model describing the mechanism of SRP RNA control of the interaction of SRP and SR.	129
Appendix A Figure 1: FRET between complexes of cy3 labeled Ffh and cy5 labeled FtsY.	144
Figure 2: FRET between complexes of cy3 labeled Ffh and cy5 labeled FtsY.	146
Figure 3: FRET accurately measures Ffh-FtsY association in the presence of 4.5S RNA.	148
Figure 4: Abnormalities in association rates for Ffh-FtsY association measured by FRET in the absence of 4.5S RNA.	150

Appendix B	Figure 1: FRET assay for monitoring signal peptide association with SRP.	158
	Figure 2: Kinetics of signal peptide exchange with SRP.	160
	Figure 3: Disulfide crosslinking of EspP-FAM to single cysteine bearing variants of Ffh.	162
Appendix C	Figure 1: Incorporation of cy3-labeled L29 into ribosomes.	170
	Figure 2: FRET between cy3 labeled ribosomes and cy5 labeled FFh.	172
	Figure 3: Affinity of ribosome Ffh complexes measured by FRET.	174
	Figure 4: Affinity of ribosome SRP complexes measured by FRET.	176
	Figure 5: Association and dissociation rate constants for the Ffh-ribosome interaction.	178

Introduction:

All cells require secreted and transmembrane proteins to sense and interact with their environment. It is essential that these proteins are accurately and efficiently delivered to the membrane to perform their functions. Additionally, failure to properly target proteins to the membrane can lead to protein aggregation or aberrant signaling^{1,2}. This thesis describes work conducted to understand the mechanism of this process; both because of its fundamental biological importance, and to serve as a paradigm for how multistep biological pathways may be coordinated.

The protein targeting machinery:

Cotranslational protein targeting is the major conserved route to target secretory and transmembrane proteins to the membrane of the endoplasmic reticulum (or plasma membrane in prokaryotes). The cotranslational protein targeting machinery was identified over 20 years ago and consists of the signal recognition particle (SRP), a protein/RNA complex that binds ribosomes translating secretory and membrane proteins, and the SRP receptor (SR), which resides at the membrane and binds to SRP³.

In the first step of cotranslational protein targeting, SRP binds the signal sequence of a nascent polypeptide chain emerging from the ribosome³⁻⁵. The resulting SRP-ribosome-nascent chain complex (RNC) then binds SR to deliver the ribosome to the membrane^{6,7}. The RNC is then transferred to the protein translocation channel (translocon), and synthesis of the protein continues directly through the membrane. The cotranslational nature of the targeting pathway ensures that proteins are not folded or

aggregated as they pass through the membrane, but requires that ribosomes translating secretory proteins are recognized and delivered to the membrane rapidly.

SRP and SR associate with each other through related GTPase modules, but only when GTP-bound⁸⁻¹⁰. After transfer of the ribosome to the protein translocation channel (translocon), SRP and SR hydrolyze their respective bound GTPs, which causes them to dissociate and allows for a new round of targeting¹¹. SRP and SR both have low basal GTPase activity in their free forms, but complex formation activates their GTPase activities. Thus, SRP and SR are GTPase-activating proteins (GAPs) for each other¹². GTP hydrolysis provides the energy that powers the targeting reaction, and the coordination of GTP hydrolysis by SRP and SR with ribosome recruitment by SRP is therefore critical for efficient targeting.

Although SRP-dependent protein targeting is conserved in all organisms, the prokaryotic system has the fewest components and therefore represents the minimal functional unit^{13,14}. In *Escherichia coli*, SRP consists of a single protein, Ffh, and a small RNA, 4.5S RNA¹⁴. Ffh consists of two domains: the M domain, which contains both the binding site for signal sequences and 4.5S RNA, and the NG domain, which includes the GTPase module that binds the SRP receptor FtsY. A flexible linker joins the two domains of Ffh^{15,16}. In *E. coli*, Ffh, FtsY, and the 4.5S RNA are all essential genes.

SRP RNA is an almost universally conserved component of the SRP targeting system. However, its role in the targeting reaction has remained a mystery since its identification over 25 years ago. In *E. coli*, 4.5S RNA has two known biochemical activities: to catalyze the interaction of Ffh and FtsY, accelerating both the on and off rate of complex formation by over two orders of magnitude without changing the K_D , and to

enhance the GTPase activity of the Ffh·FtsY complex by about seven-fold (this RNA-dependent stimulation of GTPase activity is distinct from the much larger GTPase stimulation caused directly by the interaction of Ffh and FtsY; ^{17,18}).

Questions:

When I began work in the Walter lab, we sought to address three central questions about the mechanism of the cotranslational protein targeting machinery:

What is the role of SRP RNA in the protein targeting reaction?

Despite its near universal conservation, the role of SRP RNA in the protein targeting reaction was unknown. Early efforts to understand the role of SRP RNA focused on its potential to affect SRP association with the ribosome through direct RNA-RNA interactions. Paul Peluso took an alternate approach to the problem, defining a biochemical activity for SRP RNA in a highly purified in vitro system^{17,18}. Paul discovered that SRP RNA catalytically accelerates the interaction of SRP and SR. We were interested in following up this work to determine what role SRP RNA catalysis plays in the protein targeting reaction.

A clue to the role of SRP RNA catalysis came from structural work, which shows that the signal sequence-binding pocket (a deep groove lined by hydrophobic amino acids) is spatially contiguous with the SRP RNA^{15,19}. Moreover, the hydrophobic groove can assume multiple conformations, indicating that its open state may not be stable in an aqueous environment but closes so that hydrophobic residues are buried²⁰. Because this conformational variability occurs in close juxtaposition to SRP RNA, it is plausible that it

might monitor the occupancy of the signal sequence-binding pocket to modulate SRP binding to SR. However, it was unresolved how SRP RNA might be linked to these conformational dynamics.

The work presented in Chapters 1 and 2 of this thesis seeks to address this question.

How does SRP RNA catalyze the SRP-SR interaction?

Recently it has become clear that RNA is capable of performing diverse biological functions including the enzymatic catalysis of a wide variety of reactions. SRP RNA catalysis of a protein-protein interaction is a remarkable example of the capabilities of RNA. We were therefore interested in exploring the mechanism of SRP RNA catalysis.

At the time we began this work there were several hypotheses for how SRP RNA might catalyze the SRP-SR interaction. First, based on solution fluorescence resonance energy transfer (FRET) studies it was proposed that the signal sequence binding domain of SRP occludes the binding site on SRP for SR in the absence of SRP RNA. SRP RNA binding to SRP would then displace the signal sequence binding domain to promote complex formation with SR. Second, SRP RNA might induce a conformational change in the GTPase domain of SRP that lowers the energy barrier to its interaction with SR, while not affecting the conformation of SRP in the complex with SR. Third, SRP RNA might tether SRP and SR to each other in a transient, low affinity transition state complex that would increase the rate of their interaction.

The work described in Chapters 1 and 3 seeks to distinguish between these hypotheses and give a more detailed description of the mechanism of SRP RNA catalysis.

How is the energy of GTP hydrolysis by SRP and SR coupled to productive targeting?

Hydrolysis of GTP provides the energy that drives cotranslational protein targeting, yet, how the energy of GTP hydrolysis is coupled to productive targeting was unknown. GTP hydrolysis drives the disassembly of the SRP-SR complex, liberating SRP and SR for successive rounds of targeting, and may play additional secondary roles in targeting. However, it was not known what would prevent the SRP and SR from undergoing rapid futile rounds of association and GTP hydrolysis in the absence of delivering cargo to the membrane. Furthermore, GTPases coordinate diverse biological processes, and commonly act as molecular timers or switches²¹. We were therefore interested in exploring whether the SRP GTPases similarly coordinate cotranslational protein targeting.

Most GTPases alternate between two long-lived states, either GTP bound or GDP bound, and accessory proteins regulate switching between these states. GTP hydrolysis is very slow under basal conditions and requires the action of a GTPase activating protein (GAP) to stimulate GTP hydrolysis to drive the transition to the GDP state. GAPs commonly function by providing critical catalytic residues in trans to complete the active site of the GTPase and promote hydrolysis. By contrast, SRP and SR contain all of their catalytic residues and are primarily kept in an inactive basal state by a conformational switch that holds the free proteins in an inactive state. The mechanism of this critical

regulatory conformational switch was unknown, and we sought to understand it in more detail.

Most GTPases release GDP very slowly and require a guanosine nucleotide exchange factor (GEF) to drive the transition back to the GTP state. SRP and SR both rapidly exchange GDP for GTP, and thus do not require a GEF or have a stable GDP bound state. Because of these unique features of the SRP GTPases, we wished to determine if the GTPase activities of SRP and SR still function as a switch to coordinate the steps of the targeting cycle.

Chapters 2 and 3 address this question.

Approaches:

Chapter 1

There has been a great deal of new structural information about the core GTPase subunits of SRP and SR, as well as SRP RNA. However, there was also substantial evidence that SRP is conformationally dynamic, and that these dynamics are functionally important. We were therefore interested in determining if the conformations of SRP revealed in these structural snapshots were relevant to the mechanism of SRP RNA catalysis of SRP-SR binding.

We therefore generated a panel of mutant versions of Ffh, focusing on conserved residues in conformationally dynamic regions, as revealed by the crystal structures. We expressed and purified each of the proteins and assayed the ability of 4.5S RNA to accelerate complex formation with FtsY. We found a number of mutations that did not perturb 4.5S RNA binding to Ffh but dramatically reduced the activity of 4.5S RNA.

These mutations also disrupted protein targeting *in vivo*, demonstrating that the biochemically defined catalytic activity of 4.5S RNA is required for efficient targeting. Interestingly, the mutations in Ffh that disrupted 4.5S RNA activity were in positions of the signal sequence binding pocket of Ffh that change conformation upon interacting with a signal sequence. This suggested that SRP RNA might coordinate SRP•SR interaction with ribosome recruitment and transfer to the translocon.

Chapter 2

Although we were intrigued by the possibility that 4.5S RNA catalysis of the SRP-SR interaction might be regulated to ensure that only RNC bound SRP would interact with SR, a major problem with this hypothesis was that 4.5S RNA activity appeared to be constitutive in our highly purified system in the absence of signal peptides. While Saskia Neher and I were measuring the GTPase activity of the chloroplast SRP and SR, we noticed that in this system, low concentrations of nonionic detergent that had been included in our reaction buffer was critical for rapid complex formation. Intrigued, we repeated these experiments in the *E. coli* system that had been more carefully characterized. We found that the detergent was required for 4.5S RNA to stimulate SRP-SR association. When we removed the detergent, 4.5S RNA only catalyzed the interaction of signal peptide-bound Ffh with FtsY. These results, coupled with analysis of the signal peptide SRP interaction, demonstrated that SRP RNA renders the SRP-SR GTPase responsive to signal peptide recruitment, coupling GTP hydrolysis to productive protein targeting.

Chapter 3

Understanding the mechanism of 4.5S RNA acceleration of SRP•SR association was complicated by the fact that 4.5S RNA is catalytic, and thus acts on a transition state. To circumvent the experimental difficulties inherent in studying a transient state, we asked what barriers to complex formation are present in free SRP and SR, slowing the SRP•SR interaction in the absence of 4.5S RNA. By comparing structures of the SRP and SR alone and in complex, we noticed that the N-terminal helices of both proteins were displaced in the complex. We found that truncated forms of Ffh and FtsY lacking these helices bound at nearly the RNA catalyzed rate in the absence of 4.5S RNA, but that 4.5S RNA had no additional effect on their binding rate. GTP hydrolysis assays and NMR spectroscopy demonstrated that the truncated SR adopts an SRP bound conformation in the absence of SRP. This and other evidence led us to suggest that SRP RNA accelerates complex formation by relieving autoinhibition to binding by the N-terminal helices.

1. Bernstein, H.D. & Hyndman, J.B. Physiological basis for conservation of the signal recognition particle targeting pathway in *Escherichia coli*. *J Bacteriol* **183**, 2187-97 (2001).
2. Garrison, J.L., Kunkel, E.J., Hegde, R.S. & Taunton, J. A substrate-specific inhibitor of protein translocation into the endoplasmic reticulum. *Nature* **436**, 285-9 (2005).
3. Keenan, R.J., Freymann, D.M., Stroud, R.M. & Walter, P. The signal recognition particle. *Annu Rev Biochem* **70**, 755-75 (2001).
4. Halic, M. et al. Structure of the signal recognition particle interacting with the elongation-arrested ribosome. *Nature* **427**, 808-14 (2004).
5. Walter, P. & Blobel, G. Translocation of proteins across the endoplasmic reticulum III. Signal recognition protein (SRP) causes signal sequence-dependent and site-specific arrest of chain elongation that is released by microsomal membranes. *J Cell Biol* **91**, 557-61 (1981).

6. Gilmore, R., Walter, P. & Blobel, G. Protein translocation across the endoplasmic reticulum. II. Isolation and characterization of the signal recognition particle receptor. *J Cell Biol* **95**, 470-7 (1982).
7. Gilmore, R., Blobel, G. & Walter, P. Protein translocation across the endoplasmic reticulum. I. Detection in the microsomal membrane of a receptor for the signal recognition particle. *J Cell Biol* **95**, 463-9 (1982).
8. Focia, P.J., Shepotinovskaya, I.V., Seidler, J.A. & Freymann, D.M. Heterodimeric GTPase core of the SRP targeting complex. *Science* **303**, 373-7 (2004).
9. Egea, P.F. et al. Substrate twinning activates the signal recognition particle and its receptor. *Nature* **427**, 215-21 (2004).
10. Miller, J.D., Wilhelm, H., Gierasch, L., Gilmore, R. & Walter, P. GTP binding and hydrolysis by the signal recognition particle during initiation of protein translocation. *Nature* **366**, 351-4 (1993).
11. Connolly, T., Rapiejko, P.J. & Gilmore, R. Requirement of GTP hydrolysis for dissociation of the signal recognition particle from its receptor. *Science* **252**, 1171-3 (1991).
12. Powers, T. & Walter, P. Reciprocal stimulation of GTP hydrolysis by two directly interacting GTPases. *Science* **269**, 1422-4 (1995).
13. Larsen, N. & Zwieb, C. The signal recognition particle database (SRPDB). *Nucleic Acids Res* **21**, 3019-20 (1993).
14. Poritz, M.A. et al. An E. coli ribonucleoprotein containing 4.5S RNA resembles mammalian signal recognition particle. *Science* **250**, 1111-7 (1990).
15. Keenan, R.J., Freymann, D.M., Walter, P. & Stroud, R.M. Crystal structure of the signal sequence binding subunit of the signal recognition particle. *Cell* **94**, 181-91 (1998).
16. Egea, P.F., Stroud, R.M. & Walter, P. Targeting proteins to membranes: structure of the signal recognition particle. *Curr Opin Struct Biol* **15**, 213-20 (2005).
17. Peluso, P., Shan, S.O., Nock, S., Herschlag, D. & Walter, P. Role of SRP RNA in the GTPase cycles of Ffh and FtsY. *Biochemistry* **40**, 15224-33 (2001).
18. Peluso, P. et al. Role of 4.5S RNA in assembly of the bacterial signal recognition particle with its receptor. *Science* **288**, 1640-3 (2000).
19. Batey, R.T., Rambo, R.P., Lucast, L., Rha, B. & Doudna, J.A. Crystal structure of the ribonucleoprotein core of the signal recognition particle. *Science* **287**, 1232-9 (2000).
20. Rosendal, K.R., Wild, K., Montoya, G. & Sinning, I. Crystal structure of the complete core of archaeal signal recognition particle and implications for interdomain communication. *Proc Natl Acad Sci U S A* **100**, 14701-6 (2003).
21. Bourne, H.R. GTPases: a family of molecular switches and clocks. *Philos Trans R Soc Lond B Biol Sci* **349**, 283-9 (1995).

Chapter 1

The Signal Recognition Particle (SRP) RNA links conformational changes in the SRP to protein targeting

The material in this chapter was originally published online May 16, 2007 and appeared in print July 2007 (*Mol Biol Cell.* 18(7):2728-34) Copyright © 2007 by the American Society for Cell Biology. This article is available online at:

<http://www.molbiolcell.org/cgi/content/full/18/7/2728>

The SRP RNA links conformational changes in the SRP to protein targeting

Niels Bradshaw and Peter Walter

Howard Hughes Medical Institute and
Department of Biochemistry and Biophysics
University of California at San Francisco
San Francisco, CA 94158

Running head:

The role of the SRP RNA in protein targeting

Abbreviations:

SRP; signal recognition particle, SR; SRP receptor.

e-mail: pwalter@biochem.ucsf.edu

phone: (415) 476 5017

fax: (415) 476 5233

Abstract

The RNA component of the signal recognition particle (SRP) is universally required for co-translational protein targeting. Biochemical studies have shown that SRP RNA participates in the central step of protein targeting by catalyzing the interaction of the SRP with the SRP receptor (SR). SRP RNA also accelerates GTP hydrolysis in the SRP•SR complex once formed. Using a reverse-genetic and biochemical analysis, we identified mutations in the *E. coli* SRP protein, Ffh, that abrogate the activity of the SRP RNA and cause corresponding targeting defects *in vivo*. The mutations in Ffh that disrupt SRP RNA activity map to regions that undergo dramatic conformational changes during the targeting reaction, suggesting that the activity of the SRP RNA is linked to the major conformational changes in the signal sequence binding subunit of the SRP. In this way, the SRP RNA may coordinate the interaction of the SRP and the SR with ribosome recruitment and transfer to the translocon, explaining why the SRP RNA is an indispensable component of the protein targeting machinery.

Introduction

Co-translational protein targeting is a major route by which proteins are targeted to the membrane of the endoplasmic reticulum (or plasma membrane in prokaryotes). The machinery required for co-translational protein targeting consists of the signal recognition particle (SRP), a protein/RNA complex that binds ribosomes translating secretory and membrane proteins, and the SRP receptor (SR), which resides at the membrane and binds to the SRP (Keenan *et al.*, 2001). One of the highly conserved features of the targeting machinery is that SRP requires an RNA subunit to function (Walter and Blobel, 1982). This study elaborates the mechanism by which the SRP RNA subunit contributes to the protein targeting reaction.

In the first step of cotranslational protein targeting, the SRP binds to the signal sequence of a nascent polypeptide chain emerging from the ribosome (Walter *et al.*, 1981; Keenan *et al.*, 2001; Halic *et al.*, 2004). The resulting SRP-ribosome-nascent chain complex then binds to the SR, which resides at the target membrane (Gilmore *et al.*, 1982a; Gilmore *et al.*, 1982b). The SRP and the SR associate with each other through related GTPase modules, but only when GTP-bound (Miller *et al.*, 1993; Egea *et al.*, 2004; Focia *et al.*, 2004). Following transfer of the ribosome to the protein translocation channel (translocon), the SRP and the SR hydrolyze their respective bound GTPs, which causes them to dissociate, and allows for a new round of targeting (Connolly *et al.*, 1991). The SRP and the SR reciprocally activate the other's GTPase, and are therefore GTPase activating proteins (GAPs) for each other (Powers and Walter, 1995).

Although SRP-dependent protein targeting is conserved in all organisms, the prokaryotic system has the fewest components and is therefore the simplest (Poritz *et al.*, 1990; Larsen and Zwieb, 1993). In *E. coli*, the SRP consists of a single protein, Ffh, and a small RNA, the 4.5S RNA (Poritz *et al.*, 1990). Ffh consists of two domains: the M domain, which contains both the binding site for signal sequences and the 4.5S RNA, and the NG domain, which includes the GTPase module that binds the SRP receptor FtsY. A flexible linker joins the two domains of Ffh (Keenan *et al.*, 1998; Egea *et al.*, 2005). In *E. coli*, Ffh, FtsY, and the 4.5S RNA are all essential genes.

The SRP RNA is an almost universally conserved component of the SRP targeting system. The only known exception is chloroplast SRP, which lacks an SRP RNA but also functions in a different, post-translational mode by binding to proteins entering the chloroplast from the cytosol and targeting them to the thylakoid membrane. In *E. coli*, the 4.5S RNA has two known biochemical activities: to catalyze the interaction of Ffh and FtsY, accelerating both the on and off rate of complex formation by over two orders of magnitude without changing the K_D , and to enhance the GTPase activity of the Ffh•FtsY complex by about seven-fold (this RNA dependent stimulation of GTPase activity is distinct from the much larger GTPase stimulation caused directly by the interaction of Ffh and FtsY)(Peluso *et al.*, 2000; Peluso *et al.*, 2001). Thus, the 4.5S RNA represents an amazing example of an RNA that modulates the behavior of proteins. However, the relationship between the biochemically defined activities of the 4.5S RNA

and the universal requirement for an RNA in co-translational protein targeting is unknown.

A clue to the role of the 4.5S RNA comes from structural work, which shows that the signal sequence binding pocket (a deep groove lined by hydrophobic amino acids) is spatially contiguous with the 4.5S RNA (Keenan *et al.*, 1998; Batey *et al.*, 2000).

Moreover, the hydrophobic groove can assume multiple conformations, indicating that its open state may not be stable in an aqueous environment but closes so that hydrophobic residues can pack against each other and thus be shielded from water (Rosendal *et al.*, 2003). Because this conformational variability occurs in close juxtaposition to the 4.5S RNA, it is plausible that the RNA might monitor the occupancy of the signal sequence binding pocket and transmit that information to the NG domain, thereby modulating its interaction with FtsY. However, it has remained unresolved how the 4.5S RNA might be linked to these conformational dynamics.

Solution studies looking at the conformation of Ffh suggested that in the absence of the 4.5S RNA, the Mdomain may occlude the binding site for FtsY. 4.5S RNA binding to Ffh may relieve this inhibition to promote complex formation (Buskiewicz *et al.*, 2005a; Buskiewicz *et al.*, 2005b; Halic *et al.*, 2006a; Halic *et al.*, 2006b; Mainprize *et al.*, 2006; Schaffitzel *et al.*, 2006). Although this model provides a plausible mechanism for 4.5S RNA activity, it would suggest that the role of 4.5S RNA is limited to mediate a single Ffh activation step during SRP assembly. Once bound, it would be an inert bystander that would not contribute actively to regulation of the SRP cycle, as there is currently no evidence that 4.5S RNA dissociates from Ffh after binding.

Here, we describe a reverse-genetic and biochemical analysis designed to ask if and how the 4.5S RNA facilitates communication between the M and NG domains of Ffh. We describe mutants in Ffh that bind 4.5S RNA normally and interact normally with FtsY when the 4.5S RNA is absent, but impair the rate of association or GTP hydrolysis when the 4.5S RNA is present. These mutations map to regions of Ffh that undergo major conformational rearrangements during the targeting cycle, suggesting that the 4.5S RNA coordinates the steps of the targeting reaction.

Materials and Methods

Reagents

Proteins and 4.5S RNA were purified as described in (Peluso et al., 2001). Mutations in Ffh were introduced using the QuickChange Mutagenesis protocol (Stratagene, La Jolla, California, United States). For all *in vitro* experiments, a truncated form of FtsY (aa 47-497) was used, as previously described (Powers and Walter, 1997). In all cases, assays were performed at 25° C in 50 mM HEPES, pH 7.5, 150 mM potassium acetate, 2 mM magnesium acetate, 0.01% Nikkol, 2 mM dithiothreitol. The NG domain of Ffh was generated by limited digestion as described (Zopf et al., 1993). The M domain was removed by flowing the digested protein over SP Sepharose, and the NG domain was further purified by gel filtration on Superdex 75.

Fluorescence Binding Assays

Fluorescence binding experiments were performed as described (Peluso et al., 2000). Rapid reactions (wt and Ffh(L301P) +RNA) were performed on a stopped flow fluorimeter (KinTek). Slow reactions were performed on a SLM fluorimeter. For on-rates, data were fit to a single exponential and observed rate constants were plotted as a function of concentration. Rate constants were calculated using the equation $k_{\text{obs}} = k_{\text{on}} * [\text{Ffh}] + k_{\text{off}}$. Off-rates were calculated by preforming complexes of 2 μM of each Ffh (+/- 4.5S RNA) and FtsY and then trapping dissociated components with an excess of GDP. Curves were fit to a single exponential function.

GTPase Assays

Assays were performed as described (Peluso et al., 2001) with slight modifications. To calculate the basal activities of Ffh mutants, trace amounts of [³²P] GTP were added to varying concentrations of Ffh and reactions were followed to completion. The data were fit to a single exponential equation to calculate the k_{obs} . In contrast, we used a multiple-turnover regime to measure the stimulated GTPase activity of the Ffh variants. A fixed concentration of Ffh (0.1 μ M for Ffh(wt) + 4.5S RNA and other fast reactions, 0.5 μ M for Ffh(wt) – 4.5S RNA and other slow reactions) was used with varying concentrations of FtsY. The initial linear portion of the reaction was followed, corrected for the contribution of basal hydrolysis from FtsY (less than 20% of total hydrolysis observed) and fit to the equation: $turnovers / complex = k_{obs} * time$.

Gel Shift Assays

Gel shift analysis of binding of the 4.5S RNA to Ffh mutants was carried out by mixing trace amounts of [³²P]-end-labeled 4.5S RNA with 0.25 μ M cold 4.5S RNA and 0.25 μ M Ffh (cold RNA was important to help prevent aggregation of Ffh and RNA in the well) in assay buffer supplemented with 10% glycerol. This mixture was separated in TAE buffer (40 mM Tris-acetate, 20 mM sodium acetate, 1 mM EDTA) supplemented with 2.5 mM magnesium acetate on a 7% (29:1 acrylamide:bisacrylamide) polyacrylamide gel.

Biotinylation Experiments

Wam121 cells [MC4100 ara⁺ ffh::kan attB:: (OriR6K P_{BAD}-ffh tet)] (Phillips and Silhavy, 1992) were transformed with plasmid pHP44 (pBR322-acrR'acrA acrB576-PSBT; (Tian

and Beckwith, 2002)) and pHDB7 (pACYC184-Ffh; (Lee and Bernstein, 2001)) or variants in which point mutations were introduced. Transformants were selected on plates in the presence of arabinose and were then grown overnight at 37° C in liquid media in the absence of arabinose. Cells were then diluted back and harvested during log phase as described (Tian and Beckwith, 2002). Western blots were performed using streptavidin-HRP conjugate (Amersham). HRP was inactivated with azide and the blots were reprobbed with an antibody to Ffh (Poritz et al., 1990) and visualized using chemiluminescence.

Results

To assess how 4.5S RNA promotes Ffh•FtsY complex formation, we first asked whether the Ffh M-domain inhibits the rate of binding of Ffh and FtsY. It has been proposed that 4.5S RNA may enhance the rate of complex formation by relieving this putative inhibition (Buskiewicz et al., 2005a; Buskiewicz et al., 2005b). To test this possibility, we generated the NG domain of Ffh (“Ffh-NG”) by removal of the M domain by V8 protease digestion (Fig. 1A). Next, we monitored the kinetics of complex formation by two independent assays: i) measuring the change in intrinsic tryptophan fluorescence of FtsY (Jagath et al., 2000; Peluso et al., 2000) and ii) measuring the stimulation of GTP hydrolysis (Peluso et al., 2001). In both assays, Ffh-NG behaved as full-length Ffh in the absence of 4.5S RNA, and by contrast to full-length Ffh could not be accelerated by addition of the RNA (Fig.1B-E).

As shown in Figure 1B, binding of Ffh-NG to FtsY caused an increase in fluorescence intensity and blue shift of the fluorescence emission peak similar to full-length Ffh (Jagath et al., 2000; Peluso et al., 2000). We used this fluorescence shift to measure binding of Ffh-NG to FtsY. The rate of Ffh-NG•FtsY complex formation ($k_{on} = 99 \text{ M}^{-1}\text{s}^{-1}$, Fig. 1C and D) was within error from that of full-length Ffh in the absence of the 4.5S RNA ($k_{on} = 180 \text{ M}^{-1}\text{s}^{-1}$) and over 500 times slower than full-length Ffh in the presence of the SRP RNA ($k_{on} = 5.7 \times 10^4 \text{ M}^{-1}\text{s}^{-1}$) (Peluso et al., 2000).

Following Ffh-NG•FtsY complex formation by monitoring stimulation of GTP hydrolysis yielded similar results. The stimulated GTPase reaction measures the entire interaction cycle of Ffh and FtsY. At low concentrations of FtsY the GTP hydrolysis rate is primarily dependent on the rate of binding of Ffh and FtsY, whereas at higher concentrations the catalytic step of GTP hydrolysis becomes rate limiting (Peluso et al., 2001). Thus, the k_{\max} is a direct measure of the catalytic rate, and the $K_{1/2}$ depends on both the binding rate and the k_{\max} . As the 4.5S RNA affects both the binding rate and the rate of catalysis, we observe an increase in the k_{\max} as well as a decrease in the $K_{1/2}$ upon addition of the 4.5S RNA (Fig. 1E compare filled circles and open circles). When we compared the stimulated GTPase activity of Ffh-NG to that of full-length Ffh, we saw that both the k_{\max} and the $K_{1/2}$ were nearly identical to that measured for full-length Ffh in the absence of the 4.5S RNA (Fig. 1E, Table 1). Furthermore, addition of 4.5S RNA in ten-fold excess of the $0.5 \mu\text{M } K_D$ for the 4.5S RNA and the Ffh-NG domain (Buskiewicz et al., 2005a) had no effect on either parameter of the GTPase reaction for Ffh-NG. These results indicate that the Ffh-M domain is required for 4.5S RNA to accelerate Ffh•FtsY complex formation. 4.5S RNA bound to the M domain therefore actively enhances the rate of complex formation, rather than the RNA-free M domain slowing it down.

We next asked whether the M-domain merely provides a binding site for the 4.5S RNA, or if it actively participates in the Ffh•FtsY interaction. To answer this question, we sought mutations in Ffh that abrogate 4.5S RNA activity, without impairing 4.5S RNA binding to Ffh. We chose conserved residues in the M domain and in the linker that

tethers the M and NG domains and changed these residues by site-directed mutagenesis. We then expressed and purified each of the Ffh mutants and assayed their ability to bind the 4.5S RNA and their basal GTPase activity. Mutants that behaved indistinguishably from wild-type Ffh were further tested for their ability to form a complex with FtsY and stimulate GTP hydrolysis in the complex.

Through this analysis, we identified four point mutations in Ffh (L301P, L303D, L350D, and L354D) that impair the activity of 4.5S RNA in interesting ways. All four Ffh mutants bind to the 4.5S RNA (Fig. 2A) and hydrolyze GTP in a manner indistinguishable from wild-type Ffh (the measurement refers to basal GTPase in the absence of FtsY; Fig. 2B).

Ffh mutations L303D, L350D, and L354D impair 4.5S RNA-catalyzed Ffh•FtsY complex formation

Three of the mutations (L303D, L350D, and L354D) led to dramatically reduced rates of Ffh•FtsY complex formation in the presence of the 4.5S RNA (Fig. 3A and 3B, Table 2). Compared to wild type Ffh bound to 4.5S RNA, complex formation was slowed in each case by more than 100-fold (Fig. 3B, black bars). By contrast, the binding rates were only modestly affected in the absence of the 4.5S RNA (a 2- to 10-fold decrease) (Fig. 3B, grey bars).

Since the K_D of the wild type Ffh•FtsY complex is the same in the presence or absence of 4.5S RNA (Peluso et al., 2000), mutations that affect the activity of the 4.5S RNA should affect the on- and off-rates of complex formation to the same degree. To test this prediction, we determined the off-rates of the Ffh mutants in the presence of the 4.5S RNA by following tryptophan fluorescence after addition of GDP to trap Ffh and FtsY in their dissociated, GDP-bound states. As shown in Figures 3C and 3D, all three Ffh mutants bound to 4.5S RNA showed dissociation rates comparable to those of complexes containing wild type Ffh lacking 4.5S RNA (Fig. 3D, black bars). In summary, these data demonstrate that the mutations L303D, L350D, and L354D abrogate the activity of 4.5S RNA to catalyze complex formation between Ffh and FtsY but, importantly, do not impair the affinity with which Ffh and FtsY interact (Fig. 3D, K_D 's plotted as grey bars).

Ffh mutations L301P and L303D diminish the rate of stimulated GTP hydrolysis in the Ffh•FtsY complex

In addition to catalyzing Ffh•FtsY complex formation, the 4.5S RNA also stimulates the rate of GTP hydrolysis by the complex (k_{max}), albeit to a lesser extent (Peluso et al., 2001). All four Ffh mutants analyzed here showed some reduction of RNA stimulation of GTPase activity by the complex. Ffh(L350D) and Ffh(L354D) had less than a two-fold reduction of maximal GTP hydrolysis activity in the presence of the 4.5S RNA (Fig. 4C and D, Table 1). The Ffh(L303D) and Ffh(L301P)•FtsY complex showed k_{max} levels that were reduced to near the level of the wild type Ffh•FtsY complex lacking 4.5S RNA (Fig. 4A, 4B and 4D, Table 1). In contrast to the other three mutants, Ffh(L301P) binds

to FtsY with normal rates (Fig. 3B and Table 2). Although the 4.5S RNA stimulation of Ffh•FtsY GTPase activity is small, the effects of the mutations were consistent across at least three independent experiments and two independent preparations of protein for each Ffh variant.

Thus taken together, our data show that the L301P mutation primarily impairs the activity of the 4.5S RNA to stimulate the GTPase activity of the complex, the L350D and L354D mutations primarily impair the activity of the 4.5S RNA to stimulate the rate of complex formation and GTP hydrolysis, and the L303D mutation impairs both.

Mutations that impair either activity of the 4.5S RNA lead to *in vivo* protein targeting defects

Previously it was unknown how the biochemical activities of the 4.5S RNA related to the cellular function of the 4.5S RNA in co-translational protein targeting. Having identified Ffh mutants that specifically impair the activities of the 4.5S RNA, we were able to assess the importance of these activities for protein targeting *in vivo* without directly perturbing the 4.5S RNA. To do this, we expressed the Ffh mutants in cells that harbor a reporter for co-translational protein targeting and conditionally express wild type Ffh.

To monitor co-translational protein targeting, we used the elegant system developed by Tian and Beckwith (Tian and Beckwith, 2002) in which the multispanning membrane protein, AcrB is fused to the *Propionibacterium shermanii* transcarboxylase (PSBT)

biotinylation domain. When this fusion protein is targeted to the membrane by SRP, the PSBT is targeted to the periplasm, where it is not biotinylated (Fig. 5A). However, if the SRP targeting system is defective, the protein accumulates in the cytoplasm and is biotinylated. We introduced plasmids to direct the expression of either wild type Ffh or Ffh bearing the L301P, L303D, L350D, and L354D mutations into *E. coli* cells harboring the AcrB-PSBT fusion and in which the sole genomic copy of Ffh was conditionally expressed by the presence of arabinose (Phillips and Silhavy, 1992).

Cells were grown to mid log phase in media lacking arabinose to shut-off genomic Ffh expression. Cells were harvested and extracts were electrophoresed and blotted for biotin using streptavidin-HRP. We found significant accumulation of biotinylated AcrB in all of the strains expressing mutant Ffh but not in control cells expressing wild type Ffh (Figure 5B, upper panel). The most dramatic accumulation of biotinylated AcrB was seen in cells expressing Ffh(L303D), which *in vitro* showed defects in both complex formation and stimulated GTPase activity. When the AcrB fusion protein was expressed, all four strains bearing mutant Ffh-expressing plasmids grew significantly slower than wild type controls (data not shown). These results are consistent with previous studies, which demonstrate that SRP targeting may be significantly impaired without substantially affecting cell growth (Ulbrandt *et al.*, 1997). Reduced levels of active SRP in combination with overexpression of an SRP substrate such as AcrB, however, can lead to pronounced synthetically toxic effects (Ulbrandt *et al.*, 1997; Bernstein and Hyndman, 2001). Western blotting of cell extracts with an Ffh-specific antibody showed that all Ffh variants were expressed to comparable levels (Fig. 5B, lower panel).

Taken together, these data therefore indicate that both biochemical activities of the 4.5S RNA—stimulating Ffh•FtsY complex formation and stimulating GTPase activity in the complex—are critical for protein targeting *in vivo*.

Discussion

The 4.5S RNA accelerates the interaction of Ffh with FtsY and the GTPase activities of the two proteins in the complex. In this study, we have shown that the slow rates of complex formation and GTP hydrolysis that are observed in the absence of the 4.5S RNA are recapitulated with Ffh lacking the signal sequence binding M domain, ruling out the possibility that the 4.5S RNA relieves an inhibition imposed by the RNA-free M domain. This finding led us to ask whether the 4.5S RNA requires specific features of Ffh beyond the binding site for its activity. We discovered point mutations in conserved Ffh residues that selectively abolish or diminish the catalytic effects of the 4.5S RNA on complex formation and on the simulated GTPase activity in the complex. These results demonstrate that the activity of the 4.5S RNA is intimately linked to features of the M domain and the linker that joins it to the NG domain, which interacts with the SR. Moreover, we show that mutations perturbing either activity of the 4.5S RNA significantly reduce the efficiency of the SRP-dependent protein targeting system.

A striking feature of the mutations characterized here is that all four are found in positions of Ffh that are conformationally dynamic, based on comparison of available crystal structures (Fig. 6). In particular, L350 and L354 are both part of a short helix in the finger loop of the M-domain. In one crystal structure of the M-domain (*T. aquaticus*; (Keenan et al., 1998), Fig. 6A, top), the residues line the top of one side of the signal sequence binding groove. By contrast, in another crystal structure (*S. solfataricus*; (Rosendal et al., 2003), Fig. 6B, top) the residues point away from the signal sequence

binding pocket. It is interesting to note that in the Keenan structure, two adjacent M-domains in the crystal lattice intertwine, such that hydrophobic residues from one M-domain partially occupy the signal sequence binding groove of the other. Thus, the conformational differences in the two M-domain structures may represent a change in conformation from a closed state (*T. aquaticus* structure) to an open state (*S. solfataricus* structure) that occurs when the signal sequence binding pocket becomes occupied. This view suggests that the activity of the SRP RNA may be dependent on the occupancy of the signal sequence binding groove. For example, binding of the SRP to a signal sequence may enhance the activity of the SRP RNA giving cargo bound SRP a kinetic advantage to interact with FtsY.

Similarly, the other two mutated residues, L301 and L303, are part of a small helix, which together with the loop that connects it to the NG domain, are flipped across the surface of the compactly folded NG domain in the two structures (Fig 6A and 6B, bottom). Conformational flexibility is also observed in single particle reconstructions using cryo-EM techniques when the SRP is bound to the ribosome. In the absence of the SRP receptor, all of SRP54 (the metazoan ortholog of Ffh) could be fitted into defined density, indicating that the ribosome locks the M and NG domains into a fixed conformation relative to each other. By contrast, when SRP receptor is added, no density for the NG domains of either SRP54 or the NG-domain of SR α (the metazoan ortholog of FtsY) was observed, indicating that binding to the SR induces a conformational change (Halic et al., 2006b). Solution studies further support the notion that complex formation between the SRP and SR induce a conformational change in this region (Buskiewicz et

al., 2005a; Spangord et al., 2005). Taken together with our results, these data indicate that a specific conformation of the linker is required for GTPase stimulation by the 4.5S RNA and that factors affecting the relative conformation of the M and NG domains of Ffh could affect the rate of Ffh•FtsY dissociation driven by GTP hydrolysis. For example, a ribosome bound to SRP may inhibit the conformation required for RNA dependent GTPase stimulation and thus delay Ffh•FtsY dissociation until the ribosome has been transferred to the translocon.

Significantly, we found that the two activities of the 4.5S RNA, to promote complex formation and promote GTP hydrolysis, are differentially sensitive to the mutations in Ffh that mimic the absence of 4.5S RNA *in vitro*. Whereas the two mutations in the signal sequence binding domain, L350D and L354D, primarily affect 4.5S RNA stimulation of binding rate to FtsY, L301P primarily affects 4.5S RNA stimulation of GTPase activity, and L303D causes dramatic reductions in both binding rate and GTPase activity. While these distinctions are not absolute, the differences contrast with previously reported mutations in the tetraloop region of the 4.5S RNA that act similarly to the L303D mutation and compromise both the rate of complex formation and the maximal rate of GTP hydrolysis in the complex (Jagath et al., 2001; Siu et al., 2006). Thus, the data presented here demonstrate that the two activities can be differentially affected. Therefore the activities of the 4.5S RNA to promote complex formation and disassembly could, in principle, be differentially regulated, consistent with the models presented above.

Taken together, the mutations identified in this study support the model that the SRP RNA links the major conformational changes in the signal sequence binding subunit of the SRP to the interaction cycle of the SRP and the SR. Such molecular communication within SRP provides an attractive mechanism for coordination of the interaction of the SRP and the SR with ribosome recruitment and transfer to the translocon and an explanation for the centrality of the SRP RNA to efficient protein targeting

Acknowledgments

The authors would like to thank Harris D. Bernstein , Julia R. Kardon, Saskia Neher, Beaker, and members of the Walter Lab for helpful comments. Our special appreciation goes to Shu-ou Shan for her extensive mentoring of NB in the art of pre-steady state kinetic analyses. This work was supported by a grant from the NIH to PW. PW is an Investigator of the Howard Hughes Medical Institute. NB was supported by a predoctoral fellowship from the NSF.

References

- Batey, R.T., Rambo, R.P., Lucast, L., Rha, B., and Doudna, J.A. (2000). Crystal structure of the ribonucleoprotein core of the signal recognition particle. *Science* 287, 1232-1239.
- Bernstein, H.D., and Hyndman, J.B. (2001). Physiological basis for conservation of the signal recognition particle targeting pathway in *Escherichia coli*. *J Bacteriol* 183, 2187-2197.
- Buskiewicz, I., Kubarenko, A., Peske, F., Rodnina, M.V., and Wintermeyer, W. (2005a). Domain rearrangement of SRP protein Ffh upon binding 4.5S RNA and the SRP receptor FtsY. *Rna* 11, 947-957.
- Buskiewicz, I., Peske, F., Wieden, H.J., Gryczynski, I., Rodnina, M.V., and Wintermeyer, W. (2005b). Conformations of the signal recognition particle protein Ffh from *Escherichia coli* as determined by FRET. *J Mol Biol* 351, 417-430.
- Connolly, T., Rapiejko, P.J., and Gilmore, R. (1991). Requirement of GTP hydrolysis for dissociation of the signal recognition particle from its receptor. *Science* 252, 1171-1173.
- Egea, P.F., Shan, S.O., Napetschnig, J., Savage, D.F., Walter, P., and Stroud, R.M. (2004). Substrate twinning activates the signal recognition particle and its receptor. *Nature* 427, 215-221.
- Egea, P.F., Stroud, R.M., and Walter, P. (2005). Targeting proteins to membranes: structure of the signal recognition particle. *Curr Opin Struct Biol* 15, 213-220.
- Focia, P.J., Shepotinovskaya, I.V., Seidler, J.A., and Freymann, D.M. (2004). Heterodimeric GTPase core of the SRP targeting complex. *Science* 303, 373-377.
- Gilmore, R., Blobel, G., and Walter, P. (1982a). Protein translocation across the endoplasmic reticulum. I. Detection in the microsomal membrane of a receptor for the signal recognition particle. *J Cell Biol* 95, 463-469.
- Gilmore, R., Walter, P., and Blobel, G. (1982b). Protein translocation across the endoplasmic reticulum. II. Isolation and characterization of the signal recognition particle receptor. *J Cell Biol* 95, 470-477.
- Halic, M., Becker, T., Pool, M.R., Spahn, C.M., Grassucci, R.A., Frank, J., and Beckmann, R. (2004). Structure of the signal recognition particle interacting with the elongation-arrested ribosome. *Nature* 427, 808-814.

Halic, M., Blau, M., Becker, T., Mielke, T., Pool, M.R., Wild, K., Sinning, I., and Beckmann, R. (2006a). Following the signal sequence from ribosomal tunnel exit to signal recognition particle. *Nature* *444*, 507-511.

Halic, M., Gartmann, M., Schlenker, O., Mielke, T., Pool, M.R., Sinning, I., and Beckmann, R. (2006b). Signal recognition particle receptor exposes the ribosomal translocon binding site. *Science* *312*, 745-747.

Jagath, J.R., Matassova, N.B., de Leeuw, E., Warnecke, J.M., Lentzen, G., Rodnina, M.V., Luirink, J., and Wintermeyer, W. (2001). Important role of the tetraloop region of 4.5S RNA in SRP binding to its receptor FtsY. *Rna* *7*, 293-301.

Jagath, J.R., Rodnina, M.V., and Wintermeyer, W. (2000). Conformational changes in the bacterial SRP receptor FtsY upon binding of guanine nucleotides and SRP. *J Mol Biol* *295*, 745-753.

Keenan, R.J., Freymann, D.M., Stroud, R.M., and Walter, P. (2001). The signal recognition particle. *Annu Rev Biochem* *70*, 755-775.

Keenan, R.J., Freymann, D.M., Walter, P., and Stroud, R.M. (1998). Crystal structure of the signal sequence binding subunit of the signal recognition particle. *Cell* *94*, 181-191.

Larsen, N., and Zwieb, C. (1993). The signal recognition particle database (SRPDB). *Nucleic Acids Res* *21*, 3019-3020.

Lee, H.C., and Bernstein, H.D. (2001). The targeting pathway of Escherichia coli presecretory and integral membrane proteins is specified by the hydrophobicity of the targeting signal. *Proc Natl Acad Sci U S A* *98*, 3471-3476.

Mainprize, I.L., Beniac, D.R., Falkovskaia, E., Cleverley, R.M., Gierasch, L.M., Ottensmeyer, F.P., and Andrews, D.W. (2006). The structure of Escherichia coli signal recognition particle revealed by scanning transmission electron microscopy. *Mol Biol Cell* *17*, 5063-5074.

Miller, J.D., Wilhelm, H., Gierasch, L., Gilmore, R., and Walter, P. (1993). GTP binding and hydrolysis by the signal recognition particle during initiation of protein translocation. *Nature* *366*, 351-354.

Peluso, P., Herschlag, D., Nock, S., Freymann, D.M., Johnson, A.E., and Walter, P. (2000). Role of 4.5S RNA in assembly of the bacterial signal recognition particle with its receptor. *Science* *288*, 1640-1643.

Peluso, P., Shan, S.O., Nock, S., Herschlag, D., and Walter, P. (2001). Role of SRP RNA in the GTPase cycles of Ffh and FtsY. *Biochemistry* *40*, 15224-15233.

- Phillips, G.J., and Silhavy, T.J. (1992). The *E. coli* *ffh* gene is necessary for viability and efficient protein export. *Nature* 359, 744-746.
- Poritz, M.A., Bernstein, H.D., Strub, K., Zopf, D., Wilhelm, H., and Walter, P. (1990). An *E. coli* ribonucleoprotein containing 4.5S RNA resembles mammalian signal recognition particle. *Science* 250, 1111-1117.
- Powers, T., and Walter, P. (1995). Reciprocal stimulation of GTP hydrolysis by two directly interacting GTPases. *Science* 269, 1422-1424.
- Powers, T., and Walter, P. (1997). Co-translational protein targeting catalyzed by the *Escherichia coli* signal recognition particle and its receptor. *Embo J* 16, 4880-4886.
- Rosendal, K.R., Wild, K., Montoya, G., and Sinning, I. (2003). Crystal structure of the complete core of archaeal signal recognition particle and implications for interdomain communication. *Proc Natl Acad Sci U S A* 100, 14701-14706.
- Schaffitzel, C., Oswald, M., Berger, I., Ishikawa, T., Abrahams, J.P., Koerten, H.K., Koning, R.I., and Ban, N. (2006). Structure of the *E. coli* signal recognition particle bound to a translating ribosome. *Nature* 444, 503-506.
- Shan, S.O., and Walter, P. (2003). Induced nucleotide specificity in a GTPase. *Proc Natl Acad Sci U S A* 100, 4480-4485.
- Siu, F.Y., Spangord, R.J., and Doudna, J.A. (2006). SRP RNA provides the physiologically essential GTPase activation function in cotranslational protein targeting. *RNA* 2, 240-250.
- Spangord, R.J., Siu, F., Ke, A., and Doudna, J.A. (2005). RNA-mediated interaction between the peptide-binding and GTPase domains of the signal recognition particle. *Nat Struct Mol Biol* 12, 1116-1122.
- Tian, H., and Beckwith, J. (2002). Genetic screen yields mutations in genes encoding all known components of the *Escherichia coli* signal recognition particle pathway. *J Bacteriol* 184, 111-118.
- Ulbrandt, N.D., Newitt, J.A., and Bernstein, H.D. (1997). The *E. coli* signal recognition particle is required for the insertion of a subset of inner membrane proteins. *Cell* 88, 187-196.
- Walter, P., and Blobel, G. (1982). Signal recognition particle contains a 7S RNA essential for protein translocation across the endoplasmic reticulum. *Nature* 299, 691-698.

Walter, P., Ibrahimi, I., and Blobel, G. (1981). Translocation of proteins across the endoplasmic reticulum. I. Signal recognition protein (SRP) binds to in-vitro-assembled polysomes synthesizing secretory protein. *J Cell Biol* *91*, 545-550.

Zopf, D., Bernstein, H.D., and Walter, P. (1993). GTPase domain of the 54-kD subunit of the mammalian signal recognition particle is required for protein translocation but not for signal sequence binding. *J Cell Biol* *120*, 1113-1121.

Table 1

4.5S RNA:	k_{\max} (s^{-1}) +	k_{\max} (s^{-1}) -	$K_{1/2}$ (μM) +	$K_{1/2}$ (μM) -
Ffh(wt)	0.354	0.034	1.39	16.3
Ffh(NG)	0.053	0.040	18.66	15.2
Ffh(L301P)	0.077	0.041	0.34	11.6
Ffh(L303D)	0.087	0.045	10.99	17.2
Ffh(L350D)	0.187	0.034	23.98	15.5
Ffh(L354D)	0.199	0.033	29.02	12.5

Table 2

4.5S RNA:	k_{on} ($\text{M}^{-1}\text{s}^{-1}$) +	k_{on} ($\text{M}^{-1}\text{s}^{-1}$) -	k_{off} (s^{-1}) +	K_{D} ^a (nM) +
Ffh(wt)	57,000	180	0.0018	33
Ffh(L301P)	17,000	47	n.d.	n.d.
Ffh(L303D)	280	43	0.000014	20
Ffh(L350D)	410	99	0.000006	68
Ffh(L354D)	310	21	0.000026	120

^a K_{D} values are calculated from the ratio of the k_{off} and the k_{on} . Equilibrium binding experiments independently confirmed showed that the affinity of the interaction of Ffh and FtsY was unaffected by the mutations in Ffh (data not shown).

Figure 1.

Removal of the M-domain does not alter the interaction kinetics of Ffh and FtsY in the absence of the 4.5S RNA.

(A) The NG domain was severed from Ffh by limited proteolysis with V8 protease and purified as described in Materials and Methods. A Coomassie blue-stained SDS polyacrylamide gel displaying selected fractions from the purification procedure is shown. The lane labeled “SP FT” contains the flow through fraction from an SP Sepharose column, which binds to the liberated M-domain, and the lane labeled “NG” contains purified Ffh-NG after gel filtration. This fraction was used in the subsequent assays. (B) Binding of the purified Ffh-NG fragment to FtsY produces a change of the tryptophan fluorescence of FtsY. Solid circles represent the intensity of fluorescence from the complex of Ffh-NG and FtsY when excited with 290 nm light, whereas the open circles represent the fluorescence spectrum of unbound Ffh-NG and FtsY. Complex formation was initiated by addition of Mg^{2+} in excess over EDTA as previously described (Shan and Walter, 2003). (C) Representative data monitoring the increase in tryptophan fluorescence intensity as a function of time. The time course shown was obtained at 0.85 μ M Ffh-NG and 0.1 μ M FtsY and no 4.5S RNA. Data points represent intensity measurements taken when the sample was excited at 290 nm and emission was measured at 340 nm. (D) Ffh-NG binds to FtsY with rates indistinguishable from full length Ffh in the absence of the 4.5S RNA. Observed rate constants from data such as in C are plotted as a function of concentration of Ffh (●-solid line: full length Ffh + 4.5S RNA, ○-solid line: full length Ffh - 4.5S RNA, ▲-dashed line: Ffh NG - 4.5S RNA). The inset graph is magnified to show the slow reactions. (E) Stimulated GTP hydrolysis reactions for

Ffh•FtsY and Ffh-NG•FtsY. Hydrolysis rates (per complex, per second) are plotted as a function of concentration of FtsY (●-solid line: full length Ffh + 4.5S RNA, ○-solid line: full length Ffh - 4.5S RNA, ▲-dashed line: Ffh NG - 4.5S RNA, △-dashed line: Ffh NG + 4.5S RNA).

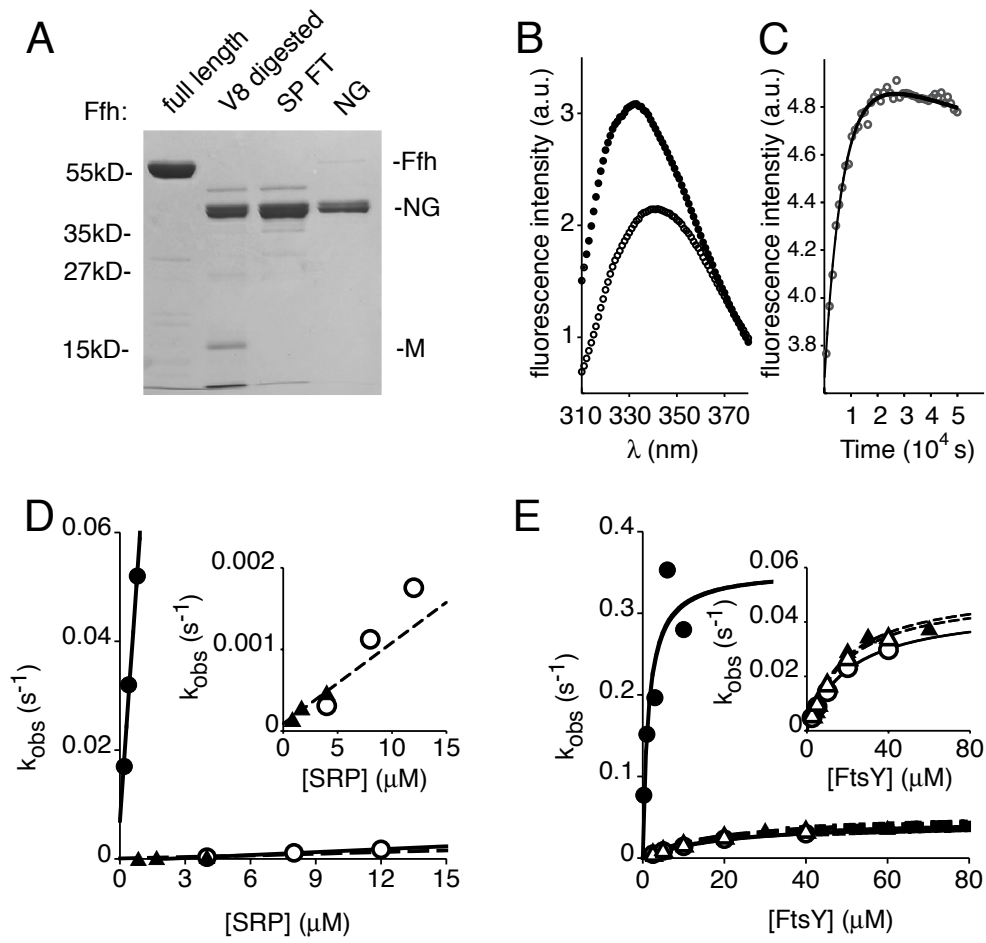


Figure 1 Chapter 1

Figure 2.

Binding to 4.5S RNA and basal GTPase activity is not affected by mutations L301P, L303D, L350D, and L354D.

(A) Gel shift analysis using 0.25 μM Ffh and 0.25 μM [^{32}P]-labeled 4.5S RNA shows that all mutant variants quantitatively shift the RNA. (B) Single turnover GTP hydrolysis assays of wild type (●), Ffh(L301P) (○), Ffh(L303D) (□), Ffh(L350D) (◇), and Ffh(L354D) (▽). Reactions were performed with trace [^{32}P]-GTP and varying amounts of Ffh. Curves (solid line Ffh(wt), dashed lines for Ffh mutants) were fit to the equation $k_{\text{obs}} = k_{\text{cat}} * [\text{Ffh}] / (K_{\text{M}} + [\text{Ffh}])$. Values of k_{cat} are: Ffh(wt) 0.070 min^{-1} , Ffh(L301P) 0.077 min^{-1} , Ffh(L303D) 0.092 min^{-1} , Ffh(L350D) 0.10 min^{-1} , and Ffh(L354D) 0.10 min^{-1} .

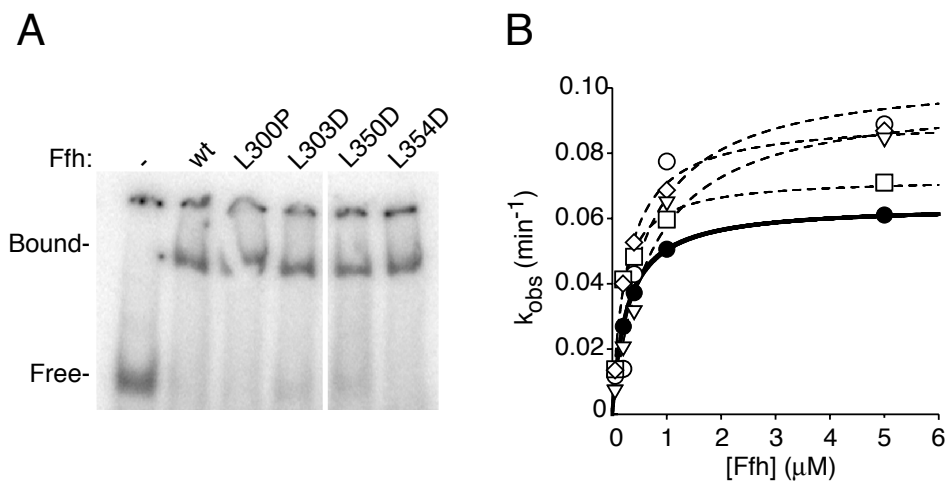


Figure 2 Chapter 1

Figure 3.

Ffh mutations of L303D, L350D, and L354D abrogate the activity of the 4.5S RNA to catalyze association of Ffh and FtsY.

(A) Observed rate constants for binding of wild type Ffh (●,○) or Ffh(L303D) (■,□) in the presence (filled symbols) or absence (open symbols) of 4.5S RNA are plotted as a function of Ffh concentration. Lines represent fits to the equation $k_{\text{obs}} = k_{\text{on}} * [\text{Ffh}] + k_{\text{off}}$ (solid lines for wt Ffh, dashed lines for Ffh(L303D)). (B) The mutations selectively affect the binding rate in the presence but not absence of the 4.5S RNA. The binding rates relative to wt Ffh are plotted (note log-scaled Y axis). (C) Dissociation of wild type (●) or Ffh(L303D) (▲) from FtsY was measured in the presence of the 4.5S RNA by adding GDP to trap dissociated complexes and monitored by changes in tryptophan fluorescence. Samples were excited at 290 nm and fluorescence emission at 340 nm was recorded. The x-axis in the inset is expanded to show the curve for wild type Ffh. Data were fit to a single exponential equation to calculate the k_{off} . (D) Plot of the k_{off} or K_{D} of Ffh mutants relative to wild type Ffh in the presence of the 4.5S RNA. k_{on} , k_{off} , and K_{D} values are summarized in Table 2.

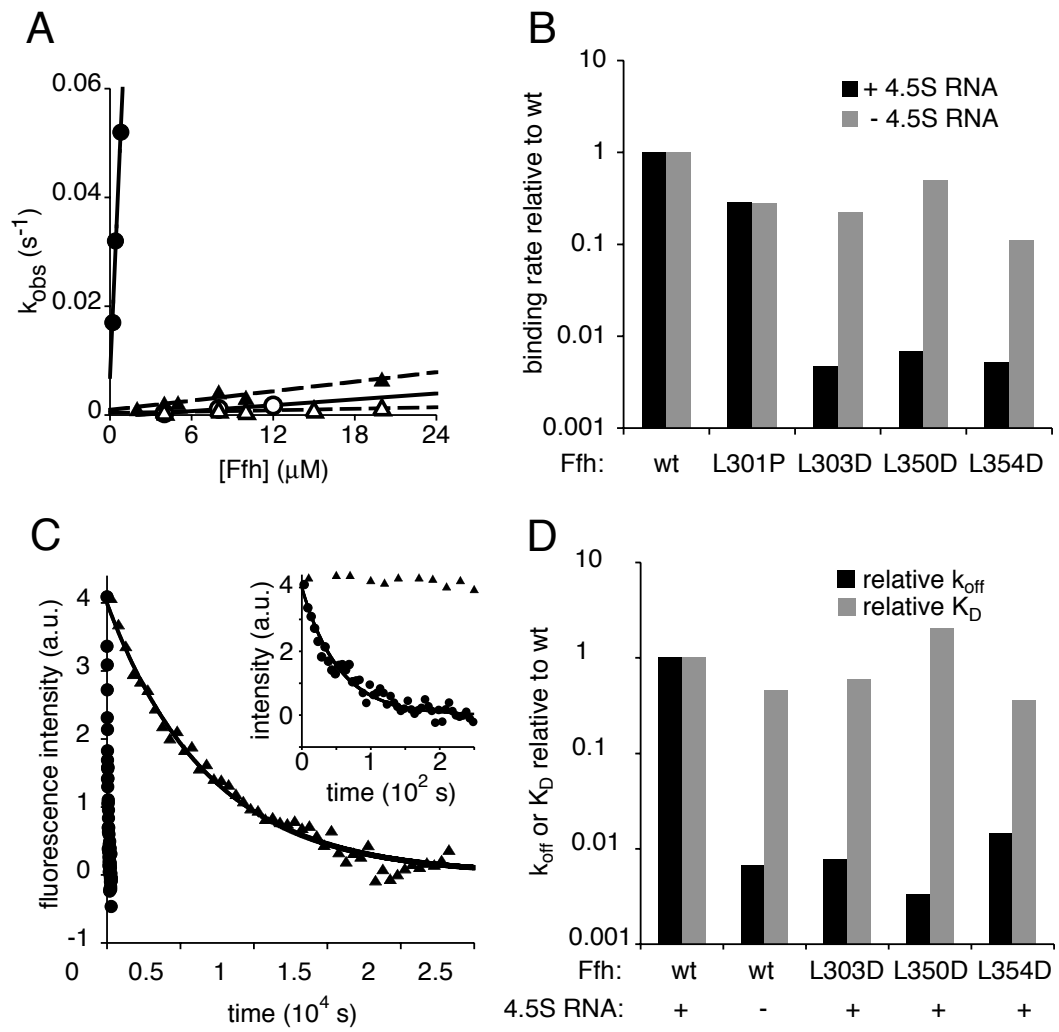


Figure 3 Chapter 1

Figure 4.

Mutations L301P and L303D abrogate the activity of the 4.5S RNA to enhance the stimulated GTPase activity of the SRP and FtsY.

Multiple turnover GTP hydrolysis reactions were carried out in which wild type Ffh (●) or Ffh mutants (▲) were mixed with varying concentrations of FtsY in the presence (filled symbols) or absence (open symbols) of the 4.5S RNA. The Ffh mutants shown are: Ffh(L301P) (Panel A), Ffh(L303D) (Panel B), and Ffh(L350D) (Panel C). Solid lines are curve fits to reactions containing wild type Ffh and dashed lines to reactions containing Ffh mutants. (D) Plot of k_{\max} in the presence and absence of 4.5S RNA. The values for k_{\max} and $K_{1/2}$ are summarized in Table 1. Error bars represent the accuracy of the fits to the data.

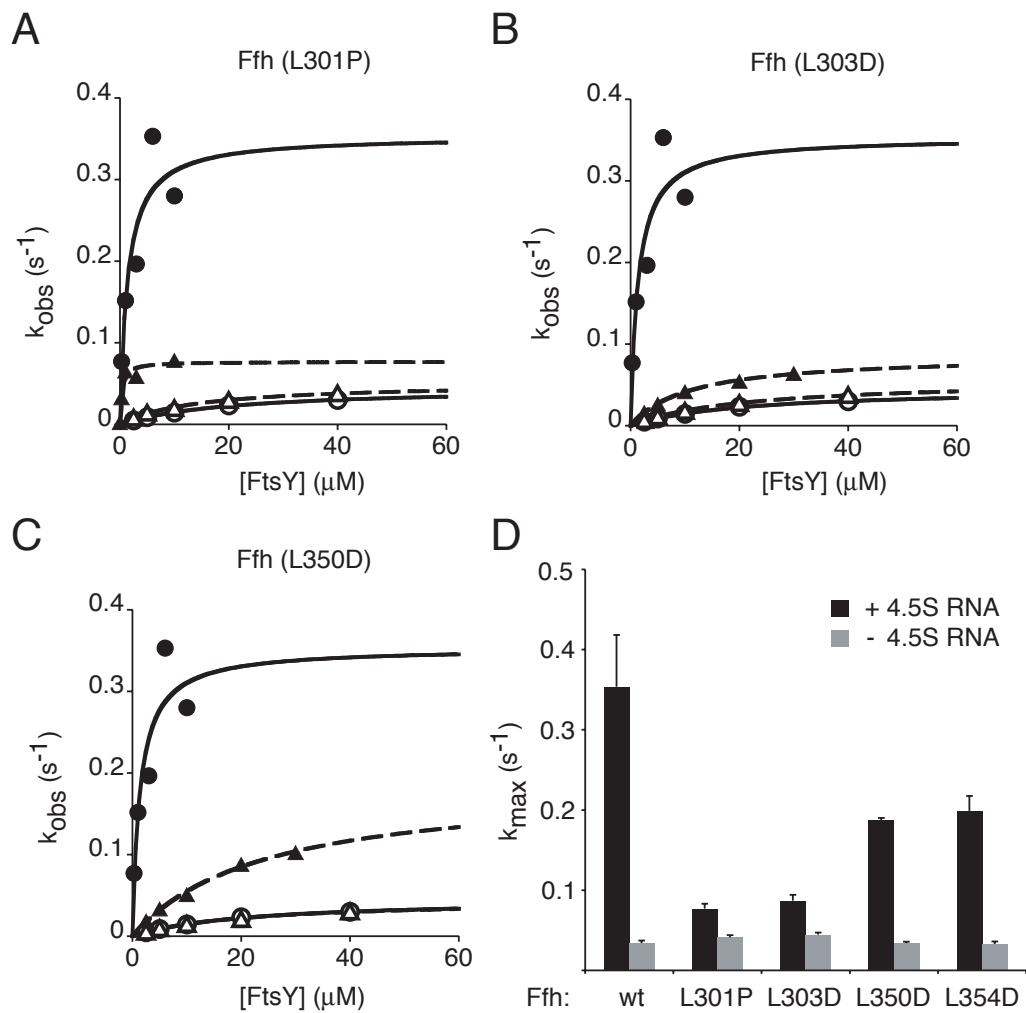


Figure 4 Chapter 1

Figure 5.

Ffh mutations L301P, L303D, L350D, and L354D show membrane protein integration defects *in vivo*.

(A) The multispinning transmembrane protein AcrB fused to the PSBT biotinylation domain is efficiently targeted and integrated in cells expressing wild type SRP, locating the PSBT biotinylation domain to the periplasmic space, where it is not biotinylated. If SRP-dependent protein targeting is impaired, AcrB accumulates in the cytoplasm, where it is biotinylated. (B) *E. coli* cells containing a genomic deletion of Ffh and a genomically inserted copy of wt Ffh that is exclusively expressed in the presence of arabinose and bearing two plasmids: one containing wild type or mutant Ffh, and the other containing AcrB fused to the PSBT biotinylation domain were grown in the absence of arabinose. Cell extracts were fractionated by SDS polyacrylamide electrophoresis and gels were blotted using a streptavidin-HRP conjugate (upper panel) or anti-Ffh antibodies followed by HRP-conjugated secondary antibodies (lower panel). HRP was visualized by chemiluminescence.

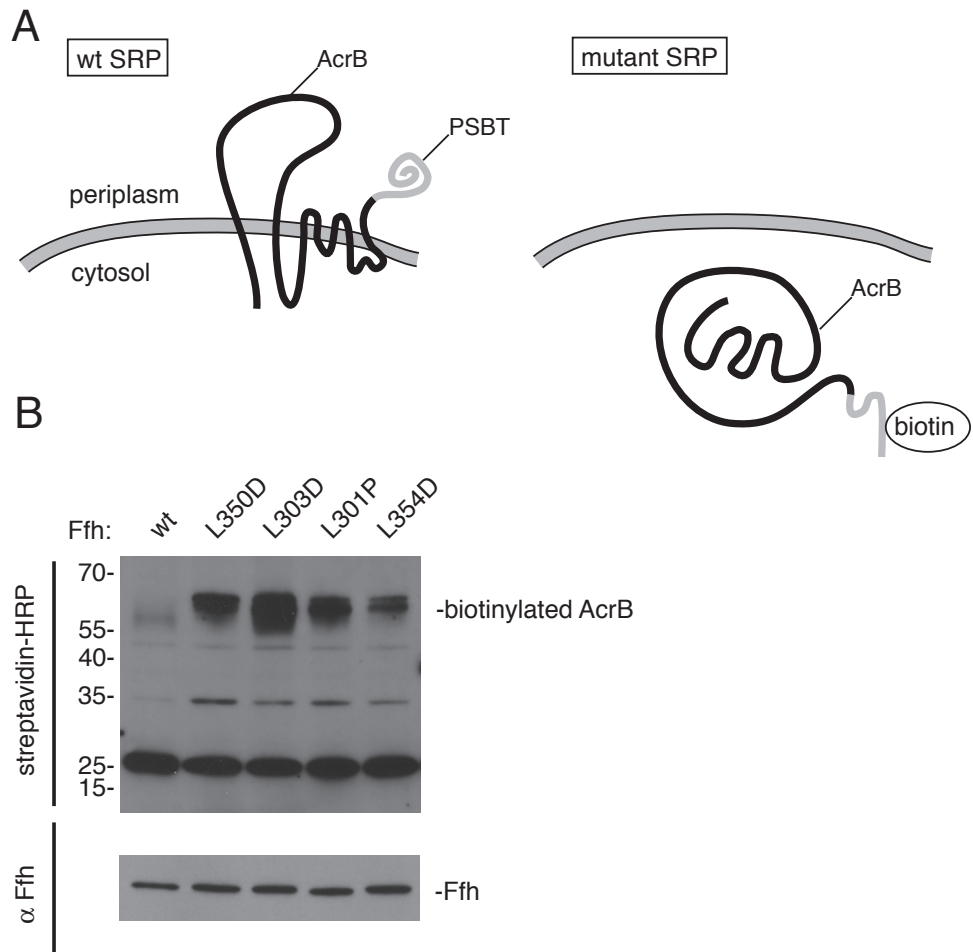


Figure 5 Chapter 1

Figure 6.

Mutations in Ffh that lead to defects in 4.5S RNA activity map to conformationally dynamic regions.

Comparison of X-ray crystal structures from *T. aquaticus* (A) and *S. solfataricus* (B) reveals that the linker between the NG and M domains (bottom) and the finger loop of the M domain (top) are mobile. The corresponding amino acid positions of the mutations in *E. coli* Ffh described in this manuscript are indicated: L301 (298 in *T. aquaticus* and 298 in *S. solfataricus*) and L303 (300,300) in the linker and L350(341,348) and L354(345,352) lead to defects in 4.5S RNA activity.

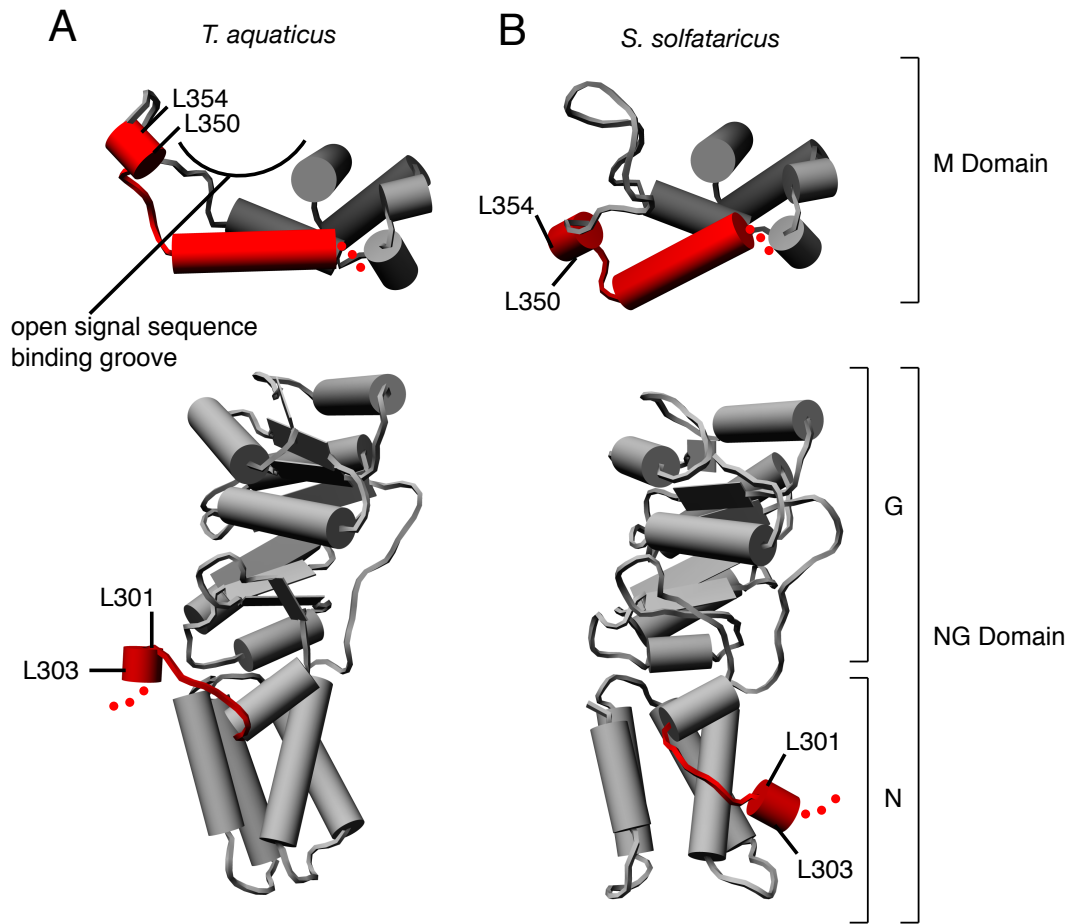


Figure 6 Chapter 1

Chapter 2

Signal Sequences Activate the Catalytic Switch of SRP RNA

From Bradshaw N, Neher SB, Booth DS, and Walter P. (2009) Signal sequences activate the catalytic switch of SRP RNA. *Science*. 323(5910): 127-30. Reprinted with permission from AAAS.

This article is available online at:

<http://www.sciencemag.org/cgi/content/full/323/5910/127>

Signal Sequences Activate the Catalytic Switch of SRP RNA

Niels Bradshaw*, Saskia B. Neher*, David S. Booth, and Peter Walter†

Howard Hughes Medical Institute
4000 Jones Bridge Road
Chevy Chase, MD 20815-6789 USA, and
Department of Biochemistry and Biophysics
Genentech Hall, MC 2200
600 16th Street
San Francisco, CA 94158-2517 USA

†To whom correspondence should be addressed. E-mail: pwalter@biochem.ucsf.edu

*These authors made equal contributions

The signal recognition particle (SRP) recognizes polypeptide chains bearing a signal sequence as they emerge from the ribosome, and then binds its membrane-associated receptor (SR) delivering the ribosome-nascent chain complex to the membrane. SRP RNA catalytically accelerates SRP-SR interaction, which stimulates their GTPase activities and drives complex dissociation. The catalytic activity of SRP RNA appeared to be constitutive. By contrast, here we have found that SRP RNA only accelerated complex formation when SRP was bound to a signal sequence. This crucial control step was obscured because detergent commonly included in the reaction buffer acted as a signal peptide mimic. Thus, SRP RNA is a molecular switch that renders the SRP-SR GTPase engine responsive to signal peptide recruitment, coupling GTP hydrolysis to productive protein targeting.

Secretory and transmembrane proteins are delivered to the membrane cotranslationally by SRP and SR(1). SRP recognizes signal sequences as they emerge from the ribosome(2) and then associates with SR at the membrane where the ribosome is transferred to the translocon. The GTPase domains of SRP and SR mediate this interaction cycle(3). Interaction of SRP with SR leads to the reciprocal stimulation of their GTPase activities, and GTP hydrolysis dissociates the complex(4, 5). In *E. coli*, SR is a single protein, FtsY, and SRP consists of 4.5S RNA and a single protein, Ffh(6). 4.5S RNA catalyzes the interaction of Ffh and FtsY, accelerating both on and off rates by over 100 fold(7).

To harness the energy of GTP hydrolysis for protein targeting, recruitment of targeting substrates by SRP should be coupled to the SRP-SR interaction cycle. Both signal sequences and 4.5S RNA bind to the M-domain of Ffh, suggesting that the catalytic activity of 4.5S RNA could be responsive to signal sequence binding(8). However, under typical assay conditions, 4.5S RNA is constitutively active, negating this role for the RNA(4, 7, 9, 10). A small amount of the non-ionic detergent octaethyleneglycol dodecylether (C₁₂E₈) has been used in assays for SRP function, including kinetic characterization of the Ffh-FtsY interaction(4, 7, 9-11). We found that C₁₂E₈ was required for the dramatic stimulation of Ffh-FtsY binding rate caused by 4.5S RNA (**Fig. 1A; Table 1**).

Assembly of the Ffh•FtsY complex can be measured by tryptophan fluorescence (7, 9). In the presence of 4.5S RNA, C₁₂E₈ stimulated the rate of Ffh-FtsY association by 70-fold (**Fig. 1A**). Likewise, the dramatic stimulation of Ffh-FtsY disassembly caused by

4.5S RNA required $C_{12}E_8$ (23-fold faster with $C_{12}E_8$ than without; **Fig. 1B**; **Table 1**). Importantly, $C_{12}E_8$ had no effect on the assembly or disassembly reactions in the absence of 4.5S RNA (**Fig. 1A-B**). Thus $C_{12}E_8$ is not a neutral stabilizing additive but “activates” 4.5S RNA to accelerate Ffh-FtsY complex formation. Moreover, as most previous studies characterizing 4.5S RNA catalysis of the Ffh-FtsY interaction were carried out with detergent, they monitored this activated state.

The molecular properties of $C_{12}E_8$ important for activating 4.5S RNA suggested that it acts as a signal peptide mimic. We tested E_8 , the nonionic head group of $C_{12}E_8$, and the detergents cetyltrimethylammonium bromide (CTABr) and sodium dodecyl sulfate (SDS), which share a long carbon chain with $C_{12}E_8$, but are positively and negatively charged, respectively (**Fig. 1C-D**). CTABr stimulated binding similarly to $C_{12}E_8$, while SDS and E_8 did not (**Fig. 1D**). Thus, the long carbon chain of $C_{12}E_8$ with a neutral or positively charged head group is sufficient to activate 4.5S RNA. This suggests that $C_{12}E_8$ acts as a signal peptide mimic because signal peptides generally have a hydrophobic core and positively but not negatively charged amino acids(12). Additionally, Ffh was crystallized with detergents(13), and density in the signal-sequence binding groove may have been attributable to it. Finally, the Hill coefficient ($n = 5.8$) for $C_{12}E_8$ stimulation of Ffh-4.5SRNA•FtsY complex formation (**Fig. 2A**), suggested that at least 6 detergent molecules cooperate to activate each Ffh-4.5S RNA and corresponded well with the size of the putative signal sequence binding pocket in Ffh (**Fig. 1B**).

We sought to determine whether signal peptides activate 4.5S RNA in the absence of C₁₂E₈. Because most signal peptides are insoluble(14), we chose the ΔEspP signal peptide(15), which is less hydrophobic than most signal peptides. We measured binding of ΔEspP peptide labeled with carboxyfluorescein (ΔEspP-FAM) to Ffh by fluorescence anisotropy. ΔEspP-FAM bound Ffh-4.5S RNA with a K_d of 1.5 ± 0.4 μM (**Fig. 3A**). Intriguingly, the K_d for Ffh alone was 19.6 ± 6.4 μM (**Fig. 3A**), demonstrating that 4.5S RNA contributes to the binding of signal peptides as predicted(8). The addition of C₁₂E₈ weakened ΔEspP-FAM binding to Ffh-4.5S RNA (K_d = 5.5 ± 1.5 μM), but not to Ffh alone (21.6 ± 7.9 μM) (**Fig. 3B**), suggesting that ΔEspP and detergent compete for binding to SRP. ΔEspP-FAM did not bind Ffh lacking its signal sequence binding M-domain (**Fig. 3A**), binding was reversible (**Fig. 4A**), and ΔEspP-FAM did not impair the solubility of Ffh-4.5S RNA (**Fig. 4B-C**).

To test if saturating concentrations of ΔEspP stimulate the activity of 4.5S RNA, we used ΔEspP with added lysines at the C-terminus to improve its solubility (ΔEspP* (16)). Like C₁₂E₈, ΔEspP* dramatically accelerated Ffh-4.5S RNA•FtsY association (over 40-fold; **Fig. 3C**; **Table 1**) and dissociation (approximately 10-fold; **Table 1**) but had no effect in the absence of 4.5S RNA (**Table 1**). In the presence of both C₁₂E₈ and ΔEspP*, the rate of Ffh-4.5SRNA•FtsY complex formation was not substantially changed relative to individual additions (**Table 1**). Thus, the ΔEspP peptide and C₁₂E₈ act by the same mechanism.

If ΔEspP^* activates 4.5S RNA by associating with SRP, then the rate of Ffh-4.5S RNA-FtsY interaction should correlate with the fraction of ΔEspP^* -bound SRP (calculated from the K_d in figure 2A). We measured the rate of Ffh-4.5S RNA and FtsY interaction as a function of ΔEspP^* concentration (**Fig. 3D**). When we compared the observed Ffh/FtsY binding rates to the rate predicted from the fraction SRP bound to ΔEspP^* (**Fig. 3A**), the data matched this model exceptionally well (**Fig. 3D**).

In addition to accelerating Ffh-FtsY association, 4.5S RNA increases the rate of GTP hydrolysis by $^{\text{GTP}}\text{Ffh}\cdot\text{FtsY}^{\text{GTP}}$ complexes. However, neither ΔEspP^* nor C_{12}E_8 affected this rate (**Fig. 5**). Thus, signal peptides specifically affect the ability of 4.5S RNA to accelerate Ffh \cdot FtsY complex formation.

To assess the specificity of 4.5S RNA activation, we used a version of ΔEspP^* bearing mutations (F12A and L15T) that reduces SRP-dependent targeting in vivo(15). In the presence of 10 μM $\Delta\text{EspP}(\text{F12A}, \text{L15T})^*$, the 4.5S RNA-stimulated association and dissociation of Ffh and FtsY was approximately 5-fold slower than that measured with “wildtype” ΔEspP^* (**Fig. 6A, Table 1**). Similar to ΔEspP^* , $\Delta\text{EspP}(\text{F12A}, \text{L15T})^*$ had no effect in the absence of 4.5S RNA (**Fig. 6A**). To determine if this was due to reduced binding of $\Delta\text{EspP}(\text{F12A}, \text{L15T})$ to SRP, we measured the K_d by fluorescence anisotropy and found that binding was substantially weaker ($K_d=87\mu\text{M} \pm 18\mu\text{m}$, **Fig. 6B**).

Consistent with this, increasing concentrations of $\Delta\text{EspP}(\text{F12A}, \text{L15T})^*$ increased the observed rate for SRP-FtsY association (**Fig. 7**).

Thus, SRP RNA acts as a switchable regulatory module at the center of the SRP protein targeting machine to link recruitment of cargo (a signal peptide) to the next step in the targeting reaction (binding to SR). If free SRP and SR interacted efficiently with each other, they would undergo futile cycles of binding and GTP hydrolysis. Cargo dependent activation of SRP RNA prevents this, harnessing the energy of GTP hydrolysis for protein targeting.

High affinity interaction of SRP with ribosomes can occur prior to SRP interaction with the signal peptide when a short nascent chain is still inside the ribosome, raising the question of how SRP selectively targets signal sequence containing substrates(17). Our results demonstrate that the interaction of the signal peptide with SRP accelerates SRP·SR complex formation, thereby providing a mechanism for selective delivery of appropriate substrates to the membrane. This is conceptually analogous to the kinetic mechanism by which translation achieves fidelity, where cognate codon-anticodon pairing accelerates GTP hydrolysis by EF-Tu(18, 19).

Our results provide an intuitive model for how each step of the targeting process activates the next to achieve productive, directional targeting (**Fig. 8**). Signal peptides bind to SRP's conformationally flexible M-domain that forms a continuous surface with SRP RNA(8, 13). Binding induces a conformational change that activates SRP RNA(20). Activated SRP RNA facilitates the displacement of the N-terminal helices of SRP and SR that slow their association without SRP RNA(21). This commits the ribosome nascent chain complex to membrane targeting. The kinetic control described here, where

substrate recruitment accelerates downstream interactions, provides a generalizable principle for coordination of multistep pathways(22).

Materials and Methods

Reagents. Full length untagged *E. coli* Ffh, 6-his tagged *E. coli* FtsY (amino acids 47-497), and *E. coli* 4.5S RNA were purified as previously described(4). As previously, Ffh was purified in the absence of detergents. Synthetic signal peptides were ordered from Elim Biosciences (unlabeled) or Anaspec (FAM labeled). All peptides were purified to >80% purity and the molecular mass of the peptides were confirmed by mass spectrometry. In all cases, a single peak was present at the predicted mass. Peptides for kinetic assays, denoted by an *, were used at higher concentrations and therefore contain four additional lysines appended at the C-terminus to enhance solubility and a C-terminal phenylalanine converted to tryptophan to facilitate concentration measurements. Peptides used in this study are; Δ EspP* (MKK HKR ILA LCF LGL LQS SYS WAK KKK), Δ EspP(F12A, L15T)* (MKK HKR ILA LCA LGT LQS SYS WAK KKK), Δ EspP-FAM (MKK HKR ILA LCF LGL LQS SYS FA K(5-FAM)-NH₂), and Δ EspP(F12A, L15T)-FAM (MKK HKR ILA LCA LGT LQS SYS FA K(5-FAM)-NH₂).

Ffh/FtsY binding assays. Fluorescence assays monitoring the association of Ffh and FtsY were performed as described(4). Assays were performed at 23°C in 50mM Hepes pH7.5, 150mM KOAc, 2mM Mg(OAc)₂, 2mM DTT and 100μM GppNHp. Data were collected on a stopped-flow fluorimeter (KinTek) for fast reactions or a SLM 8100 for slow reactions with an excitation wavelength of 290 nm and an emission wavelength of 340 nm.

Observed binding rates were calculated by fitting the fluorescence data to a single exponential equation. To determine association rate constants, observed binding rates were plotted as a function of [Ffh] and fit to the equation $k_{\text{obs}}=k_{\text{on}}[\text{Ffh}]+k_{\text{off}}$. For experiments with ΔEspP peptide, Ffh, FtsY and ΔEspP were mixed and binding was initiated by the addition of GppNHp. Peptides were always used at 10 μM concentration unless otherwise noted.

To ensure that the increase in tryptophan fluorescence observed in the presence of ΔEspP^* was caused by the specific interaction of Ffh and FtsY rather than by nonspecific aggregation induced by the peptide, reactions were performed by premixing Ffh, 4.5SRNA, FtsY, and ΔEspP^* , and initiating the reaction by adding GppNHp. Additionally, pelleting assays (**Fig. S2C**) and gel filtration (data not shown) confirmed that the peptide did not induce aggregation of the proteins.

Dissociation rate constants were determined by forming complexes with 4 μM of each protein and then mixing with an equal volume of 4mM GDP•Mg²⁺. The fluorescence data was then fit to a single exponential equation corrected for photobleaching to determine the k_{off} .

Peptide-Ffh binding assays. Fluorescence anisotropy was measured on a ISS K2 fluorimeter in 50mM Hepes pH7.5, 150mM KOAc, 2mM Mg(OAc)₂, 2mM DTT with or without 185 μM C₁₂E₈ as noted in the text. FAM-labeled peptides (0.5 μM) were combined with varying concentrations of Ffh or Ffh-4.5S RNA and allowed to

equilabrate for at least 10 minutes at room temperature. Samples were excited at 492 nm and measured at 520 nm. Each reading was taken for 30 seconds, averaged and corrected against a minus peptide sample for light scattering.

1. R. J. Keenan, D. M. Freymann, R. M. Stroud, P. Walter, *Annu Rev Biochem* **70**, 755 (2001).
2. D. Zopf, H. D. Bernstein, A. E. Johnson, P. Walter, *Embo J* **9**, 4511 (Dec, 1990).
3. J. D. Miller, H. Wilhelm, L. Gierasch, R. Gilmore, P. Walter, *Nature* **366**, 351 (Nov 25, 1993).
4. P. Peluso, S. O. Shan, S. Nock, D. Herschlag, P. Walter, *Biochemistry* **40**, 15224 (Dec 18, 2001).
5. T. Powers, P. Walter, *Science* **269**, 1422 (Sep 8, 1995).
6. M. A. Poritz *et al.*, *Science* **250**, 1111 (Nov 23, 1990).
7. P. Peluso *et al.*, *Science* **288**, 1640 (Jun 2, 2000).
8. R. T. Batey, R. P. Rambo, L. Lucast, B. Rha, J. A. Doudna, *Science* **287**, 1232 (Feb 18, 2000).
9. J. R. Jagath, M. V. Rodnina, W. Wintermeyer, *J Mol Biol* **295**, 745 (Jan 28, 2000).
10. X. Zhang, S. Kung, S. O. Shan, *J Mol Biol* **381**, 581 (Sep 5, 2008).
11. P. Walter, G. Blobel, *Proc Natl Acad Sci U S A* **77**, 7112 (Dec, 1980).
12. G. von Heijne, *J Mol Biol* **184**, 99 (Jul 5, 1985).
13. R. J. Keenan, D. M. Freymann, P. Walter, R. M. Stroud, *Cell* **94**, 181 (Jul 24, 1998).
14. J. F. Swain, L. M. Gierasch, *J Biol Chem* **276**, 12222 (Apr 13, 2001).
15. J. H. Peterson, C. A. Woolhead, H. D. Bernstein, *J Biol Chem* **278**, 46155 (Nov 14, 2003).
16. See SOM methods
17. T. Bornemann, J. Jockel, M. V. Rodnina, W. Wintermeyer, *Nat Struct Mol Biol* **15**, 494 (May, 2008).
18. T. Pape, W. Wintermeyer, M. Rodnina, *Embo J* **18**, 3800 (Jul 1, 1999).
19. J. M. Ogle, V. Ramakrishnan, *Annu Rev Biochem* **74**, 129 (2005).
20. N. Bradshaw, P. Walter, *Mol Biol Cell* **18**, 2728 (Jul, 2007).
21. S. B. Neher, N. Bradshaw, S. N. Floor, J. D. Gross, P. Walter, *Nat Struct Mol Biol* (Aug 10, 2008).
22. The authors thank J. Weissman, C. Gross, P. Egea, C. Gallagher, and A. Korennykh, A. Acevedo, W. Weare, and J. Kardon for assistance and comments. This work was supported by grants to P.W. from the National Institutes of Health. P.W. is an Investigator of the Howard Hughes Medical Institute. N.B. was supported by the NSF. The JCC Fund supports S.B.N. An NIGMS Fellowship supports D.S.B.
23. M. Le Maire, S. Kwee, J. P. Andersen, J. V. Moller, *Eur J Biochem* **129**, 525 (Jan 1, 1983).

Table and Legend.

Table 1: Association and dissociation rate constants for Ffh/FtsY association and dissociation. Rate constants were measured as described in methods in the presence or absence of detergent and peptides. In all cases, peptides were used at 10 μ M concentration and C₁₂E₈ was used at 185 μ M.

	$k_{on} (M^{-1}s^{-1})$		$k_{off} (s^{-1})$	
	+	-	+	-
RNA:				
Additive:				
-	830 \pm 50	110 \pm 50	0.00010 \pm 0.000003	0.0000056 \pm 0.0000004
C ₁₂ E ₈	60,000 \pm 7000	140 \pm 20	0.0023 \pm 0.0001	0.0000089 \pm 0.000001
Δ EspP*	36,000 \pm 700	44 \pm 20	0.0010 \pm 0.00003	0.000014 \pm 0.0000005
Δ EspP* + C ₁₂ E ₈	83,000 \pm 3000	N.D.	N.D	N.D
Δ EspP(F12A, L15T)*	7,000 \pm 900	82 \pm 10	0.00023 \pm 0.000009	0.0000044 \pm 0.0000005

Figure legends:

Figure 1. Detergent activates 4.5S RNA to catalyze the Ffh-FtsY interaction. **A.** $C_{12}E_8$ stimulates the binding of Ffh and FtsY only in the presence of 4.5S RNA. Observed binding rates for formation of Ffh•FtsY complexes are plotted as a function of Ffh concentration in the presence and absence of 4.5S RNA and 185 μM $C_{12}E_8$. Lines represent fits to the equation $k_{\text{obs}}=k_{\text{off}}+k_{\text{on}}[\text{Ffh}]$. Inset shows the slow reactions with an expanded scale. **B.** $C_{12}E_8$ activates 4.5S RNA stimulation of Ffh•FtsY complex dissociation. Dissociation rate constants are plotted in the absence and presence of $C_{12}E_8$. **C.** Chemical structures of $C_{12}E_8$, E_8 , CTABr, and SDS. **D.** Association rate constants for Ffh-4.5SRNA•FtsY complex formation with no detergent, 185 μM $C_{12}E_8$, 100 μM E_8 , 70 μM CTABr, and 100 μM SDS. Error bars in B. and D. are standard errors of the fits.

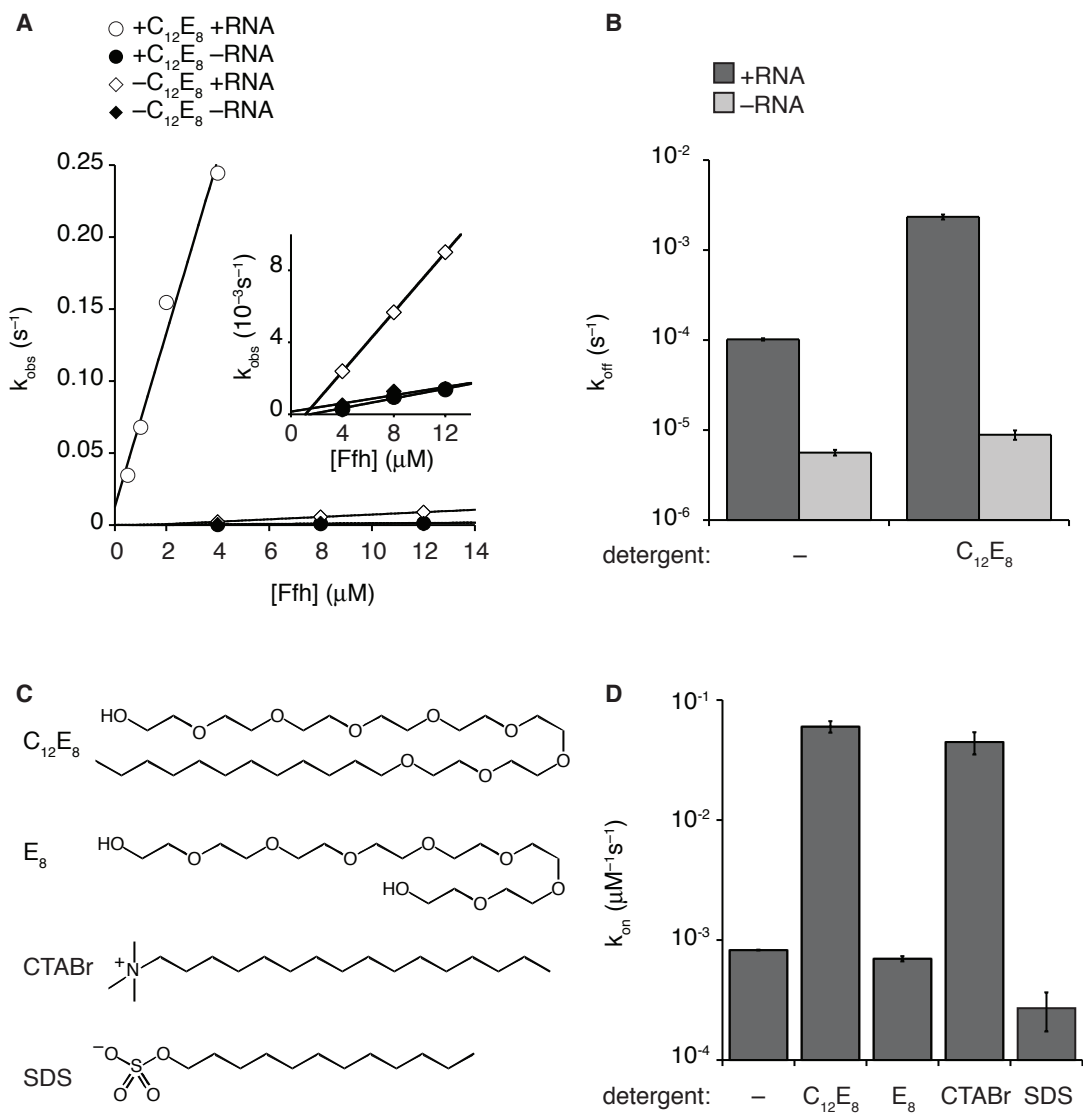


Figure 1 Chapter 2

Figure 2. A. Concentration dependence of C₁₂E₈ activation of 4.5S RNA. Observed binding rates were determined for reactions with 1μM Ffh, 0.1μM FtsY, and 1.5μM 4.5SRNA as a function of C₁₂E₈ concentration. Data were fit to the equation $k_{obs} = [C_{12}E_8]^n / ([C_{12}E_8]^n + K_{1/2}^n)$ giving $K_{1/2} = 60 \pm 0.7 \mu M$ and $n = 5.8 \pm 0.4$. Half-maximal stimulation (60μM) was achieved below the critical micelle concentration of C₁₂E₈ (90 μM(23)), suggesting that free detergent molecules activate 4.5S RNA. This is also supported by the fact that CTABr activates 4.5S RNA at concentrations significantly below its CMC (approximately 1mM). **B.** C₁₂E₈ may act as a signal peptide mimic. Hypothetical model of C₁₂E₈ binding in the putative signal sequence binding groove of the M-domain of Ffh (PDBID 2FFH)(13). In this crystal form of Ffh, M-domains from adjacent molecules in the crystal packing are twinned so that the hydrophobic groove of each M-domain is partially occupied by the other. Due to the size and hydrophobic nature of the groove it is assumed to be the signal peptide binding site. We therefore generated a molecular model of C₁₂E₈ in the groove using ChemDraw3D. Six C₁₂E₈ molecules were placed into the signal sequence binding pocket manually and the energy of the detergent was minimized by an MM2 minimization.

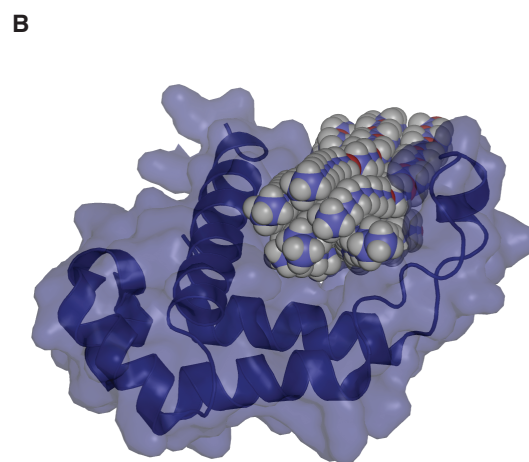
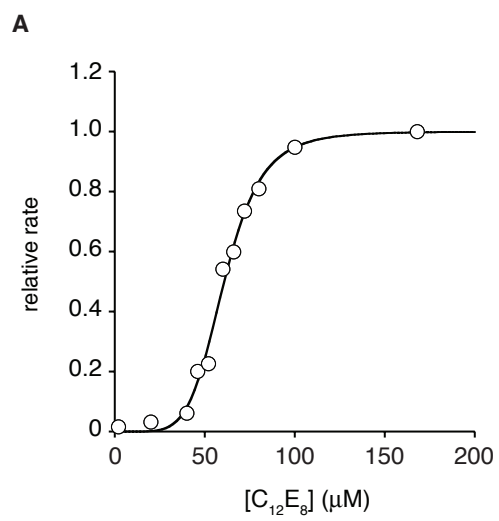


Figure 1 Chapter 2

Figure 3. Δ EspP binds SRP with micromolar affinity and stimulates 4.5S RNA catalysis of Ffh-FtsY interaction. **A.** Fluorescence anisotropy of Δ EspP-FAM is plotted as a function of [Ffh]. Lines represent fits to the equation $\text{Anisotropy} = \text{Anisotropy}_{\text{free}} + \text{Anisotropy}_{\text{bound}}([\text{Ffh}]/(\text{K}_d + [\text{Ffh}]))$. **B.** C_{12}E_8 increased the K_d of Δ EspP for Ffh-4.5S RNA. Equilibrium dissociation constants for Δ EspP binding to Ffh from fluorescence anisotropy in the presence and absence of 4.5S RNA are plotted. Dark bars represent K_d in the presence of 185 μM C_{12}E_8 . Error bars are standard errors of the fits. **C.** In the presence of 4.5S RNA, Δ EspP stimulates the association rate for Ffh•FtsY complex formation. Observed rate constants are plotted as a function of [Ffh]. Lines are fits to the equation $k_{\text{obs}} = k_{\text{off}} + k_{\text{on}}[\text{Ffh}]$. The dashed line is a reference to the binding rate in the presence of C_{12}E_8 from figure 1. **D.** Δ EspP* activates 4.5S RNA by binding to SRP. Observed rates for 1 μM Ffh/4.5SRNA binding to 1 μM FtsY are plotted as a function of Δ EspP* concentration. The dashed line represents the equation $k_{\text{obs}} = (\text{fraction bound}) * (\text{max stimulated rate}) + (\text{fraction unbound}) * (\text{unstimulated rate})$, where the fraction bound was calculated from the K_d measured in part A, $\chi^2 = 5.4 * 10^{-6}$.

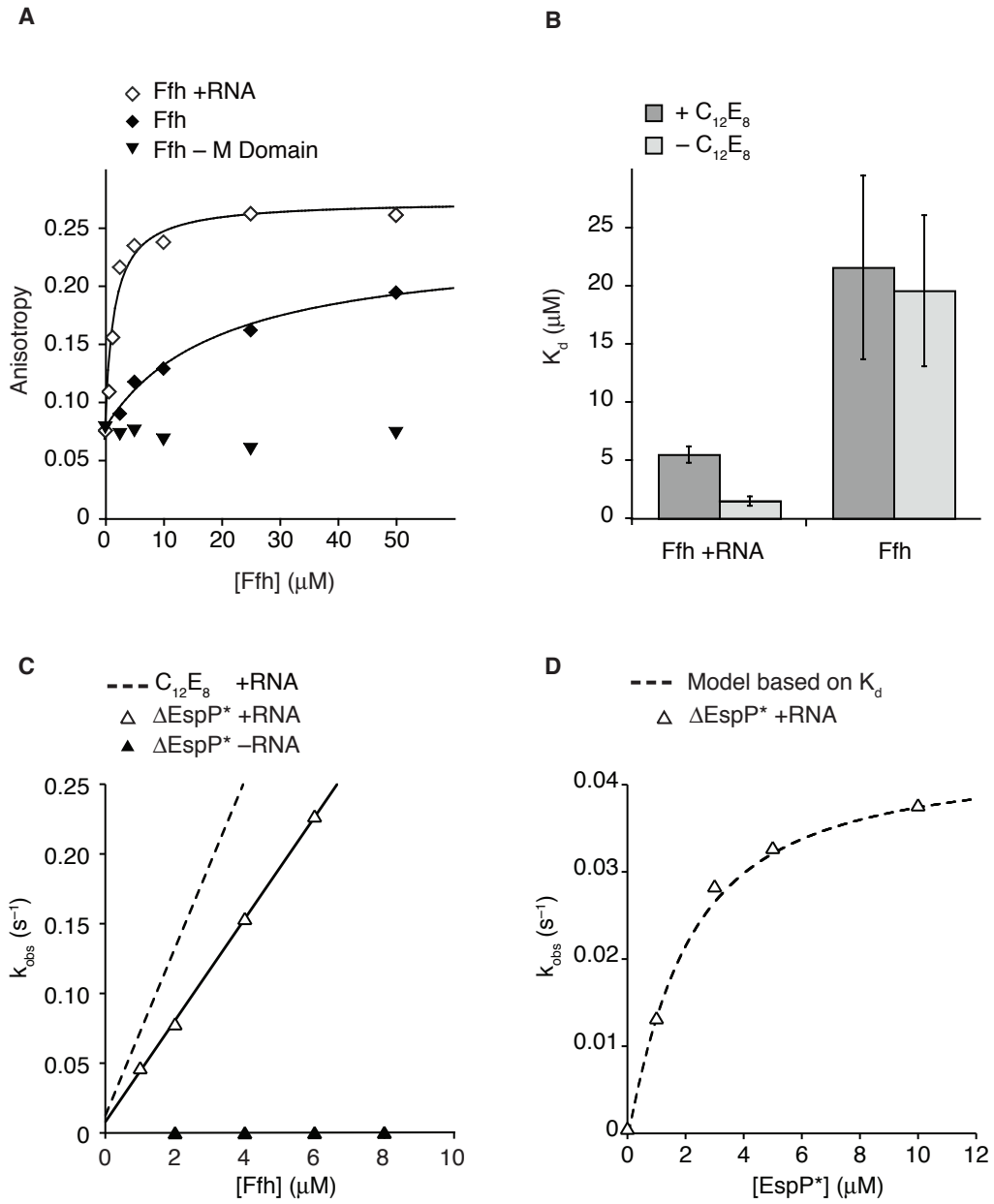


Figure 3 Chapter 2

Figure 4. Addition of peptide does not induce aggregation of SRP under the assay conditions used. **A.** Binding of peptide to SRP is reversible. When peptide bound to 5 μM SRP is diluted 5 fold, the anisotropy returns to that seen for 1 μM SRP. Error bars represent the standard deviation of 3 independent measurements. **B.** Addition of 0.5 μM ΔEspP -FAM peptide to 50 μM SRP as used in anisotropy assays does not decrease the amount of Ffh still soluble after 1 hr. at 390,000 x g. **C.** No decrease in the fraction of soluble Ffh is observed upon addition of 10 μM ΔEspP^* peptide to Ffh/FtsY binding reactions using 5 μM Ffh. Centrifugation is as per part B.

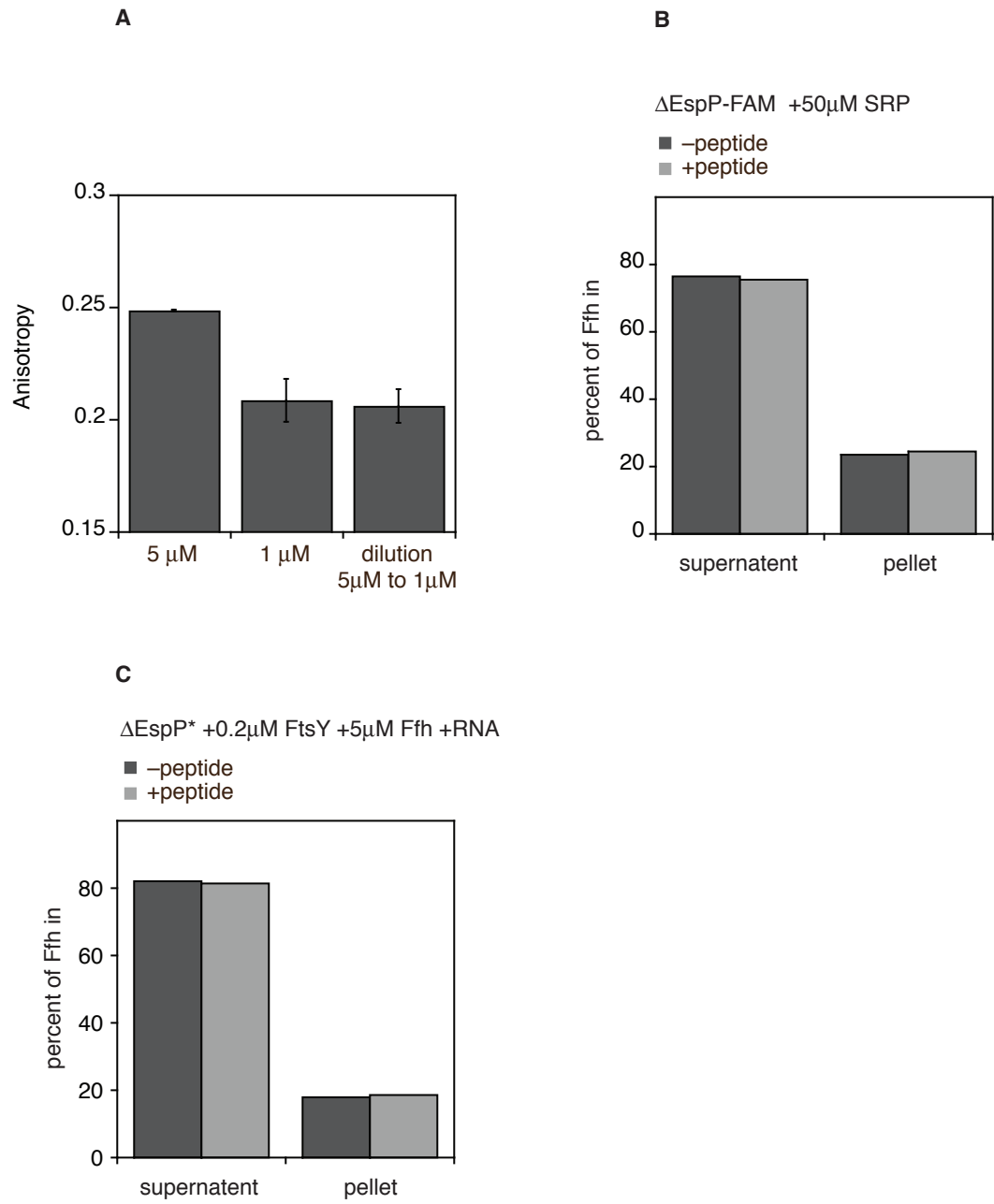


Figure 4 Chapter 2

Figure 5. The GTP hydrolysis-driven disassembly of the Ffh•FtsY complex is insensitive to 4.5S RNA activation. In addition to catalyzing Ffh•FtsY complex formation, 4.5S RNA stimulates the GTPase activity of the $^{GTP}\text{Ffh}/4.5\text{S RNA}\cdot\text{FtsY}^{GTP}$ complex approximately 4-fold. To explore whether C₁₂E₈ and ΔEspP* also affect GTPase activity, we measured the rate of GTP hydrolysis-driven disassembly of $^{GTP}\text{Ffh}/4.5\text{SRNA}\cdot\text{FtsY}^{GTP}$ complexes by a pulse chase procedure. $^{GTP}\text{Ffh}/4.5\text{SRNA}\cdot\text{FtsY}^{GTP}$ complexes were formed and then rapidly mixed with an excess of GDP^{Mg⁺⁺}. Complex disassembly was monitored by a decrease in tryptophan fluorescence. The disassembly rate is equal to the maximal rate of GTP hydrolysis by the $^{GTP}\text{Ffh}/4.5\text{SRNA}\cdot\text{FtsY}^{GTP}$ complex. C₁₂E₈ and ΔEspP* had no effect on the maximal rate of GTP hydrolysis by the $^{GTP}\text{Ffh}/4.5\text{SRNA}\cdot\text{FtsY}^{GTP}$ complex.

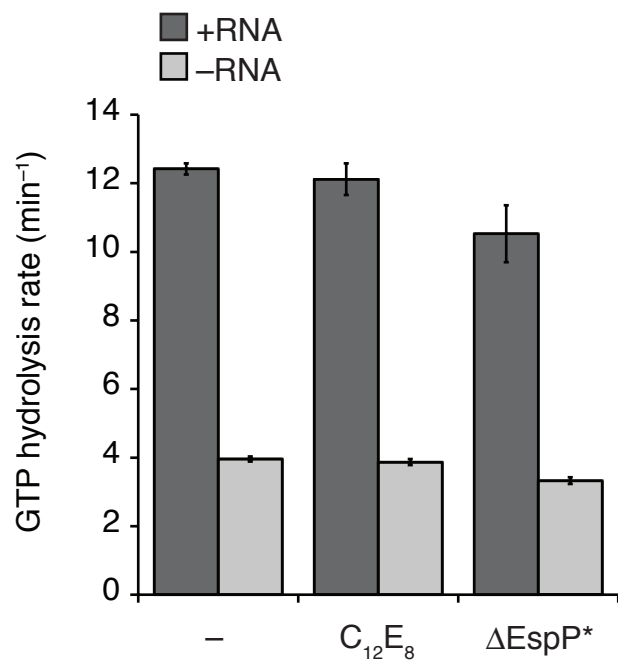


Figure 5 Chapter 2

Figure 6. Mutations in Δ EspP that impair SRP-mediated targeting show decreased binding to SRP and decreased stimulation of 4.5S RNA. **A.** The Δ EspP (F12A, L15T) stimulates SRP•FtsY complex formation less than Δ EspP. The dashed line represents the +RNA + Δ EspP* peptide binding rate from figure 2C. **B.** Fluorescence anisotropy of FAM-labeled Δ EspP (F12A, L15T) is plotted as a function of [SRP].

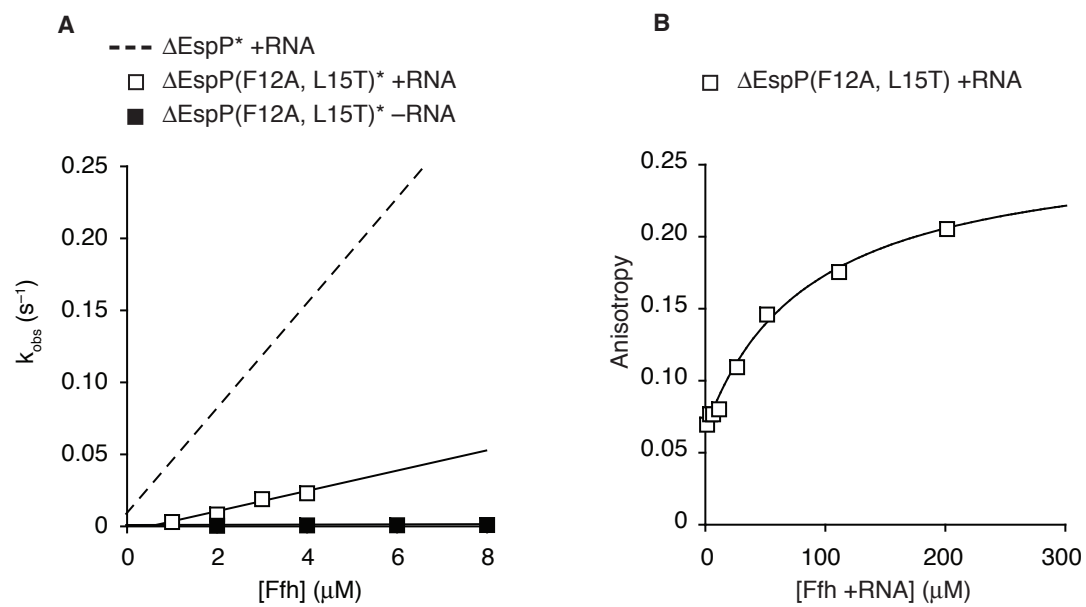


Figure 6 Chapter 2

Figure 7. In figure 3, Ffh/4.5SRNA/FtsY binding assays were done at subsaturating concentrations (10 μ M) of Δ EspP (F12A, L15T)* peptide (K_d 87 μ M, figure 3A). Addition of increasing amounts of the Δ EspP (F12A, L15T)* peptide to 1 μ M FtsY with 2 μ M Ffh/4.5SRNA increased the k_{obs} for Ffh/4.5SRNA•FtsY complex formation.

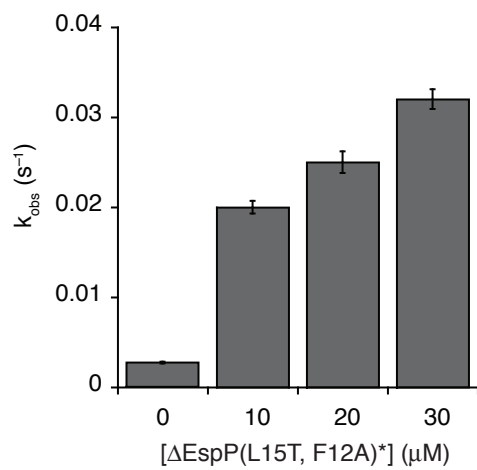


Figure 7 Chapter 2

Figure 8. Model for the role of 4.5S RNA in cotranslational protein targeting. Signal peptides bind to the M-domain of Ffh as they emerge from ribosomes. Contact with signal peptide induces a conformational change in 4.5S RNA (Step 1), which activates the RNA. Activated 4.5S RNA communicates with the NG domain of Ffh (Step 2), priming it for interaction with FtsY by displacing the autoinhibitory helix α -N1 (Step 3). Encountering FtsY relaxes this transition state by displacing helix α -N1 of FtsY (Step 4), resulting in productive targeting of the ribosome nascent chain complex to the translocon. It is not known whether the displacement of helices N1 from Ffh and from FtsY occurs stepwise as depicted or in a concerted reaction only upon Ffh encountering FtsY. Next, the SRP/SR complex is disassembled by GTP hydrolysis to recycle the components for subsequent rounds of targeting.

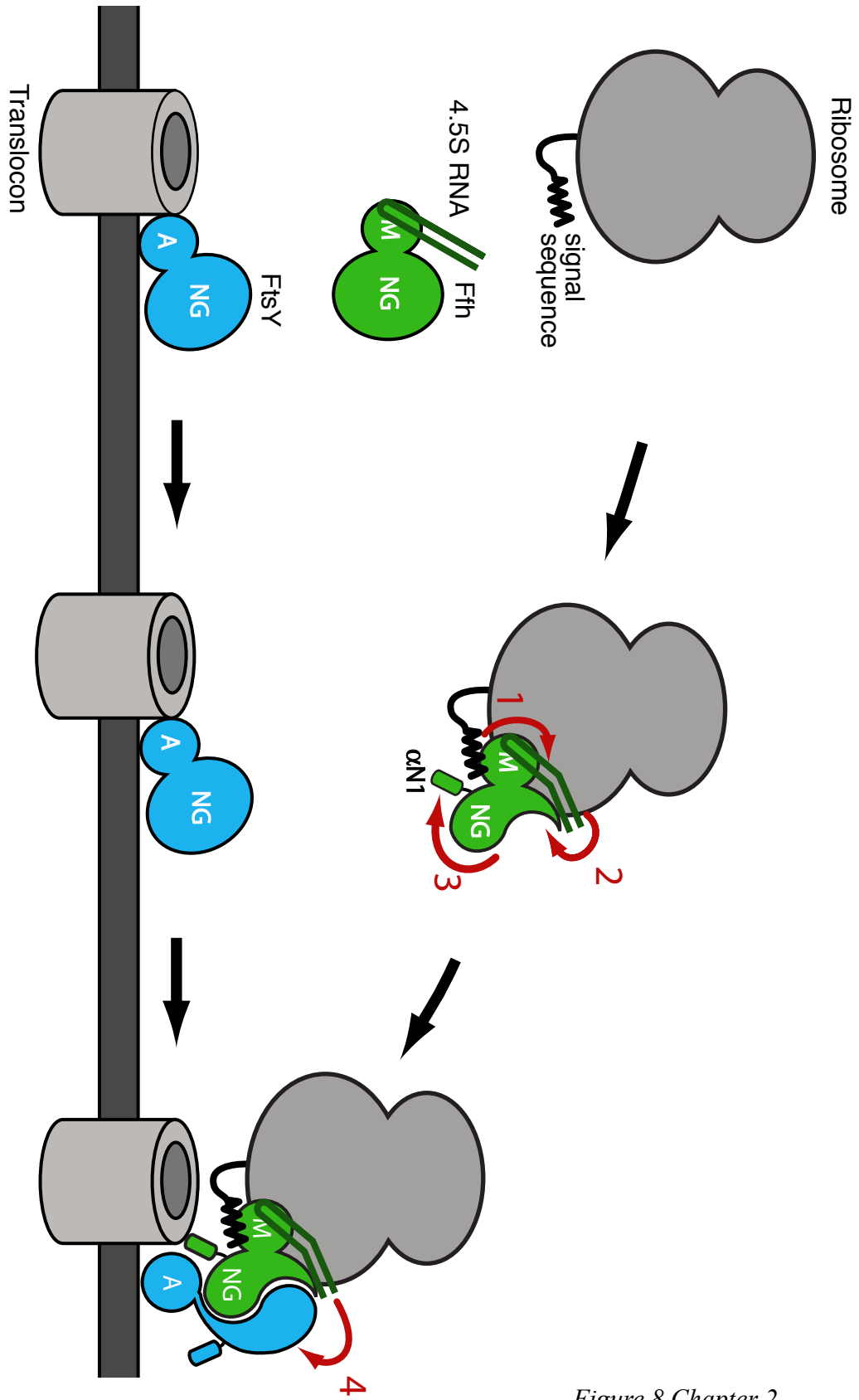


Figure 8 Chapter 2

Chapter 3

SRP RNA controls a conformational switch that regulates SRP-SRP receptor interaction

From Neher, S.B., Bradshaw, N., Floor, S.N., Gross, J.D., & Walter, P. (2008) SRP RNA controls a conformational switch regulating the SRP-SRP receptor interaction. *Nature Structural & Molecular Biology*. 15(9): 916-923 .

This article is available online at:

<http://www.nature.com/nsmb/journal/v15/n9/pdf/nsmb.1467.pdf>

**SRP RNA controls a conformational switch that regulates SRP-SRP receptor
interaction**

Saskia B. Neher*^{1,2}, Niels Bradshaw*^{1,2}, Stephen N. Floor³, John D. Gross³, and
Peter Walter^{1,2}

Howard Hughes Medical Institute¹
4000 Jones Bridge Road
Chevy Chase, MD 20815-6789, and
Departments of Biochemistry and Biophysics²
Genentech Hall, MC 2140
60016th Street, Suite S222
San Francisco, CA 94158-2517 and
Pharmaceutical Chemistry³
600 16th Street
Suite 518,Box 2280
San Francisco, CA 94143-2280,
University of California at San Francisco

Corresponding author: Peter Walter (pwalter@biochem.ucsf.edu)*These authors made
equal contributions

Abstract

The interaction of the signal recognition particle (SRP) with its receptor (SR) mediates cotranslational protein targeting to the membrane. SRP and SR interact via their homologous core GTPase domains and N-terminal four-helix bundles (N-domains). SRP-SR complex formation is slow unless catalyzed by SRP's essential RNA component. We show that truncation of the first helix of the N-domain (helix N1) of both proteins dramatically accelerates their interaction. SRP and SR with helix N1 truncations interact at nearly the RNA-catalyzed rate in the absence of RNA. NMR spectroscopy and analysis of GTPase activity show that helix N1 truncation in SR mimics the conformational switch caused by complex formation. These results demonstrate that the N-terminal helices of SRP and SR are autoinhibitory for complex formation in the absence of SRP RNA, suggesting a mechanism for RNA-mediated coordination of the SRP-SR interaction.

Introduction

Compartmentalization of cells requires protein targeting into and across membranes. The signal recognition particle (SRP) captures signal-sequence containing nascent chains on the ribosome, associates with its membrane-bound receptor (SR), and transfers the ribosome nascent chain complex to the translocation apparatus in the endoplasmic reticulum in eukaryotes or plasma membrane in bacteria^{1,2}. Both SRP and SR have

related GTPase domains that are an integral part of the targeting cycle. In their GTP-bound form, SRP and SR form a complex that dissociates upon GTP hydrolysis^{3,4}.

Whereas its mammalian homologue is a complex of six proteins and one RNA molecule (7S RNA), in *Escherichia coli. coli*, SRP is comprised of a smaller RNA molecule (4.5S RNA), and a single, essential protein, Ffh⁵⁻⁷. Ffh is homologous to mammalian SRP54, the central SRP component that binds to signal sequences as they emerge from the ribosome. The SR, termed FtsY in *E. coli*, is also streamlined from two proteins in mammals to a single, essential protein^{6,8}. Thus, *E. coli* contains the core, universally conserved elements of the targeting machinery, which remarkably can complement the more complex eukaryotic machinery in *in vitro* assays^{9,10}.

Ffh and FtsY share structurally and functionally related N-terminal four-helix bundles (N-domains) and Ras-like GTPase domains (G-domains; Fig. 1A)^{11,12}. Formation of Ffh•FtsY complexes occurs via extensive contact between these domains (Fig. 1B)^{13,14}. Additionally, Ffh contains a C-terminal M domain, which binds 4.5S RNA and provides the signal-sequence binding site (Fig. 1C)¹⁵⁻¹⁷. FtsY contains an N-terminal A domain, which is weakly evolutionarily conserved and is implicated in membrane binding (Fig. 1C)^{10,18,19}.

SRPs from all studied species (excepting only chloroplast SRP in higher plants) contain an RNA subunit, and in *E. coli* 4.5S RNA is essential for survival²⁰⁻²². The 4.5S RNA catalyzes the interaction of Ffh and FtsY—increasing the rate of complex formation by

over two orders of magnitude^{3,23}. In addition, 4.5S RNA enhances the maximal rate of GTP hydrolysis from the Ffh•FtsY complex³. Previous work suggested that the activity of 4.5S RNA may be linked to the signal peptide binding state of Ffh-effectively coordinating the interaction of Ffh and FtsY with cargo recruitment by SRP^{15,24}. It remains unclear, mechanistically, why Ffh and FtsY require stimulation by 4.5S RNA to bind efficiently.

Here, we investigate the structural elements of Ffh and FtsY that control the kinetics of their interaction. The N-domains of both Ffh and FtsY are four-helix bundles, and in all crystal forms of the individual proteins, the N-terminal most helix (N1) is present (Fig. 2)^{11,12,16,25}. In contrast, structures of the Ffh•FtsY complex always lack helix N1 of the N domain of FtsY, and exhibit an unstructured or repositioned helix N1 of Ffh^{13,14,26,27}. Indeed, FtsY helix N1 was found to be proteolyzed during the crystallization process, and deliberate amputation of FtsY helix N1 both enhanced complex formation and facilitated crystallization of the complex²⁸. Furthermore, helix N1 of the chloroplast FtsY has been shown to be important for its rapid binding to the chloroplast homologue of Ffh²⁹. Given these hints that helix N1, like 4.5S RNA, affects the rate of Ffh•FtsY complex formation, we set out to investigate this structural element with the goal of clarifying the mechanism of kinetic control of the Ffh•FtsY interaction.

Results

Helix N1 truncations accelerate Ffh•FtsY binding without RNA

To explore whether helix N1 regulates the Ffh•FtsY interaction, we N-terminally truncated *E. coli* FtsY and Ffh. We compared FtsY Δ N1, which lacks the A-domain and first helix of the N domain (Fig. 1A, deleted region in red), to FtsY lacking the first 46 amino acids of the A domain. This 46 amino acid truncation variant is functionally equivalent to full-length FtsY in *in vitro* studies^{3, 10, 23}, and we use it as our wildtype reference and refer to it as FtsY. Similarly, we removed the 8 most N-terminal amino acids of helix N1 from Ffh, creating Ffh Δ N1 (Fig. 1A, deleted region in red). We partially truncated Ffh helix N1 because Ffh lacking the entire N-terminal helix is poorly soluble, and the two truncated proteins displayed indistinguishable binding kinetics with FtsY (Fig. 3).

With these tools in hand, we compared the rates of Ffh•FtsY complex formation between wildtype and truncated forms of Ffh and FtsY in the absence of SRP RNA (Fig. 4A). We monitored the change in FtsY tryptophan fluorescence that reports complex formation^{23, 30}. In the absence of 4.5S RNA, FtsY Δ N1 showed a 7-fold enhanced association rate constant compared to wildtype FtsY (Fig. 4A, compare circles and diamonds; Table 1). Similarly, Ffh Δ N1 formed a complex with FtsY about 4-fold faster than its wild-type counterpart (Fig. 4A, compare squares and diamonds; Table 1). Further, when we combined the rapid-binding mutants FtsY Δ N1 and Ffh Δ N1, the association rate constant was enhanced roughly 150-fold compared to the wild type proteins (Fig. 4B, compare solid triangles and diamonds; Table 1). These experiments were performed in the absence of 4.5S RNA; yet the rate observed with the two truncated proteins approached the RNA-stimulated association rate of Ffh and FtsY to within a factor of three (Fig. 4B,

compare solid triangles and open diamonds; Table 1) indicating that the rate enhancement afforded by 4.5S RNA is quantitatively mimicked by removal of the N1 helices from both FtsY and Ffh. Thus, in the absence of 4.5S RNA, the N-terminal helices of the N-domains of Ffh and FtsY are autoinhibitory for Ffh•FtsY complex formation.

Ffh helix N1 truncation blocks RNA stimulation of Ffh•FtsY binding

If 4.5S RNA acts by relieving inhibition of complex formation caused by helix N1, then helix N1 truncation would enhance complex formation only in the absence of 4.5S RNA. However, if 4.5S RNA speeds complex formation by another mechanism, truncation of the N1 helices would enhance complex formation with and without 4.5S RNA. We therefore measured the binding rate of the truncated forms of Ffh and FtsY in the presence of 4.5S RNA. Unlike our results in the absence of 4.5S RNA, in its presence FtsY Δ N1 and wildtype FtsY associated with Ffh at similar, rapid rates (Fig. 4C, compare circles to diamonds; Table 1). Thus, truncation of helix N1 of FtsY enhances the rate of Ffh•FtsY complex formation selectively in the absence of 4.5S RNA and has no effect in its presence.

Unexpectedly, 4.5S RNA did not stimulate Ffh Δ N1•FtsY complex formation.

Ffh Δ N1•FtsY complexes formed slowly, at nearly identical rates in the presence and absence of 4.5S RNA (Figs. 4C compare open squares and open diamonds and 4D).

Similarly, the rate of Ffh Δ N1•FtsY Δ N1 complex formation is unaffected by the presence of 4.5S RNA. Multiple reports show that the isolated M domain and full-length Ffh bind 4.5S RNA with similar affinity, excluding the possibility that Ffh Δ N1 no longer binds

4.5S RNA^{15,31}. Thus, deletion of helix N1 not only failed to further accelerate complex formation in the presence of 4.5S RNA, but also abolished the stimulatory effect of the RNA.

Taken together, these results (summarized in Figure 4D) show that the N1 helices of Ffh and FtsY jointly inhibit Ffh•FtsY complex formation in the absence of 4.5S RNA. Thus, 4.5S RNA may enhance Ffh•FtsY complex formation by lowering the kinetic barrier imposed by the N1 helices in Ffh and FtsY.

Truncation of N1 helices enhances complex stability

4.5S RNA stimulates binding of Ffh and FtsY by a catalytic mechanism—increasing both the association and dissociation rates²³. Because truncation of helix N1 from both Ffh and FtsY led to an association rate constant as rapid as that observed in the presence of 4.5S RNA, we investigated if the rates of complex dissociation would also be affected. To measure the rates of Ffh•FtsY complex dissociation, we allowed complexes to form in the presence of the non-hydrolyzable GTP analog GppNHp. We then added an excess of GDP to trap dissociated proteins and followed the change of tryptophan fluorescence over time.

As summarized in Figure 5A and Table 1, the dissociation rates of Ffh and FtsY in the absence of 4.5S RNA are virtually unaffected by removal of helices N1. By contrast, in the presence of 4.5S RNA, the Ffh•FtsY complex dissociation rates decrease as the N1 helices are removed. The Ffh•FtsY Δ N1 complex dissociates approximately 5-fold

slower than the complex of the full-length proteins. Consistent with 4.5S RNA having no effect on the association rate of the Ffh Δ N1•FtsY complex, the dissociation rates for this complex are approximately equal with and without 4.5S RNA. Finally, the Ffh Δ N1•FtsY Δ N1 complex, which forms in the absence of 4.5S RNA at nearly the RNA-stimulated, wild type rate, dissociated at a rate that was largely unaffected by 4.5S RNA.

Strikingly, the decreases in dissociation rates caused by truncation of helix N1 almost precisely balances the increase in association rate we observed in Figure 4, such that the calculated K_D 's of each complex ($K_D=k_{off}/k_{on}$) are similar in the absence or presence of 4.5S RNA (Fig. 5B). Because the on-rates of the truncated proteins are increased in the absence of 4.5S RNA, it follows that the K_D 's of the complexes change correspondingly: whereas the wildtype Ffh•FtsY complex has a K_D of 83 ± 12 nM, the complexes in which the N1 helix is deleted from one protein bind 10-fold more tightly, with K_D 's of 8 ± 1 nM for Ffh•FtsY Δ N1 and 7 ± 1 nM for Ffh Δ N1•FtsY. The complex composed of both truncated proteins is around 250-fold tighter with a K_D of 0.36 ± 0.03 nM. Thus, deletion of the N1 helices thermodynamically stabilizes Ffh•FtsY complexes. It is important to note, however, that for each combination of the N1 helix truncated mutants, the principle that 4.5S RNA functions catalytically, i.e. changing the kinetics but not the equilibrium of Ffh/FtsY interactions (which we previously documented for the wildtype proteins²³), is not violated. In summary, these results demonstrate that the N1 helices of Ffh and FtsY inhibit *association* exclusively in the absence of 4.5S RNA and promote *dissociation* exclusively in the presence of 4.5S RNA.

Helix N1 truncation enhances basal GTP hydrolysis

Both Ffh and FtsY are GTPases, and the GTPase cycles of the proteins are intimately linked to their association and dissociation. In the absence of Ffh, FtsY hydrolyzes GTP at a very low, basal rate. Upon association, the GTPase activity of both Ffh and FtsY is accelerated over their respective basal levels, and is referred to as the *stimulated* GTPase activity of the complex. In contrast to other GTPases, Ffh and FtsY each contain all of their catalytic residues, and GTPase stimulation is due to induced conformational changes in each protein upon complex formation^{13,14}. We therefore hypothesized that FtsY Δ N1, which binds more rapidly to Ffh in the absence of 4.5S RNA, might exhibit enhanced basal GTPase activity if it assumes a conformation more like the Ffh bound state.

Indeed, we found that the basal GTPase activity of FtsY Δ N1 was dramatically increased compared to FtsY (Fig. 6A). The maximal GTP hydrolysis rate (k_{cat}) for wild type FtsY was 0.0098 min^{-1} , in good agreement with previous data³, whereas the k_{cat} for FtsY Δ N1 was nearly 100-fold faster (0.66 min^{-1}). Despite the dramatic increase in k_{cat} , the K_D of FtsY Δ N1 for nucleotide (equal to the K_M of the GTPase reaction) did not differ substantially from that of the wildtype FtsY, demonstrating that only the hydrolysis step and not substrate binding is affected by truncation of the N-terminus of FtsY. Thus, FtsY Δ N1 may assume an “Ffh bound” conformation in the absence of Ffh.

Ffh has a higher basal GTP hydrolysis rate than FtsY, and its enhancement upon forming a complex is less pronounced. Furthermore, the active site of Ffh requires an interaction with FtsY to be fully activated³². Consistent with these differences and in contrast to

FtsY Δ N1, the basal GTPase activity of Ffh Δ N1 was only marginally increased over that of the wildtype control (Fig. 6B, 3-fold compared to Ffh).

In summary, truncation of helix N1 of FtsY but not Ffh dramatically increases its basal GTP hydrolysis rate, suggesting that helix N1 prevents FtsY from assuming an “Ffh bound”-activated conformation in the absence of Ffh.

Helix N1 truncation does not affect stimulated GTPase activity

Upon association, the GTPase activity of both Ffh and FtsY is stimulated and drives the disassembly of the Ffh•FtsY complex. In addition to stimulating the rate of interaction between Ffh and FtsY, 4.5S RNA also enhances the rate of stimulated GTP hydrolysis by the Ffh•FtsY complex several fold³. We therefore asked if truncation of helix N1 of Ffh and FtsY affects the ability of 4.5S RNA to accelerate the stimulated GTPase activity of the complex.

Because the maximal rate of stimulated GTP hydrolysis is the same as the GTP-hydrolysis driven rate for disassembly of the $^{GTP}\text{Ffh}\cdot\text{FtsY}^{GTP}$ complex³, we measured disassembly of the $^{GTP}\text{Ffh}\cdot\text{FtsY}^{GTP}$ complex for truncation variants. For all combinations of wild type and truncated Ffh and FtsY, 4.5S RNA stimulated the GTPase activity to a similar extent (Fig. 6C). Additionally, the rates of GTP hydrolysis by Ffh•FtsY complexes and complexes of the truncation variants were similar in the absence of 4.5S RNA (Fig. 6C). This demonstrates that the kinetically different routes of assembly specified by N1 helix truncations do not affect the catalytic core of Ffh•FtsY complexes.

Furthermore, although helix N1 of Ffh is required for 4.5S RNA to accelerate complex formation, 4.5S RNA still accelerates the GTPase activity of the Ffh Δ N1•FtsY and Ffh Δ N1•FtsY Δ N1 complexes.

FtsY Δ N1's conformation resembles the Ffh bound conformation

To further probe the conformational changes of FtsY upon truncation of helix N1 and during complex formation, we analyzed FtsY that either contained or lacked helix N1 by NMR. Because the Ffh•FtsY complex is larger than 80 KDa, we selectively labeled the ultimate methyl groups of isoleucine, leucine, and valine residues with ^{13}C and recorded two-dimensional HSQC spectra of the proteins. This selective labeling scheme is particularly useful for obtaining NMR spectra of large proteins and protein complexes³³. We then compared HSQC spectra of FtsY variants to determine how the structure of FtsY is altered by truncation of helix N1. For this study, we compared FtsY Δ N1 to FtsY-204, which starts at residue 204 and includes helix N1. Like FtsY, FtsY-204 binds slowly to Ffh in the absence of 4.5S RNA (Fig. 7A). Furthermore, the basal GTPase activity of FtsY-204 is significantly slower than that of FtsY Δ N1 (Fig. 7B). Therefore, FtsY-204 is a minimal construct to probe the effects of helix N1 on FtsY structure.

In the absence of nucleotide, the spectra of FtsY-204 and FtsY Δ N1 share a vast majority of cross peaks (Fig. 7C). As expected, a number of the peaks arising from helix N1 were missing from the FtsY Δ N1 spectrum (there are two leucines and one isoleucine between residues 204 and 221). In addition, a few peaks had shifted, indicating that some residues were in different chemical environments in the different FtsY forms (Fig. 7C). Addition

of GppNHp to FtsY Δ N1 shifted numerous cross peaks, whereas addition of GppNHp to FtsY-204 led to virtually no change in the spectrum (Fig. 8A, 8B). The difference in the GppNHp spectra of FtsY-204 and FtsY Δ N1 is not accounted for by differences in affinity for nucleotide because truncation of helix N1 results in only a modest decrease in affinity of FtsY for GppNHp (FtsY-204 $K_D=2.6\mu\text{M}\pm 0.3$ FtsY Δ N1 $K_D=22\mu\text{M}\pm 8$) (Supplementary Fig. 6C). Additionally, one resonance in the FtsY-204 spectrum was broadened and resulted in formation of a new cross-peak upon the addition of GppNHp, consistent with nucleotide being bound to the protein (Fig. 8A, 8D).

Remarkably, many of the cross peaks that appeared when nucleotide was added to FtsY Δ N1 are matched by peaks in the $^{\text{GppNHp}}\text{FtsY-204}\cdot\text{Ffh}^{\text{GppNHp}}$ complex spectrum (Fig. 9). This similarity between the FtsY Δ N1 $^{\text{GppNHp}}$ spectrum and the $^{\text{GppNHp}}\text{FtsY-204}\cdot\text{Ffh}^{\text{GppNHp}}$ spectrum indicates that in the presence of nucleotide, FtsY Δ N1 adopts a conformation similar to the Ffh bound FtsY. These results are consistent with the enhanced basal GTPase activity observed for FtsY Δ N1, indicating that it assumes an active conformation in the absence of Ffh.

Helix N1 of FtsY is expelled upon binding Ffh

Thus far, our results show that helix N1 impedes FtsY's basal GTPase activity and slows complex formation with Ffh. This suggests that rearrangement of helix N1 is required for association with Ffh. By this model, helix N1 might keep FtsY in a conformation unfavorable for complex formation. To associate, FtsY would be forced into a favorable conformation, repositioning the helix in the process. Movement of the helix by complex

formation, like its deletion, could partially account for the stimulatory effect of Ffh on FtsY GTPase activity.

To gain direct evidence for such a conformational change, we used limited proteolysis to probe the structural changes that take place in FtsY helix N1 upon complex formation with Ffh. We found that, when bound to Ffh, a new site in FtsY becomes accessible to protease cleavage, resulting in an additional low molecular weight band (Fig. 10A, arrow). This additional cleavage site is dependent upon both Ffh and nucleotide. The truncation variants FtsY-197, FtsY-204 and FtsY Δ N1 allow finer mapping, and suggest that cleavage occurs at the N-terminus of FtsY, after position 204 and prior to position 221, where FtsY Δ N1 is truncated (Fig. 10B). N-terminal sequencing revealed that cleavage occurred between Ser216 and Leu217 (Fig. 10C), similar to that obtained when *Thermus aquaticus* FtsY was subjected to limited proteolysis in the presence of Ffh²⁸, demonstrating the conservation of this conformational rearrangement.

Discussion

Ribosomes translating proteins destined for insertion into the membrane must be efficiently and rapidly delivered to the translocon. Efficient delivery requires precise control of the interaction of SRP with its receptor by the combined action of their GTPase cycles and SRP RNA. In this study, we describe a conformational switch that inhibits the interaction of the SRP with its receptor in the absence of SRP RNA stimulation.

Furthermore, we show that this mechanism of inhibition is intimately linked to the catalytic effect of SRP RNA on the SRP•SRP receptor interaction.

A conformational switch regulates Ffh•FtsY interaction

Our results demonstrate that the N1 helices of Ffh and FtsY slow Ffh•FtsY association in the absence of 4.5S RNA. Combining these results with previous observations about the differences between the structures of the proteins individually and in complex, we suggest an explanation of how the helices exert their inhibitory effects^{13, 14, 28, 34, 35}.

Strikingly, in all of the unbound structures of Ffh and FtsY, evolutionarily conserved basic amino acids (Ffh-R255 and FtsY-K453) point into the dimerization interface (Fig. 11A, shown in red). In all of the complex structures, Ffh-R255 and FtsY-K453 have rotated approximately 140 degrees to hydrogen-bond to the most C-terminal helix of the NG domain. This movement places Ffh-R255 and FtsY-K453 and the C-terminal helices into the positions that formerly were occupied by helices N1 in the respective proteins (Fig. 11B). The conjecture that this conformational rearrangement is linked to displacement of the N1 helices is further supported by a GDP bound structure of *T. aquaticus* FtsY with helix N1 removed³⁴. In this structure, the homologous residue to K453 (*T. aquaticus* residue K262) is rotated to a position that is in between the Ffh-bound and unbound states.

The importance of these rearrangements to the conformational switch described in this study is underscored by mutational analyses of Ffh and FtsY. Mutations of Ffh-R255 and

FtsY-K453 inhibit complex formation, demonstrating that the contacts made by these residues are required to form a stable complex^{14,36}. Mutation of the absolutely conserved glycine residues (Ffh-G257 and FtsY-G455) that are adjacent to Ffh-R255 and FtsY-K453 also affect complex formation, demonstrating that conformational flexibility in this region is critical for binding (data not shown and^{36,37}). In the complex structure, only the first 6 amino acids of helix N1 clash with R255 or K453 and the C-terminal helices, consistent with our results that truncation of only the first 8 amino acids of Ffh mimic truncation of the entire helix (Fig. 3). Finally, the interaction of Ffh-R255 and FtsY-K453 with the C-terminal helices of the NG domains brings residues on that helix into contact with the GTPase cores of Ffh and FtsY, explaining the link between truncation of helix N1 and the increased basal GTPase activity of FtsY (and, more modestly, of Ffh).

A physical model describing the mechanism of SRP RNA catalysis

The mechanism by which SRP RNA catalyzes the interaction of SRP and SR is a mystery. The results presented here provide a thermodynamic framework that suggests a physical model for the mechanism of SRP RNA catalysis.

In the absence of SRP RNA, the energy to reach the transition state for complex formation is very high due to the requirement to move helix N1. Truncation of helix N1 from both Ffh and FtsY reduces the energy to reach the transition state for complex formation by 2.9 kcal mol⁻¹ but has virtually no effect on the dissociation reaction, suggesting that helix N1 truncation destabilizes the ground state of the unbound proteins, while not changing the energetic state of the complex. Similar to helix N1 truncations,

SRP RNA reduces the energy barrier for the association reaction by approximately 3.5 kcal mol⁻¹. SRP RNA reduces the energy of the dissociation reaction by a similar amount, suggesting that it stabilizes the transition state. We therefore hypothesize that SRP RNA moves the N1 helices of both Ffh and FtsY, which lowers the energy barrier to complex formation. A schematic representation of how each of the truncations affects the thermodynamics of the Ffh•FtsY interaction is presented in Figure 12.

The N1 helices of both Ffh and FtsY are autoinhibitory for complex formation, but only helix N1 of Ffh is required for the stimulatory effect of SRP RNA. This demonstrates a link between the conformational switch described above and the mechanism of SRP RNA catalysis. We hypothesize that SRP RNA moves Ffh helix N1 to a conformation favorable for complex formation with FtsY. Currently we cannot distinguish if this occurs through direct interaction or through an allosteric mechanism. Our results also demonstrate that helix N1 of FtsY must move for complex formation. This connection between SRP RNA and the conformation of FtsY is supported by previous results showing that the M-domain of Ffh (to which SRP RNA binds) can be cross-linked to the N-terminus of FtsY³⁸. Taken together, these observations suggest that the SRP RNA interacts with Ffh helix N1 and FtsY helix N1 in the transition state to stabilize a conformation favorable to interaction.

Implications of the conformational switch for protein targeting

The conformational switch regulating the Ffh•FtsY interaction has important implications for the mechanism of co-translational protein targeting. Structural studies of

the SRP RNA in complex with Ffh, as well as mutational analysis of Ffh suggest that the activity of the SRP RNA is controlled by the signal sequence binding state of Ffh^{15,24}. Such a link suggests that the conformational switch described here may constitute the heart of the mechanism by which the interaction of the SRP and SR is coordinated with signal sequence binding. Furthermore, recent studies have implicated helix N1 of FtsY in association of FtsY with the membrane and transfer of the ribosome from Ffh to the translocon^{39,40}. Given our result that helix N1 of FtsY is exposed by formation of the Ffh•FtsY complex, exposure of helix N1 may coordinate complex formation with membrane association, and the exposed helix N1 may directly stimulate the transfer of the nascent chain to the translocon. Thus, our results provide a conceptual framework of how the stepwise coordination of the SRP-mediated protein targeting reaction could be achieved.

Materials and Methods

Reagents. Plasmids for expression and purification of native *E. coli* FtsY variants containing amino acids 197-497, 204-497 and 221-497 and *E. coli* Ffh containing amino acids 9-454 were created by PCR amplifying the correct sequence with primers that added NdeI and BamHI sites to the 5' and 3' ends of the sequence respectively. These PCR products were cut and ligated into the NdeI and BamHI sites of pET41a (Novagen). Ffh, 4.5S RNA, and FfhΔN1, were purified as previously described³. FtsY variants were expressed in BL21 DE3 cells, and induced with 0.4 mM IPTG for 4 hours. Cell pellets

were resuspended in 200 mM NaCl, 50 mM Tris pH 8, 2 mM DTT, and lysed with a microfluidizer. After clearing the lysate, a 45-55% saturation (FtsY-197, and FtsY-204) or a 55-65% saturation (FtsY Δ N1) (NH₄)₂SO₄ cut was taken. Protein was resuspended and desalted to 75 mM NaCl, 50 mM Tris pH 8, 2 mM DTT. Desalted protein was applied to a MonoQ column, washed, and eluted to 350 mM NaCl over 6 column volumes. Peak fractions were applied to a hydroxyapatite column equilibrated with 200 mM KCl, 50 mM Tris pH 8, 2 mM DTT, washed, and eluted over 3 column volumes to 200 mM potassium phosphate pH 8, 200 mM KCl, 2 mM DTT. Peak fractions were pooled and applied to a Superdex 200 gel filtration column equilibrated in 50 mM Tris pH 8, 200 mM NaCl, 2 mM DTT, 5% (v/v) glycerol. Peak fractions were pooled and stored at -80°C. In all cases proteins were purified to >95% purity.

Fluorescence Binding Assays. Fluorescence binding assays were performed as described³. In all cases, assays were performed at 23°C in 50 mM HEPES, pH 7.5, 150 mM potassium acetate, 2 mM magnesium acetate, 0.01% (w/v) Nikkol detergent, 2 mM DTT, 100 μ M GppNHp. Data were collected on a stopped flow fluorimeter for fast association rates (KinTek) or a SLM 8100 fluorimeter for slow association with excitation wavelength of 290 nm and emission wavelength of 340 nm. For on-rates, data were fit to a single exponential function, and observed rate constants were plotted as a function of concentration. Rate constants were calculated using the equation

$$k_{\text{obs}} = k_{\text{on}}[\text{Ffh}] + k_{\text{off}}$$

Off-rates were calculated by pre-forming complexes of 2 μM of each Ffh (\pm 4.5S RNA) and FtsY with 100 μM GppNHp and then trapping dissociated complexes by mixing with 4 mM GDP-Mg²⁺. Curves were fit to a single exponential function.

GTP-hydrolysis driven dissociation was measured in a similar manner to off rate measurements using a pulse chase experiment. Complexes were formed in the presence of GTP and were then rapidly mixed with 4 mM GDP-Mg²⁺. We observed dissociation of the ^{GTP}Ffh•FtsY^{GTP} by monitoring the decrease in tryptophan fluorescence as the complex dissociates.

GTPase Assays. Assays were performed as described³ with slight modifications. To calculate the basal GTPase activities, trace amounts of γ ³²P-GTP were added to varying concentrations of protein, and reactions were followed to completion. The data were fit to a single exponential equation to calculate the k_{obs} . Observed rate constants were plotted as a function of concentration of protein and fit to the equation $k_{\text{obs}} = k_{\text{cat}}[\text{protein}]/(K_{\text{M}} + [\text{protein}])$. To ensure that changes in basal GTP hydrolysis were not due to contaminating GTPases, we compared the K_{M} for the GTP hydrolysis reaction to the inhibition constant (K_{i}) calculated by inhibiting the reaction with GppNHp. In all cases, the K_{i} was measured to be within two-fold of the K_{M} (data not shown).

NMR. Proteins for NMR were purified as described above with several modifications. Proteins were expressed in M9 minimal media made with D₂O. Thirty minutes prior to induction of protein expression, γ -¹³C labeled α -ketoacid precursors to isoleucine, leucine

and valine were added^{41, 42}. All data were collected on either a 600 Mhz Varian Inova spectrometer or an 800 Mhz Bruker Avance spectrometer outfitted with cryogenic probes. ¹³C gradient enhanced HSQC experiments were performed in 20 mM NaPO₄ pH 7, 250 mM NaCl, 2 mM DTT, and 2 mM MgCl₂. Spectra of FtsYΔN1 were taken with 300 μM protein with or without 2 mM GppNHp-Mg²⁺. Spectra of FtsY-204 were taken with 800 μM protein with or without 2 mM GppNHp-Mg²⁺ and equimolar Ffh.

Partial proteolysis and N-terminal sequencing. For partial proteolysis assays, 1 μM FtsY variants and 1.5 μM Ffh•4.5S RNA were assembled in assay buffer with 100 μM GppNHp or GDP for 10 minutes at 25°C. Proteinase K was added to 2 ng μl⁻¹ and the reaction was stopped at the appropriate time by adding the sample to a final concentration of 5% (w/v) ice-cold TCA. Samples were precipitated, washed with ice-cold acetone, resolved by SDS-PAGE, transferred to PVDF membranes, and detected by Western blot using polyclonal antibody against FtsY. N-terminal sequencing was obtained from the Stanford PAN facility.

Author contributions:

S.B.N. and N.B. prepared reagents and performed Ffh-FtsY association and dissociation assays. N.B. carried out GTPase experiments. N.B., S.N.F. and J.D.G. designed, executed, and interpreted the NMR experiments. S.B.N. performed partial proteolysis assays. S.B.N, N.B, and P.W. wrote the article.

Acknowledgements:

The authors would like to thank Christine Guthrie, Pascal Egea, and members of the Walter Lab for insightful comments and careful reading of the manuscript. This work was supported by grants to P.W. from the National Institutes of Health and the Howard Hughes Medical Institute. The Jane Coffin Childs Memorial Fund supports S.B.N. N.B was supported by a predoctoral fellowship from the National Science Foundation.

References:

1. Egea, P. F., Stroud, R. M. & Walter, P. Targeting proteins to membranes: structure of the signal recognition particle. *Curr Opin Struct Biol* 15, 213-20 (2005).
2. Keenan, R. J., Freymann, D. M., Stroud, R. M. & Walter, P. The signal recognition particle. *Annu Rev Biochem* 70, 755-75 (2001).
3. Peluso, P., Shan, S. O., Nock, S., Herschlag, D. & Walter, P. Role of SRP RNA in the GTPase cycles of Ffh and FtsY. *Biochemistry* 40, 15224-33 (2001).
4. Miller, J. D., Wilhelm, H., Gierasch, L., Gilmore, R. & Walter, P. GTP binding and hydrolysis by the signal recognition particle during initiation of protein translocation. *Nature* 366, 351-4 (1993).
5. Poritz, M. A. et al. An *E. coli* ribonucleoprotein containing 4.5S RNA resembles mammalian signal recognition particle. *Science* 250, 1111-7 (1990).
6. Miller, J. D., Bernstein, H. D. & Walter, P. Interaction of *E. coli* Ffh/4.5S ribonucleoprotein and FtsY mimics that of mammalian signal recognition particle and its receptor. *Nature* 367, 657-9 (1994).
7. Phillips, G. J. & Silhavy, T. J. The *E. coli* *ffh* gene is necessary for viability and efficient protein export. *Nature* 359, 744-6 (1992).
8. Eitan, A. & Bibi, E. The core *Escherichia coli* signal recognition particle receptor contains only the N and G domains of FtsY. *J Bacteriol* 186, 2492-4 (2004).
9. Bernstein, H. D., Zopf, D., Freymann, D. M. & Walter, P. Functional substitution of the signal recognition particle 54-kDa subunit by its *Escherichia coli* homolog. *Proc Natl Acad Sci U S A* 90, 5229-33 (1993).
10. Powers, T. & Walter, P. Co-translational protein targeting catalyzed by the *Escherichia coli* signal recognition particle and its receptor. *Embo J* 16, 4880-6 (1997).
11. Montoya, G., Svensson, C., Lührink, J. & Sinning, I. Crystal structure of the NG domain from the signal-recognition particle receptor FtsY. *Nature* 385, 365-8 (1997).
12. Freymann, D. M., Keenan, R. J., Stroud, R. M. & Walter, P. Structure of the conserved GTPase domain of the signal recognition particle. *Nature* 385, 361-4 (1997).
13. Focia, P. J., Shepotinovskaya, I. V., Seidler, J. A. & Freymann, D. M. Heterodimeric GTPase core of the SRP targeting complex. *Science* 303, 373-7 (2004).
14. Egea, P. F. et al. Substrate twinning activates the signal recognition particle and its receptor. *Nature* 427, 215-21 (2004).
15. Batey, R. T., Rambo, R. P., Lucast, L., Rha, B. & Doudna, J. A. Crystal structure of the ribonucleoprotein core of the signal recognition particle. *Science* 287, 1232-9 (2000).
16. Keenan, R. J., Freymann, D. M., Walter, P. & Stroud, R. M. Crystal structure of the signal sequence binding subunit of the signal recognition particle. *Cell* 94, 181-91 (1998).

17. Zopf, D., Bernstein, H. D., Johnson, A. E. & Walter, P. The methionine-rich domain of the 54 kd protein subunit of the signal recognition particle contains an RNA binding site and can be crosslinked to a signal sequence. *Embo J* 9, 4511-7 (1990).
18. de Leeuw, E. et al. Membrane association of FtsY, the E. coli SRP receptor. *FEBS Lett* 416, 225-9 (1997).
19. Angelini, S., Boy, D., Schiltz, E. & Koch, H. G. Membrane binding of the bacterial signal recognition particle receptor involves two distinct binding sites. *J Cell Biol* 174, 715-24 (2006).
20. Regalia, M., Rosenblad, M. A. & Samuelsson, T. Prediction of signal recognition particle RNA genes. *Nucleic Acids Res* 30, 3368-77 (2002).
21. Rosenblad, M. A. & Samuelsson, T. Identification of chloroplast signal recognition particle RNA genes. *Plant Cell Physiol* 45, 1633-9 (2004).
22. Brown, S. & Fournier, M. J. The 4.5 S RNA gene of Escherichia coli is essential for cell growth. *J Mol Biol* 178, 533-50 (1984).
23. Peluso, P. et al. Role of 4.5S RNA in assembly of the bacterial signal recognition particle with its receptor. *Science* 288, 1640-3 (2000).
24. Bradshaw, N. & Walter, P. The signal recognition particle (SRP) RNA links conformational changes in the SRP to protein targeting. *Mol Biol Cell* 18, 2728-34 (2007).
25. Reyes, C. L., Rutenber, E., Walter, P. & Stroud, R. M. X-ray structures of the signal recognition particle receptor reveal targeting cycle intermediates. *PLoS ONE* 2, e607 (2007).
26. Gawronski-Salerno, J. & Freymann, D. M. Structure of the GMPPNP-stabilized NG domain complex of the SRP GTPases Ffh and FtsY. *J Struct Biol* (2006).
27. Focia, P. J., Gawronski-Salerno, J., Coon, J. S. t. & Freymann, D. M. Structure of a GDP:Alf4 complex of the SRP GTPases Ffh and FtsY, and identification of a peripheral nucleotide interaction site. *J Mol Biol* 360, 631-43 (2006).
28. Shepotinovskaya, I. V. & Freymann, D. M. Conformational change of the N-domain on formation of the complex between the GTPase domains of Thermus aquaticus Ffh and FtsY. *Biochim Biophys Acta* 1597, 107-14 (2002).
29. Chandrasekar, S., Chartron, J., Jaru-Ampornpan, P. & Shan, S. O. Structure of the chloroplast signal recognition particle (SRP) receptor: domain arrangement modulates SRP-receptor interaction. *J Mol Biol* 375, 425-36 (2008).
30. Jagath, J. R., Rodnina, M. V. & Wintermeyer, W. Conformational changes in the bacterial SRP receptor FtsY upon binding of guanine nucleotides and SRP. *J Mol Biol* 295, 745-53 (2000).
31. Schmitz, U. et al. NMR studies of the most conserved RNA domain of the mammalian signal recognition particle (SRP). *Rna* 2, 1213-27 (1996).
32. Shan, S. O. & Walter, P. Molecular crosstalk between the nucleotide specificity determinant of the SRP GTPase and the SRP receptor. *Biochemistry* 44, 6214-22 (2005).
33. Sprangers, R. & Kay, L. E. Quantitative dynamics and binding studies of the 20S proteasome by NMR. *Nature* 445, 618-22 (2007).

34. Gawronski-Salerno, J., Coon, J. S. t., Focia, P. J. & Freymann, D. M. X-ray structure of the *T. aquaticus* FtsY:GDP complex suggests functional roles for the C-terminal helix of the SRP GTPases. *Proteins* 66, 984-95 (2007).
35. Gariani, T., Samuelsson, T. & Sauer-Eriksson, A. E. Conformational variability of the GTPase domain of the signal recognition particle receptor FtsY. *J Struct Biol* 153, 85-96 (2006).
36. Shan, S. O., Stroud, R. M. & Walter, P. Mechanism of association and reciprocal activation of two GTPases. *PLoS Biol* 2, e320 (2004).
37. Lu, Y. et al. Evidence for a novel GTPase priming step in the SRP protein targeting pathway. *Embo J* 20, 6724-34 (2001).
38. Chu, F. et al. Unraveling the interface of signal recognition particle and its receptor by using chemical cross-linking and tandem mass spectrometry. *Proc Natl Acad Sci U S A* 101, 16454-9 (2004).
39. Parlitz, R. et al. *Escherichia coli* signal recognition particle receptor FtsY contains an essential and autonomous membrane-binding amphipathic helix. *J Biol Chem* 282, 32176-84 (2007).
40. Bahari, L. et al. Membrane targeting of ribosomes and their release require distinct and separable functions of FtsY. *J Biol Chem* 282, 32168-75 (2007).
41. Gross, J. D., Gelev, V. M. & Wagner, G. A sensitive and robust method for obtaining intermolecular NOEs between side chains in large protein complexes. *J Biomol NMR* 25, 235-42 (2003).
42. Goto, N. K., Gardner, K. H., Mueller, G. A., Willis, R. C. & Kay, L. E. A robust and cost-effective method for the production of Val, Leu, Ile (δ 1) methyl-protonated ^{15}N -, ^{13}C -, ^2H -labeled proteins. *J Biomol NMR* 13, 369-74 (1999).

Table 1.

		$k_{on} (M^{-1}s^{-1})$		$k_{off} (10^6 s^{-1})$		$K_D (nM)$	
		-	+	-	+	-	+
4.5S RNA:							
FtsY:							
wt		104 ± 16	38800 ± 730	8.60 ± 0.16	2650 ± 150	82.7 ± 13	68.4 ± 4.2
wt	ΔN1	685 ± 93	40500 ± 2500	5.47 ± 0.14	605 ± 77	7.98 ± 1.1	14.9 ± 2.1
ΔN1	Wt	426 ± 66	435 ± 33	3.01 ± 0.15	6.14 ± 0.3	7.06 ± 1.1	14.1 ± 1.3
ΔN1	ΔN1	14900 ± 1100	19000 ± 4700	5.38 ± 0.16	12.2 ± 0.3	0.361 ± 0.028	0.639 ± 0.16

Figure 1 Structural and schematic representations of the FtsY and Ffh constructs used in this study. **(a)** Left is a ribbon representation of the crystal structure of *E. coli* FtsY (a subset (residues 204-495) of PDB ID 2QY9 are shown). FtsY Δ N1 begins at residue 221; residues up to 220 are colored red. Right is a ribbon representation of the crystal structure of *T. aquaticus* Ffh NG domain (residues 1-298 of PDB ID 2FFH) with amino acids 1-8, truncated in Ffh Δ N1, colored red. The G-domains are colored dark grey and the N-domains are light grey. The orientation of the individual proteins in relation to the structure is indicated. **(b)** Structure of the FtsY-Ffh complex (PDB ID 1OKK). **(c)** Domain map of FtsY and Ffh with positions of truncations indicated by arrows. The color scheme is the same as for part a and b.

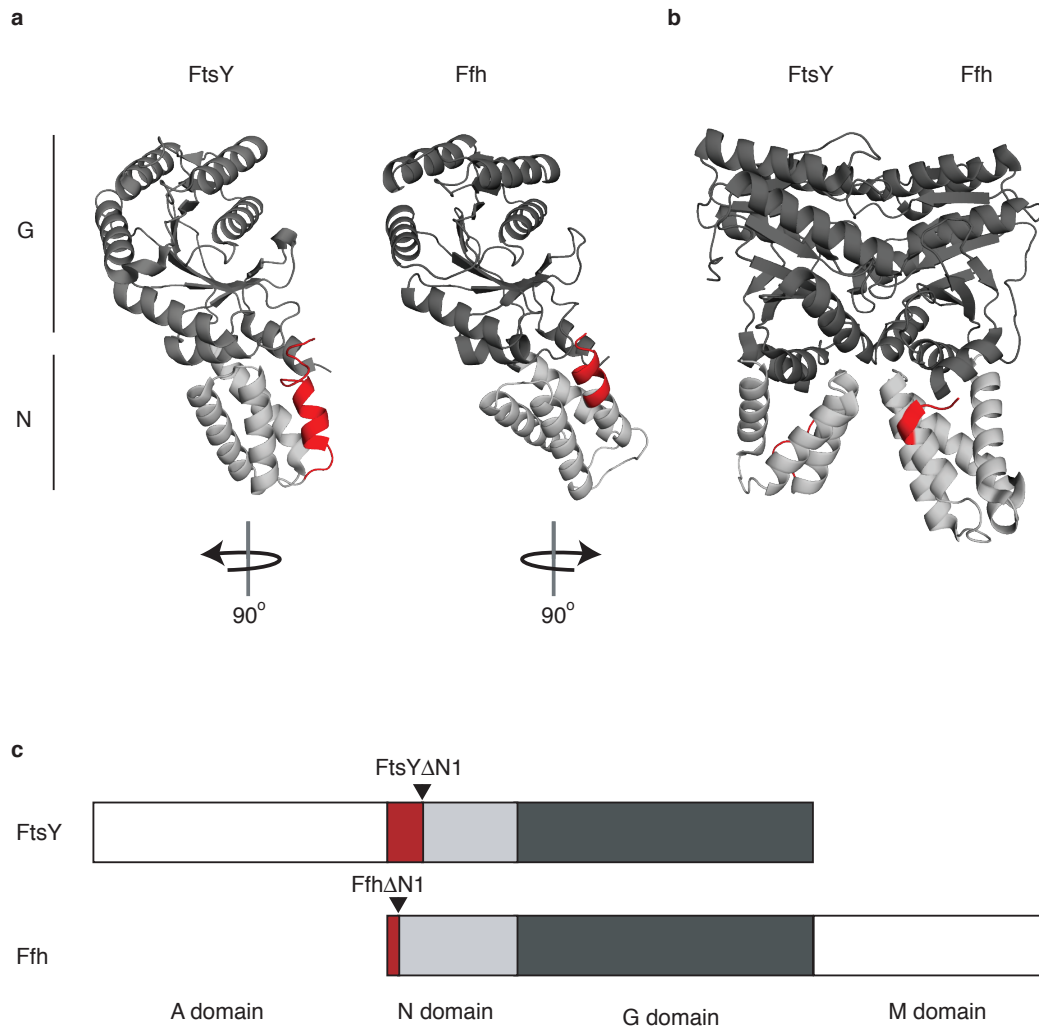


Figure 1 Chapter 3

Figure 2 Helix N1 is present in structures of uncomplexed FtsY. Alignment of FtsY structures from PDB files 1FTS, 2QY9, 1ZU4, 1ZU5, 2Q9C, 2Q9B, 2Q9A, 1VMA, 3B9Q, and 2OG2. Residues homologous to *E. coli* residues 204-221 of helix N1 are shown in red.

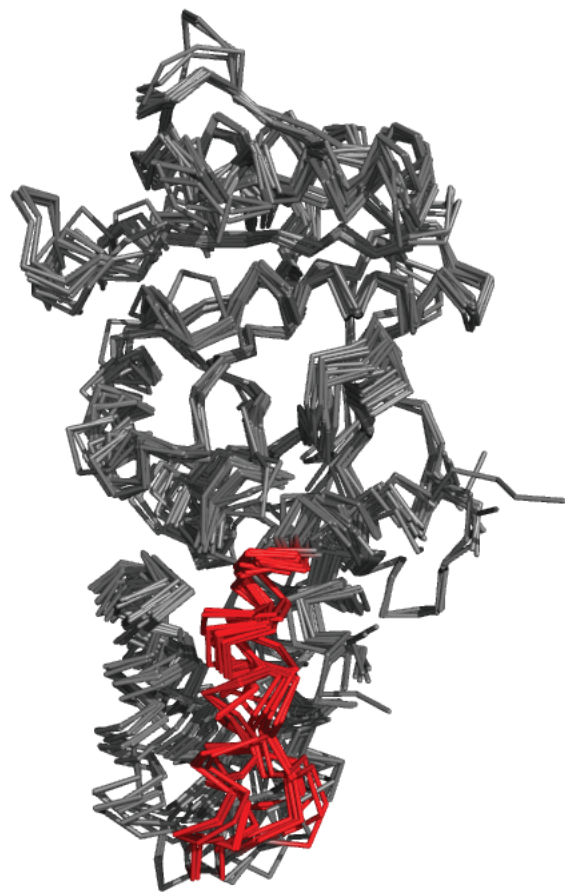


Figure 2 Chapter 3

Figure 3 Truncation of the entire Ffh helix N1 (amino acids 1-20) is functionally equivalent to truncation of the first 8 amino acids. Observed binding rates are plotted as a function of Ffh concentration for Ffh-21-FtsY –RNA (▼), Ffh Δ N1-FtsY –RNA (■) and Ffh-FtsY –RNA (◆). Lines are fits to the equation $k_{obs}=k_{on}[Ffh]+k_{off}$.

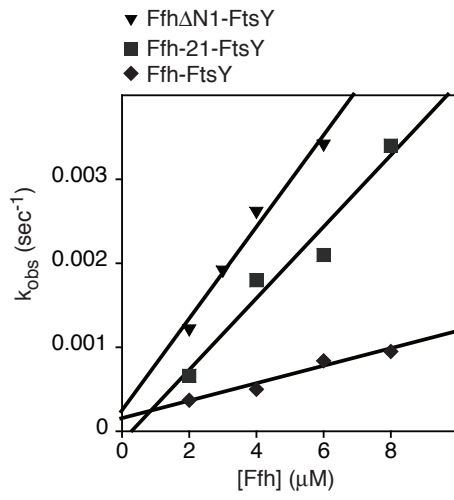


Figure 3 Chapter 3

Figure 4 The N-terminal helices of Ffh and FtsY inhibit Ffh-FtsY association in the absence of 4.5S RNA. **(a)** Truncation of helix N1 increases the rate of Ffh-FtsY association in the absence of 4.5S RNA. Observed binding rates are plotted as a function of Ffh concentration for Ffh-FtsY Δ N1 –RNA (●), Ffh Δ N1-FtsY –RNA (■) and Ffh-FtsY –RNA (◆). Lines are fits to the equation $k_{obs}=k_{on}[Ffh]+k_{off}$ in parts a, b, and c, and wild-type references are included in multiple figures for comparison. **(b)** The Ffh Δ N1-FtsY Δ N1 complex forms nearly as rapidly in the absence of 4.5S RNA as the Ffh-FtsY complex forms in the presence of 4.5S RNA. Observed binding rates are plotted as a function of Ffh concentration for Ffh-FtsY +RNA (◇), Ffh Δ N1-FtsY Δ N1 –RNA (▲), and Ffh-FtsY –RNA (◆). **(c)** Binding of Ffh Δ N1 and FtsY Δ N1 in the presence of 4.5S RNA. Observed binding rates are plotted as a function of Ffh concentration for Ffh-FtsY +RNA (◇), Ffh-FtsY Δ N1 +RNA (○), Ffh Δ N1-FtsY Δ N1 +RNA (△), and Ffh Δ N1-FtsY + RNA (□). **(d)** Summary of binding rates. On rates for each Ffh-FtsY pair are plotted in the presence and absence of 4.5S RNA. Note the log scale. Error bars represent the standard error of the linear fit to the equation $k_{obs}=k_{on}[Ffh]+k_{off}$.

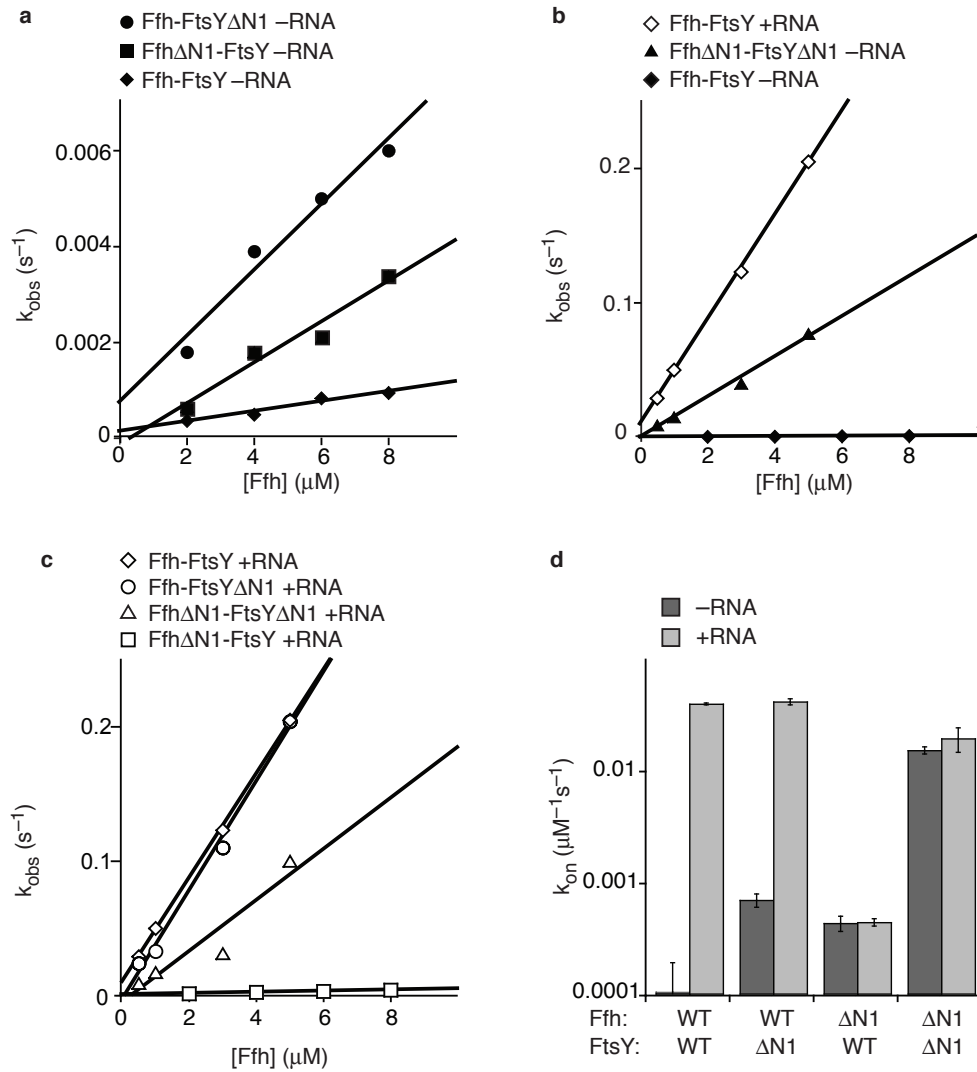


Figure 4 Chapter 3

Figure 5 The N-terminal helices of Ffh and FtsY stimulate Ffh-FtsY complex dissociation in the presence of 4.5S RNA. **(a)** Bar graphs representing the dissociation rate constants (k_{off}) for disassembly of the Ffh-FtsY complex $-$ RNA (dark grey) and $+$ RNA (light grey). The k_{offs} were measured by forming complexes in the presence of GppNHp and trapping dissociated proteins with GDP. Data were fit to a single exponential equation, and error bars represent the standard error of the fit. **(b)** Plot of equilibrium dissociation constants, \pm RNA. K_D values were calculated by the equation $K_D = k_{off}/k_{on}$. Note the log scale axes.

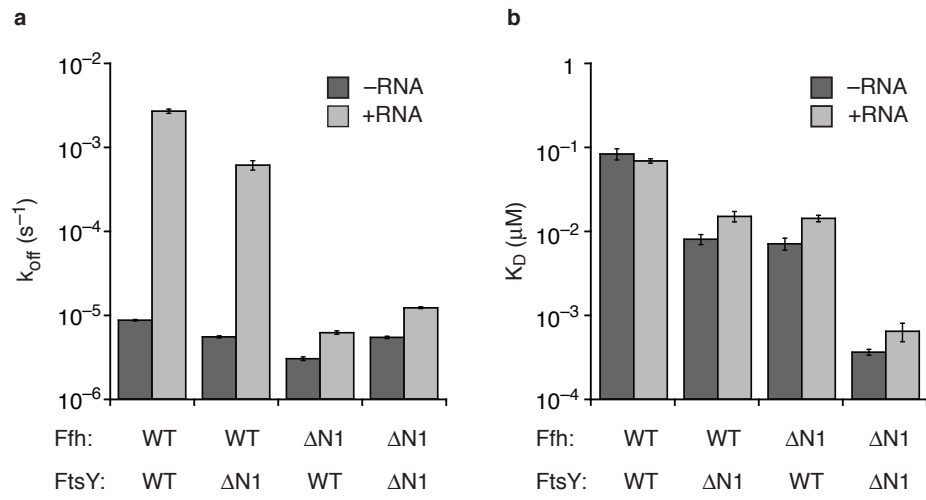


Figure 5 Chapter 3

Figure 6 The N-terminal helix of FtsY represses its basal GTPase activity. **(a)** Plot of observed rates from single turnover GTPase assays measuring GTP hydrolysis rate as a function of FtsY (◆) or FtsYΔN1 (●) concentration. A fit of the data to the equation $k_{\text{obs}}=k_{\text{cat}}[\text{FtsY}]/(K_m+[\text{FtsY}])$ gave k_{cat} of $0.00979\pm 0.0028 \text{ min}^{-1}$ for FtsY and $0.662\pm 0.24 \text{ min}^{-1}$ for FtsYΔN1. **(b)** Single turnover GTPase assays were performed for Ffh (◆) or FfhΔN1 (■) as a function of increasing concentrations of Ffh. A fit of the data to the equation $k_{\text{obs}}=k_{\text{cat}}[\text{Ffh}]/(K_M+[\text{Ffh}])$ gave k_{cat} of $0.0876\pm 0.012 \text{ min}^{-1}$ for Ffh and $0.305\pm 0.031 \text{ min}^{-1}$ for FfhΔN1. **(c)** Plot of stimulated GTP hydrolysis rates for Ffh-FtsY complexes +RNA (light grey bars) or -RNA (dark grey bars). Rates were measured as pulse chase experiments as described in the methods. Error bars are standard errors of the fit to a single exponential equation.

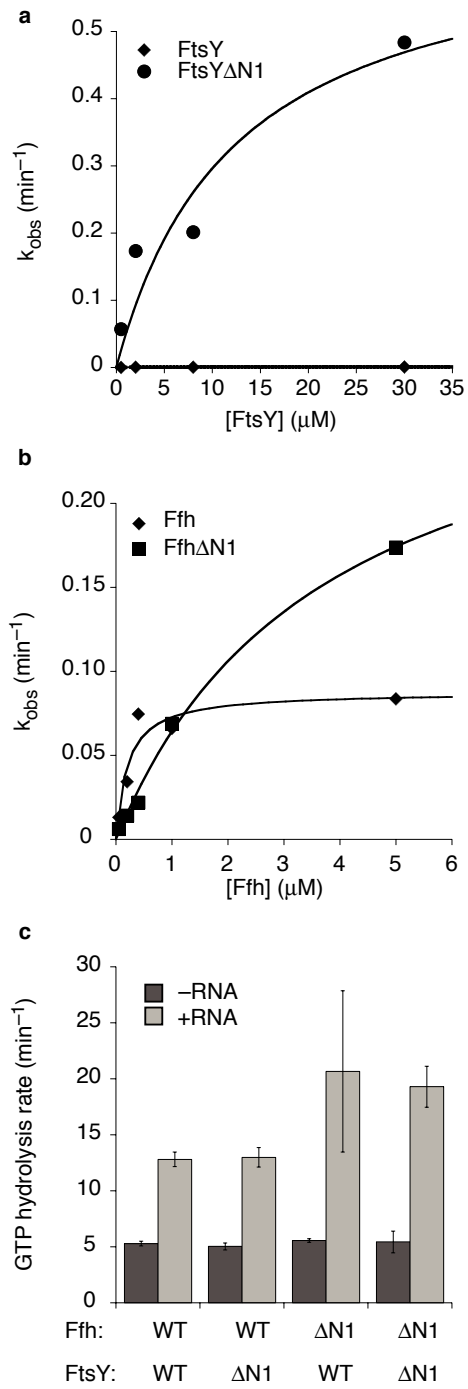


Figure 6 Chapter 3

Figure 7 NMR analysis of FtsY-204 and FtsY Δ N1. **A.** Observed binding rates are plotted as a function of Ffh concentration for Ffh-FtsY –RNA (\blacklozenge), Ffh-FtsY-204 –RNA (\blacktimes), and Ffh-FtsY Δ N1 –RNA (\bullet). Lines are fits to the equation $k_{\text{obs}}=k_{\text{on}}[\text{Ffh}]+k_{\text{off}}$. **B.** Plot of observed rates from single turnover GTPase assays measuring GTP hydrolysis rate as a function of FtsY Δ N1 (\bullet), FtsY-204 (\blacktimes), or FtsY (\blacklozenge) concentration. Lines are fits to the equation $k_{\text{obs}}=k_{\text{cat}}[\text{FtsY}]/(K_{\text{M}}+[\text{FtsY}])$. **C.** 2D CHSQC spectrum for FtsY Δ N1 (red) is overlaid on the spectrum of FtsY-204 (blue).

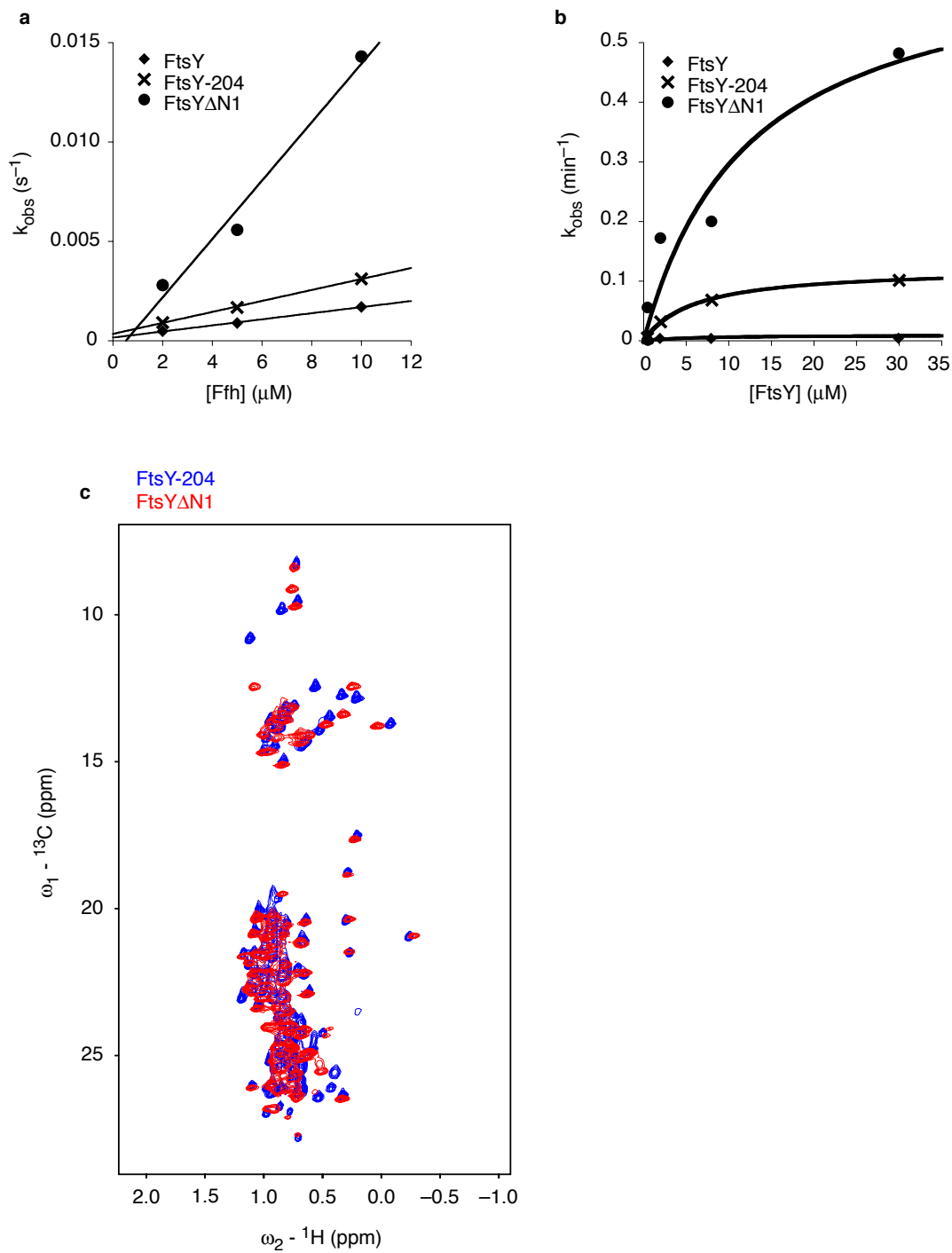


Figure 7 Chapter 3

Figure 8 FtsY Δ N1 but not FtsY-204 undergoes a GppNHp dependent conformational change. **A.** 2D CHSQC spectrum for FtsY-204+GppNHp (red) is overlaid on the spectrum of FtsY-204 (blue). A peak that broadens in the FtsY-204 spectrum +GppNHp is marked with an arrow. **B.** 2D CHSQC spectrum for FtsY Δ N1+GppNHp (red) is overlaid on the spectrum of FtsY- Δ N1 (blue). **C.** The affinity of GppNHp for FtsY Δ N1 and FtsY-204 was measured by GTPase inhibition assays. Relative rates of GTP hydrolysis are plotted as a function of concentration of GppNHp. Lines are fits to the equation $k_{rel} = K_i / (K_i + [GppNHp])$ **D.** A region of the 2D CHSQC spectrum containing the peak marked in A is magnified with decreased contour cutoff.

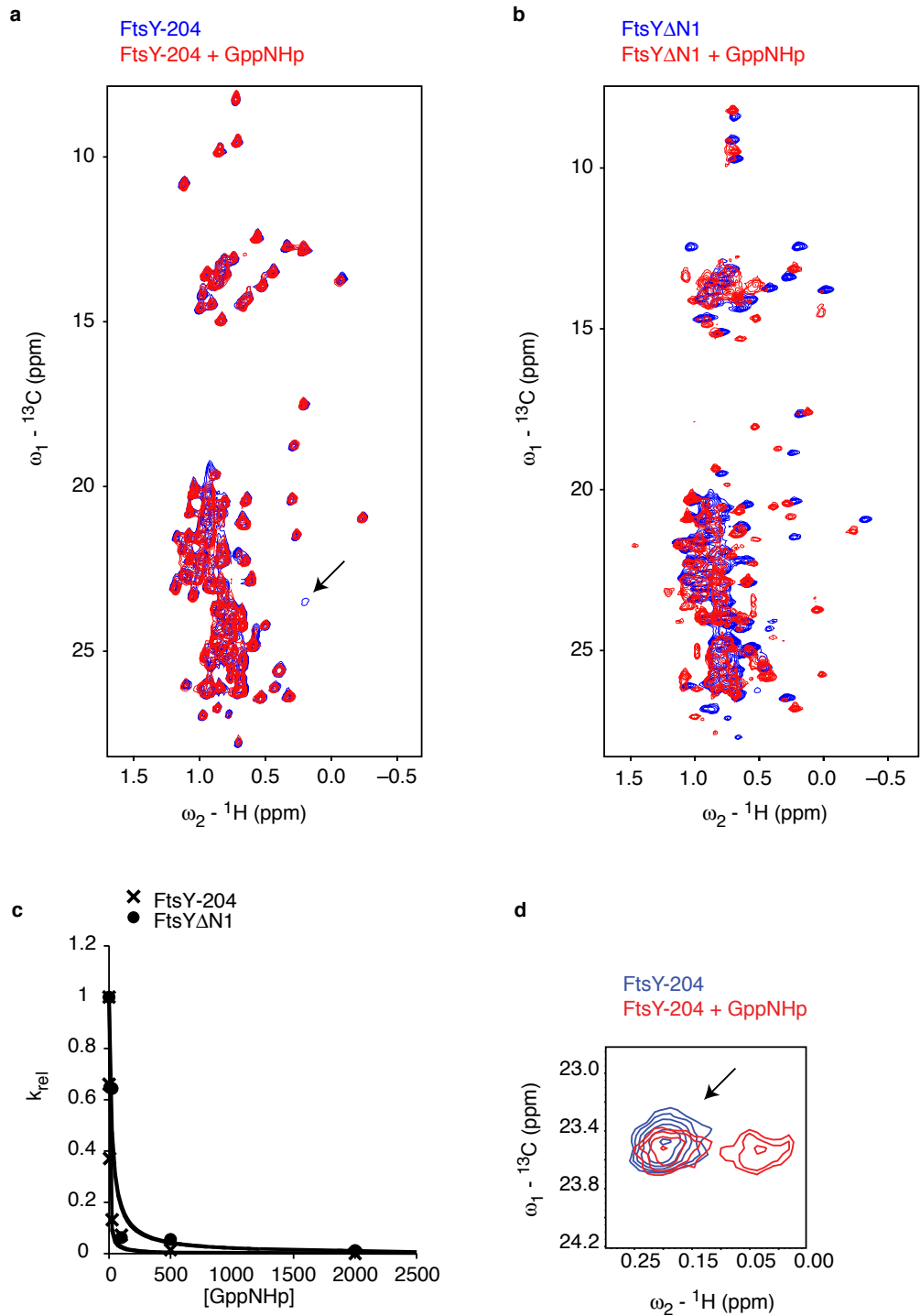


Figure 8 Chapter 3

Figure 9 FtsY Δ N1 assumes an `Ffh bound` conformation in the presence of GppNHp. NMR spectra of ^{13}C ILV labeled FtsY-204 and FtsY Δ N1 are overlaid. FtsY Δ N1+GppNHp is shown in both panels in red as a reference. FtsY-204 +GppNHp (**a**) and FtsY-204 + GppNHp + Ffh (**b**) is shown in blue. Inset panels are magnifications of a region of the spectra shown above. Notice that several peaks that are unmatched in a have partners in b (a subset of these peaks from a particularly well resolved region of the spectrum are marked with arrows).

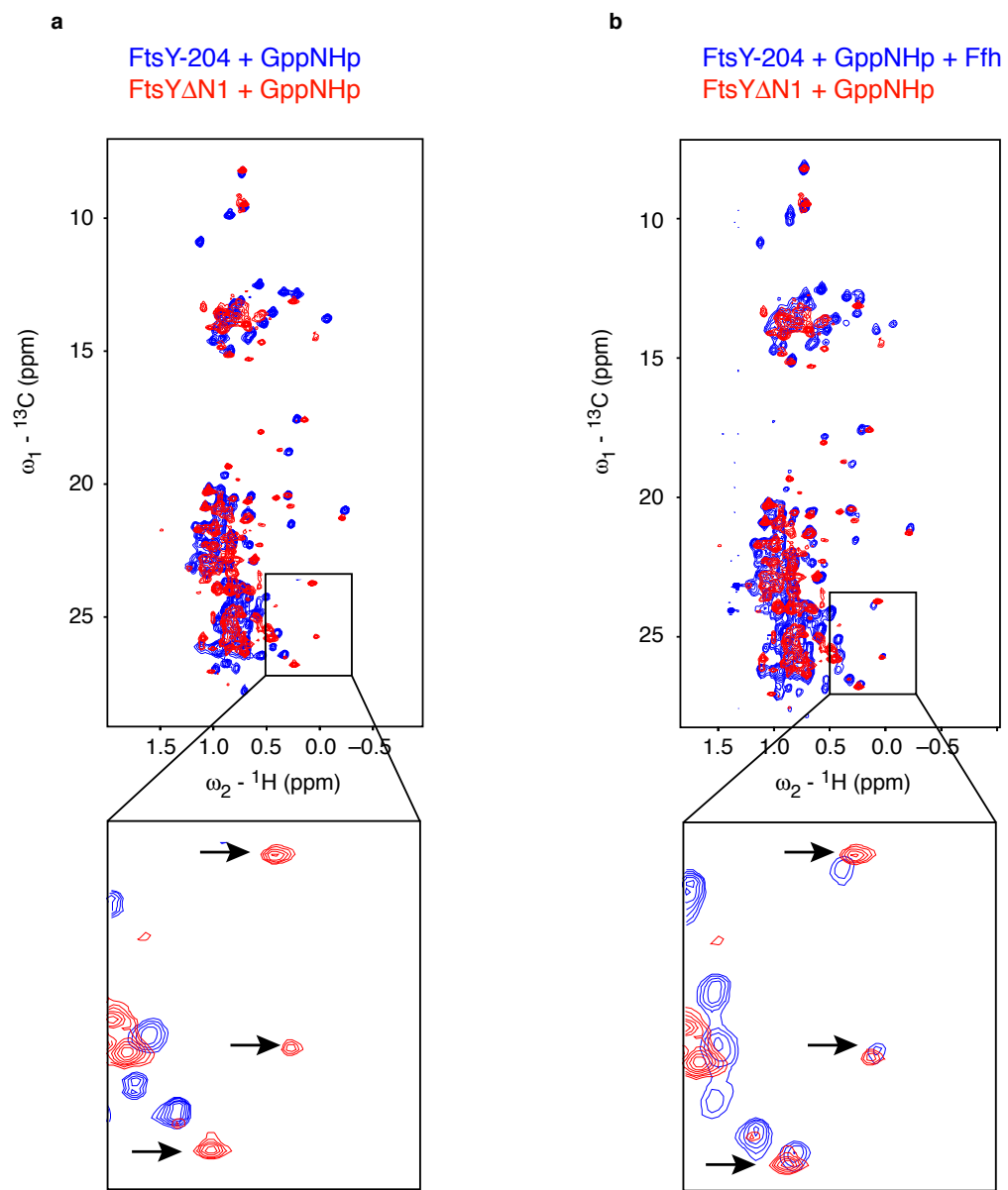


Figure 9 Chapter 3

Figure 10 Binding of Ffh to FtsY exposes the N-terminal helix of FtsY. **(a)** Western blot showing limited proteolysis of FtsY either alone or in complex with SRP (Ffh+4.5S RNA). A low molecular weight band marked with an arrow appears specifically when SRP is bound. **(b)** Western blots showing fine mapping of the location of the cleavage site in FtsY. Truncation variants of FtsY were subjected to limited proteolysis in the presence of SRP with either GppNHp (allowing complex formation) or GDP (preventing complex formation). The low molecular weight band is marked with an arrow. **(c)** Proteolysis of FtsY takes place between residues S116 and L117. The sequence of the N-terminal helix of the FtsY NG domain is shown with an arrow marking the cleavage site as determined by N-terminal sequencing.

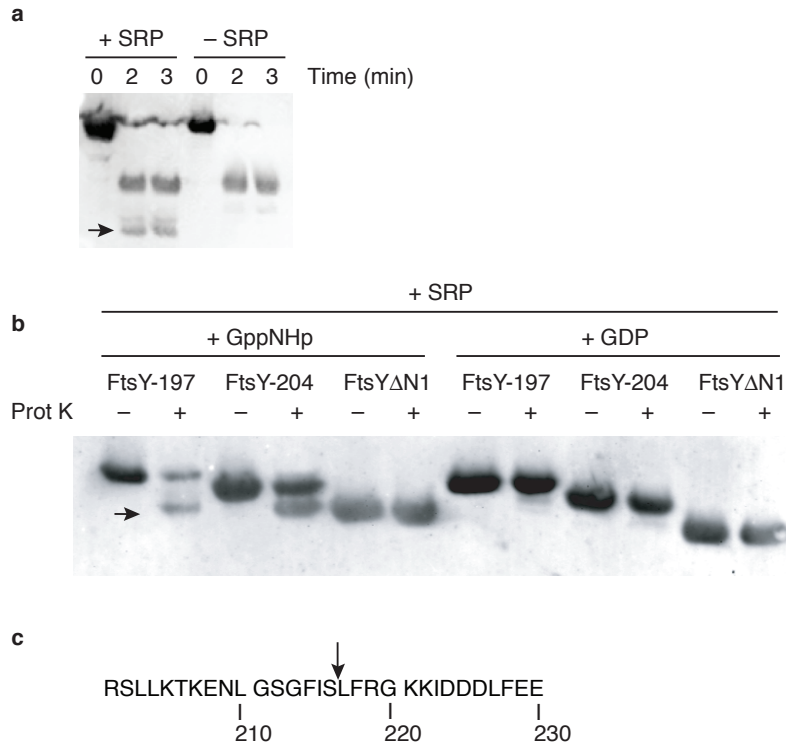


Figure 10 Chapter 3

Figure 11 Model for Ffh-FtsY structural rearrangement upon complex formation. **(a)** Ribbon representations of FtsY and Ffh in unbound form (PDB ID 2QY9 and 2FFH, respectively). Helix N1 of both proteins is shown in red. Note that in the unbound form, residue K453 of FtsY and residue R255 of Ffh (both displayed in stick form in red) protrude into the dimerization interface, conceptually represented by a dashed line. **(b)** Ribbon representation of the Ffh•FtsY complex (PDB ID 1OKK). In the bound form, K453 of FtsY and R255 of Ffh move away from the interface, into the space formerly occupied by helix N1.

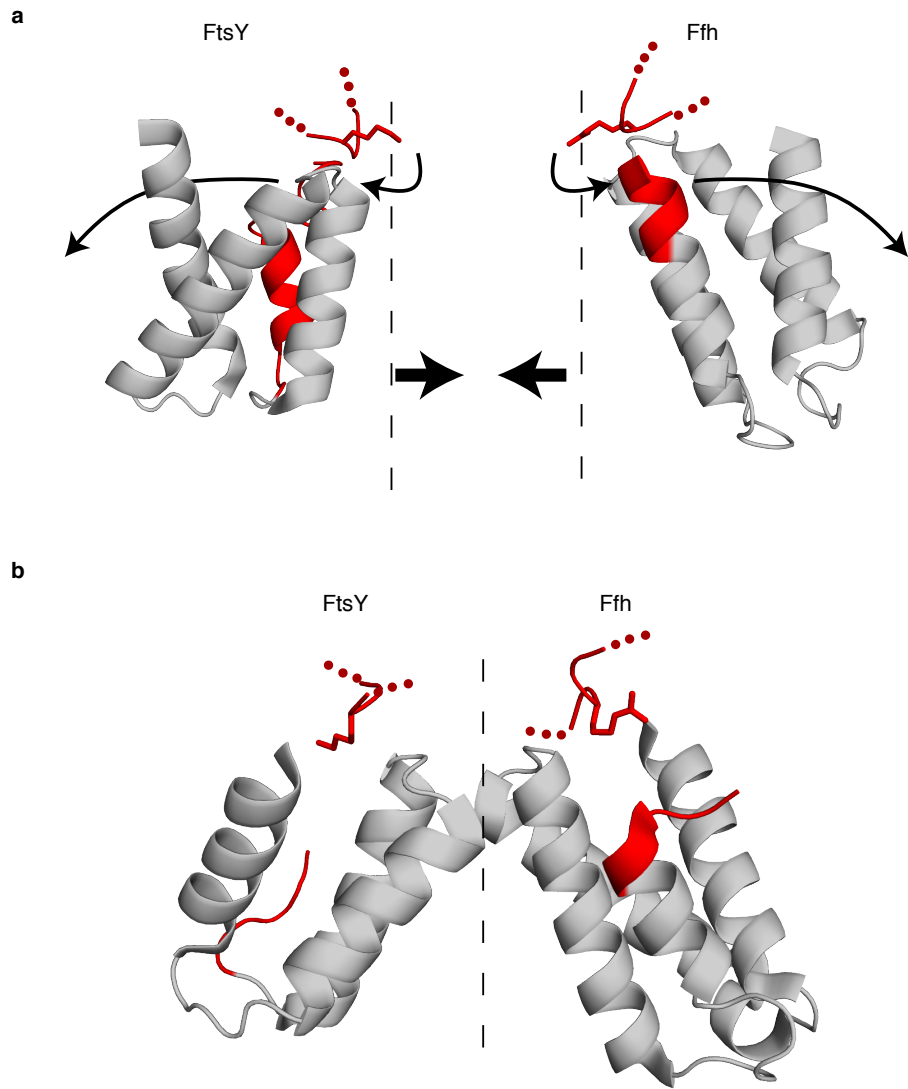


Figure 11 Chapter 3

Figure 12 Thermodynamic model describing the mechanism of SRP RNA control of the interaction of the SRP and SR. Free energy diagrams for interaction of Ffh and FtsY wild type and N-terminal truncation variants with and without 4.5S RNA. The free energy of activation is calculated from the observed association and dissociation rate constants (k) using the equation $\Delta G^\ddagger = -RT \ln(hk/k_B T)$ where h is Planck's constant, k_B is the Boltzmann constant, T is the absolute temperature and R is the universal gas constant. For forward reactions, a standard state of 1 μM was used to calculate free energy changes. Cartoons depict Ffh and FtsY with circles representing the GTPase domain and lines representing the N-terminal four-helix bundle. Helices N1 are colored red. Ffh additionally is shown with the M-domain and the 4.5S RNA (hairpin). 4.5S RNA is shown interacting with helix N1 of Ffh and FtsY in the transition state complex in a manner that is dependent on helix N1 of Ffh.

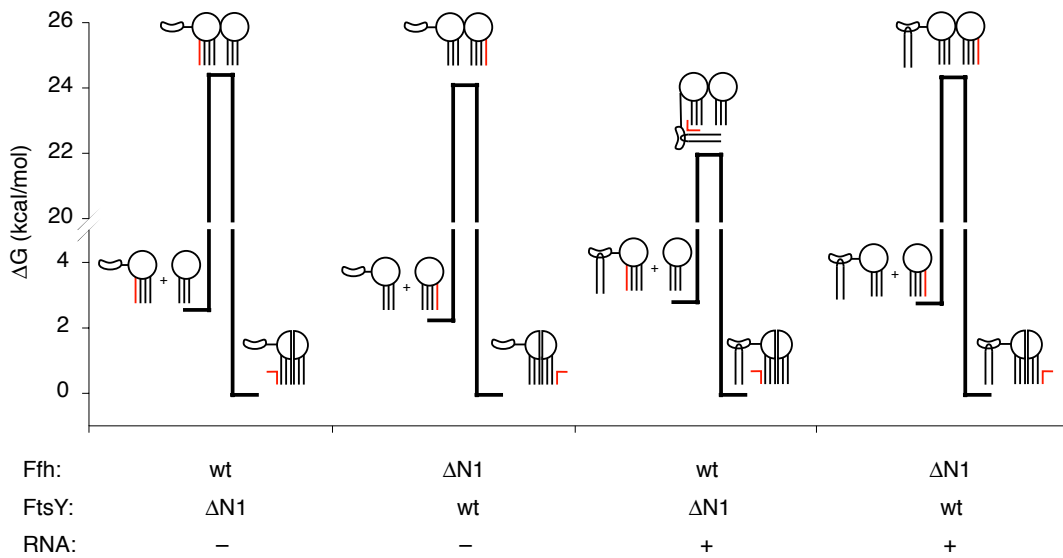
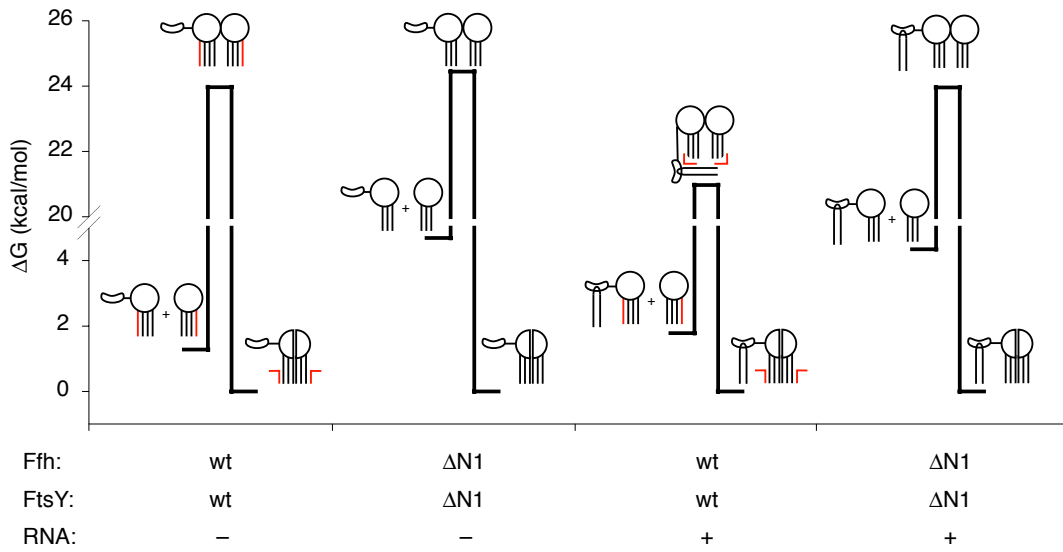


Figure 12 Chapter 3

Epilogue:

This section presents my perspective on several unresolved questions about the mechanism of cotranslational protein targeting. I will begin by revisiting the three questions posed in the introduction (What is the role of the SRP RNA in protein targeting? How does SRP RNA catalyze the SRP-SR interaction? How is the energy of GTP hydrolysis by SRP and SR coupled to productive targeting?), and conclude with several additional questions that future studies will hopefully answer.

What is the role of the SRP RNA in protein targeting?

The work presented in Chapter 2 demonstrated that SRP RNA coordinates the recruitment of a signal peptide by SRP with SRP binding to SR. This provides an attractive explanation for the role of SRP RNA in protein targeting, however it is almost certainly not the only role played by SRP RNA. This is underscored by the fact that it still remains a mystery why an RNA molecule (as opposed to a protein) is required for cotranslational targeting. Understanding what else SRP RNA does remains one of the most fascinating questions about the mechanism of protein targeting.

SRP RNA stimulates the GTPase activity of the SRP-SR complex in addition to accelerating SRP-SR association¹. The role of GTPase stimulation is unknown, but is most likely important. We made several additional findings that may help to elaborate the role of this stimulation of GTP hydrolysis. In contrast to SRP RNA catalysis of the SRP-SR interaction, SRP RNA stimulation of the GTPase activity of the SRP-SR complex does not require SRP RNA binding to a signal peptide (chapter 2) or SRP helix

N1 (chapter 3). However, mutation of the tetraloop of SRP RNA and some mutations in the M-domain and linker of SRP affect both SRP RNA catalysis and stimulation of GTPase activity (chapter 1, unpublished observations). Mutation of L301P of *E. coli* Ffh specifically blocks stimulation of GTP hydrolysis by SRP RNA and also produces a targeting defect in vivo. This mutant form of Ffh would therefore be a very useful tool for trying to understand the role of GTPase stimulation by SRP RNA. Determining the timing of GTP hydrolysis by the SRP-SR complex in the context of a complete targeting reaction with ribosomes and translocons will be key to understanding the role of GTPase stimulation by SRP RNA.

The structure of SRP RNA in complex with the M-domain revealed that SRP RNA forms a continuous surface with the signal sequence binding pocket. It was therefore postulated that SRP RNA might play a role in signal sequence recognition. Using fluorescence anisotropy we showed that for the Δ EspP signal peptide, SRP RNA dramatically enhances the affinity of peptide binding. Interestingly, detergent competed for binding of Δ EspP only in the presence but not absence of SRP RNA, suggesting that the binding mode of the peptide might significantly depend on the presence of SRP RNA. Similarly, the affinity of SRP for Δ EspP was decreased by truncation of the C-terminal helix of the M-domain in the presence of SRP RNA but not in its absence (data not shown). It is not clear how general this role of SRP RNA is and if direct contacts between SRP RNA and the signal peptide are required for stimulation of SRP-SR complex formation.

SRP RNA also affects SRP binding to the ribosome, however the significance of this is unexplored. The affinity of Ffh binding to non-translating ribosomes measured by

FRET is decreased by the presence of SRP RNA (Appendix C). Furthermore, the conformation of SRP on the ribosome is different in the presence and absence of SRP RNA². Future studies characterizing the binding of SRP to translating ribosomes in more detail will be required to determine the significance of these effects. Direct interaction between SRP RNA and ribosomal RNA would also provide an explanation for why SRP requires an RNA subunit.

How does SRP RNA catalyze the SRP-SR interaction?

Although we now understand the structural changes that must occur for SRP and SR to bind, we are far from a mechanistic understanding of how SRP RNA catalyzes SRP-SR binding.

At the time we began this work there were several hypotheses for how SRP RNA might catalyze the SRP-SR interaction. First, based on solution FRET studies it was proposed that the signal sequence binding domain of SRP occludes the binding site on SRP for SR in the absence of SRP RNA³. Second, SRP RNA might induce a conformational change in the GTPase domain of SRP that lowers the energy barrier to its interaction with SR, while not affecting the conformation of SRP in the complex with SR. Third, SRP RNA might tether SRP and SR to each other in a transient, low affinity complex that would increase the rate of their interaction.

In chapter 1, we showed that truncation of the signal sequence binding domain of SRP had no effect on the rate of SRP-SR binding, ruling out the model that the signal sequence binding domain inhibits binding in the absence of SRP RNA. To the contrary,

we found that residues in the signal sequence binding domain and linker are required for SRP RNA activity.

Our results presented in chapter 3, show that the substantial energy barrier to complex formation is due to autoinhibition of binding by the N-terminal helices of SRP and SR and that this autoinhibition is relieved by SRP RNA. One of the most surprising features of this result was helices of both SRP and SR inhibited binding, and that therefore SRP RNA must act on an encounter complex where SRP and SR are in contact. This finding was supported by FRET experiments⁴ (unpublished data). This led us to propose a combined model, where SRP RNA facilitates complex formation by displacing the N-terminal helices of SRP and SR in the encounter complex. Thus, determining how SRP RNA moves the N-terminal helices of SRP and SR and how the encounter complex forms, is central to understanding the mechanism of SRP RNA catalysis.

How is the energy of GTP hydrolysis by SRP and SR coupled to productive targeting?

Our results presented in chapter 2 demonstrated that the binding of SRP and SR, and therefore their hydrolysis of GTP is kinetically prohibited unless SRP is bound to a signal sequence. This provides a concrete explanation for why SRP and SR do not engage in futile cycles of binding and GTP hydrolysis without recruiting cargo to the membrane. However, there still remain several central questions about the role of GTP hydrolysis in the protein targeting reaction that remain to be answered.

One of the most intriguing hypotheses for an additional role of GTP hydrolysis in protein targeting is that it might drive the transfer of the ribosome from SRP to the

translocon. This hypothesis is supported by the observation that mutant forms of SR that bind SRP normally but are defective for GTP hydrolysis fail to target ribosomes to the membrane⁵. However, contradictory results were obtained when wildtype proteins were used in the presence of GPPNHP to prevent GTP hydrolysis⁶. Improved assays to monitor the individual steps in the targeting reaction will be required to directly test this hypothesis.

Whether or not GTP hydrolysis plays a direct role in transfer of the ribosome from SRP to the translocon, there must be a mechanism to ensure that SRP and SR do not hydrolyze GTP and dissociate prior to transfer, and this mechanism is not known. One possibility is that GTP hydrolysis is delayed until transfer occurs. However, signal peptide association with SRP did not affect the rate of GTP hydrolysis by the SRP-SR complex, so any inhibition of GTP hydrolysis must be mediated by the ribosome rather than the signal peptide. An alternate possibility is that transfer is much more rapid than the lifetime of an SRP-SR complex. A quantitative targeting system in which the individual steps of the targeting reaction can be monitored will also be necessary to resolve this question.

How is the signal peptide recognized by SRP?

Despite being called the Signal Recognition Particle, we know very little about how SRP recognizes its signal. Therefore a major goal in the field has been, and should be, to determine the structure of a signal peptide bound to SRP. The system we developed with the Δ EspP signal peptide is a great starting point for such studies.

Preliminary results relating to this project and a more complete discussion of these ideas are presented in Appendix B.

Why does SRP RNA act on a transition state?

SRP RNA facilitates the interaction of SRP and SR by stabilizing the transition state to binding rather than the final SRP-SR complex. As a result of this, SRP RNA catalyzes the binding reaction, accelerating the association and dissociation rates equally. However, it is not clear whether the fact that SRP RNA acts on a transition state is important to its function in the targeting reaction. This is particularly perplexing, because dissociation of SRP-SR complexes is driven by GTP hydrolysis not the off rate of the GPPNHP stabilized complex, so the off rate of the SRP-SR complex that SRP RNA accelerates is most likely not directly relevant in the context of the targeting reaction. Our recent work, and the work of others allows us to propose several hypotheses for why SRP RNA acts as a catalyst.

A plausible explanation for why SRP RNA stabilizes the transition state to binding comes from the realization that SRP RNA is only active when SRP is bound to a signal peptide. Because signal peptides exchange with SRP much faster than SRP binds SR (Appendix B), if SRP RNA stabilized the SRP-SR complex rather than the transition state to complex formation, then each time the signal peptide dissociated, the complex would in turn be destabilized. However, by stabilizing the transition state, the final SRP-SR complex is unaffected by whether or not signal peptide is bound at any moment, effectively giving the SRP-SR complex “memory” as to whether a signal peptide was

recently bound. Further exploration of the kinetics of signal peptide association with SRP will be necessary to determine if this is important.

A second possible explanation for why SRP RNA acts on the transition state to SRP-SR binding is that it facilitates transfer of the ribosome from the SRP-SR complex. If signal peptide binding to SRP led to stabilization of the SRP-SR complex, rather than the transition state to binding, signal peptides would bind the SRP-SR complex more tightly than SRP alone. This would mean that release of the RNC from SRP would be inhibited by formation of the SRP-SR complex, which is counterintuitive. However, since signal peptides stabilize the transition state for SRP-SR binding (by activating SRP RNA), they bind the transition state complex with high affinity while binding SRP and the SRP-SR complex with the same lower affinity. Thus, the switch between the transition state complex and the final stable complex could drive the dissociation of the signal peptide from SRP and transfer of the RNC to the translocon.

How is the ribosome transferred to the translocon?

The least understood step of the targeting reaction is how the ribosome is transferred from SRP to the translocon. Ribosome hand off is complicated by the fact that SRP and the translocon bind to overlapping sites on ribosomes and both directly interact with the signal sequence. Additionally, very little is known about how the SRP-SR-RNC complex interacts with the translocon and it is controversial whether or not GTP hydrolysis is required for transfer^{5,6}. There is some intriguing evidence that SRP targets ribosomes to a subpopulation of translocons that are incapable of binding SRP on their own, but how this is mediated is also a mystery⁷.

The main reason for the lack of understanding of ribosome transfer is the lack of good biochemical systems in which to study this step. Fluorescent assays to monitor SRP-ribosome association are a key ingredient in developing such a system. It is also critical to have a preparation of translocons, either purified or in microsomes, that can be added to SRP-ribosome complexes without perturbing the fluorescence signal. By monitoring the disassembly of SRP-ribosome complexes dependent on SR and translocons, it would be possible to directly and quantitatively monitor SRP-ribosome handoff to the translocon.

There are several models for how ribosomes are handed off from the SRP to the translocon. First, SR might destabilize the SRP-ribosome interaction to create a binding site on the ribosome for the translocon. This is supported by the disappearance of SRP54 density in the cryo-EM structure of SRP bound to the ribosome in the presence of SR⁸. Second, the SRP interaction with the ribosome and the signal peptide may “breathe”, transiently dissociating to allow the translocon to bind to either the signal peptide or the ribosome while SRP is still bound. Finally, it is plausible that handoff might be a more active process, in which GTP hydrolysis by the SRP-SR complex drives the transfer of the ribosome. Distinguishing between these models would be a major advance in our understanding of the targeting process.

How is high fidelity targeting achieved?

The central function of the cotranslational protein targeting machinery is to ensure high fidelity sorting of ribosomes destined for the membrane and there are likely many steps during the targeting reaction that contribute to the fidelity of targeting. The first

sorting occurs when SRP recognizes a signal peptide as it emerges from the ribosome. The affinity of SRP for ribosomes is enhanced by signal peptides, which means that SRP will preferentially bind to appropriate ribosomes. In addition, SRP binds SR much more rapidly when associated with a signal peptide, providing a potential additional sorting step. The translocon interacts directly with signal peptides providing a potential mechanism for a post-SRP sorting step. Finally, it is not known if transfer of the ribosome from SRP to the translocon is affected by signal peptides, but this would also provide a potential sorting step. If sorting occurs both before and after GTP hydrolysis by the SRP-SR complex, it is possible that kinetic proofreading, analogous to transcription or translation, occurs during cotranslational protein targeting.

1. Peluso, P., Shan, S.O., Nock, S., Herschlag, D. & Walter, P. Role of SRP RNA in the GTPase cycles of Ffh and FtsY. *Biochemistry* **40**, 15224-33 (2001).
2. Schaffitzel, C. et al. Structure of the E. coli signal recognition particle bound to a translating ribosome. *Nature* **444**, 503-6 (2006).
3. Buskiewicz, I., Kubarenko, A., Peske, F., Rodnina, M.V. & Wintermeyer, W. Domain rearrangement of SRP protein Ffh upon binding 4.5S RNA and the SRP receptor FtsY. *Rna* **11**, 947-57 (2005).
4. Zhang, X., Schaffitzel, C., Ban, N. & Shan, S.O. Multiple conformational switches in a GTPase complex control co-translational protein targeting. *Proc Natl Acad Sci U S A* **106**, 1754-9 (2009).
5. Shan, S.O., Chandrasekar, S. & Walter, P. Conformational changes in the GTPase modules of the signal reception particle and its receptor drive initiation of protein translocation. *J Cell Biol* **178**, 611-20 (2007).
6. Wilson, C., Connolly, T., Morrison, T. & Gilmore, R. Integration of membrane proteins into the endoplasmic reticulum requires GTP. *J Cell Biol* **107**, 69-77 (1988).
7. Schaletzky, J. & Rapoport, T.A. Ribosome binding to and dissociation from translocation sites of the endoplasmic reticulum membrane. *Mol Biol Cell* **17**, 3860-9 (2006).
8. Halic, M. et al. Signal recognition particle receptor exposes the ribosomal translocon binding site. *Science* **312**, 745-7 (2006).

Appendix A

A major goal for future research in protein targeting is to determine how the interaction of SRP and SR is affected by other components of the targeting reaction, specifically translating ribosomes and translocons. To this end, we developed a system to monitor the association of SRP and SR using FRET. This section describes single cysteine containing variants of Ffh and FtsY that were generated, their characterization, as well as the characterization of the fluorescence assay to monitor binding. In general the assay system proved to be reliable for monitoring the rapid interaction of Ffh and FtsY in the presence of 4.5S RNA and detergent, but not for slower reactions lacking these cofactors.

Methods:

Single cysteine containing variants of Ffh and FtsY were constructed by quickchange mutagenesis. All proteins were purified as described previously, with the exception that Ffh mutant C406S and its derivatives (all single cysteine substituted variants of Ffh) were destabilized in standard assay buffer (50mM KHEPES pH 7.5, 150mM KOAc, 2mM Mg(OAc)₂, 2mM DTT. This difficulty was overcome by the addition of 10% glycerol to the assay buffer. Proteins were labeled by exchanging into labeling buffer (5mM Tris pH 7.0, 250mM NaCl, 2mM EDTA) and incubating with a 2 molar excess of maleimide dye for 10 minutes at 25 degrees. Labeling reactions were stopped by the addition of 5mM DTT and proteins were purified away from free dye by gel filtration. Specificity of labeling was assessed by including a cysteine free variant as a control. Covalent attachment of the dye was confirmed by SDS PAGE. During the purification of cysteine

substituted proteins 2mM DTT or 2mM BmE was present at all times to prevent oxidation of the cysteine residues.

For kinetic studies, fluorescence measurements were made on an SLM fluorimeter with excitation wavelength 514nm and emission wavelength 670nm when monitoring acceptor emission, and emission wavelength 570nm when monitoring donor quenching.

Results

7 variants of FtsY and 11 variants of Ffh were generated that have single cysteine residues at surface exposed positions that do not overlap with the Ffh-FtsY interface. The proteins were expressed, purified, labeled with organic dyes, and tested for function in GTP hydrolysis assays. Two variants of FtsY labeled on the N-domain were tested with five variants of Ffh with labels distributed throughout the protein. FtsY variants were labeled with Cy5 and Ffh variants were labeled with Cy3. FRET was detected in all cases, with the FRET efficiency related to the distance between the dyes based on the structure of the Ffh-FtsY complex as expected (Fig. A-1-2). In all cases, the intensity of fluorescence from the individual proteins was measured as well as the fluorescence spectrum with both proteins in the presence and absence of GppNHp. One unexpected feature of the FRET data, was that for some dye pairs, there was FRET signal observed in the absence of GppNHp. This signal is likely attributable to the nucleotide free state Ffh-FtsY complex reported by Shan and colleagues¹.

Next we measured the kinetics of Ffh-FtsY association and dissociation by FRET. For these analyses, we used FtsY labeled at position 225 (on the N-domain) with Ffh labeled at position 72 (on the N-domain) or position 395 (on the M-domain). Association rate constants measured by FRET in the presence of Nikkol detergent and 4.5S RNA were similar to those measured by tryptophan fluorescence (Fig. A-3A+B). Similarly, the dissociation rate constants measured by FRET in the presence of Nikkol and 4.5S RNA were similar to those measured by tryptophan fluorescence (Fig. A-3C+D). One interesting feature of the dissociation reactions was that although the dissociation rate measured with the M-domain probe for Ffh fit nicely to a single exponential, the dissociation rate measured with the NG domain probe for Ffh had double exponential characteristics. This might also be accounted for by the nucleotide free association of Ffh and FtsY.

Next we measured the association of Ffh and FtsY in the absence of 4.5S RNA. In this case the binding rates measured were very similar to those measured previously by tryptophan fluorescence, however the fluorescence signal in these assays exhibited some unusual characteristics (examples are shown in Fig. A-4A-C). Binding traces exhibited clear deviation from standard exponential behavior, and this behavior was somewhat reproducible although not always identical. Therefore, it was not clear if the FRET system was revealing previously undetected features of the binding reaction or if the labeled proteins were inducing artifacts. We therefore simultaneously measured binding by tryptophan fluorescence and FRET. The tryptophan fluorescence trace showed the same aberrations that we detected by FRET (Fig. A-4C), however, we did not detect such

aberrations when an identical reaction was performed with unlabeled Ffh and FtsY. This led us to conclude that the fluorescent labels on Ffh and FtsY were perturbing binding in the absence of SRP RNA. Thus, the system requires more refinement (perhaps different dyes or positions of attachment) before it can be used reliably.

1. Zhang, X., Kung, S. & Shan, S.O. Demonstration of a multistep mechanism for assembly of the SRP x SRP receptor complex: implications for the catalytic role of SRP RNA. *J Mol Biol* **381**, 581-93 (2008).

Figure A-1

FRET between complexes of cy3 labeled Ffh and cy5 labeled FtsY. 0.2 μ M FtsY labeled with cy5 at position 225 was incubated with 0.2 μ M Ffh+4.5SRNA labeled with cy3 at position 279 (A), 153 (B), 72 (C), 28 (D), or 395 (E) in the presence or absence of 100 μ M GppNHp. An emission spectrum was recorded for each sample exciting at 550nm (the excitation maximum for cy3). Spectra were also recorded of each protein alone and were subtracted from the spectrum taken for the complex. Negative fluorescence peaking at 570nm (the emission maximum for cy3) therefore represents quenching, while positive fluorescence peaking at 670nm represents energy transfer to cy5. (F) The positions of fluorophores are mapped onto the crystal structure of the $GppNHp$ Ffh-FtsY $GppNHp$ complex from *thermus aquaticus* (PDB ID1okk) and the M-domain of Ffh (PDB ID 2ffh).

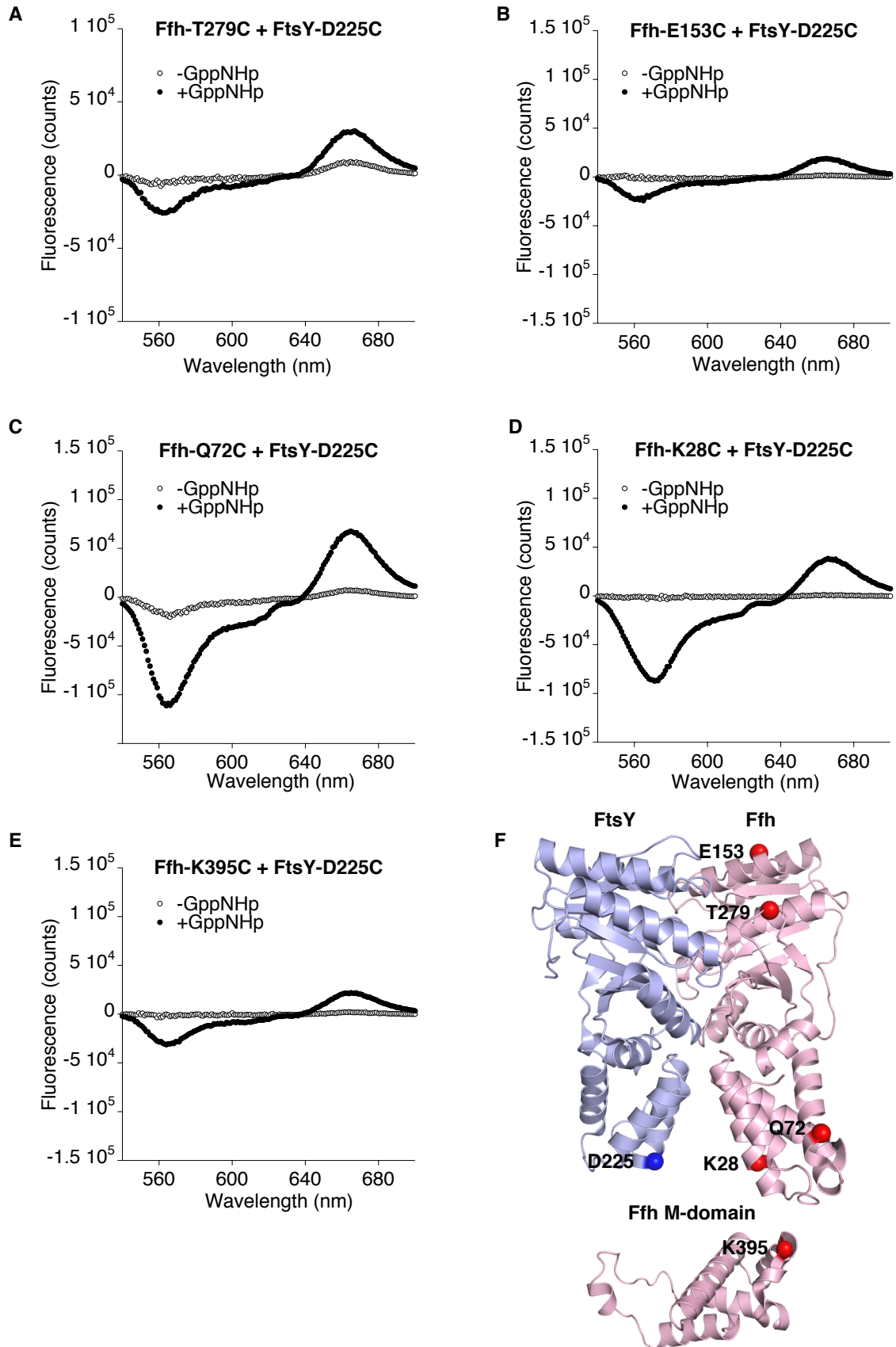


Figure A-2

FRET between complexes of cy3 labeled Ffh and cy5 labeled FtsY. 0.2 μ M FtsY labeled with cy5 at position 230 was incubated with 0.2 μ M Ffh+4.5SRNA labeled with cy3 at position 279 (A), 153 (B), 72 (C), 28 (D), or 395 (E) in the presence or absence of 100 μ M GppNHp. An emission spectrum was recorded for each sample exciting at 550nm (the excitation maximum for cy3). Spectra were also recorded of each protein alone and were subtracted from the spectrum taken for the complex. Negative fluorescence peaking at 570nm (the emission maximum for cy3) therefore represents quenching, while positive fluorescence peaking at 670nm represents energy transfer to cy5. (F) The positions of fluorophores are mapped onto the crystal structure of the $GppNHp$ Ffh-FtsY $GppNHp$ complex from *thermus aquaticus* (PDB ID1okk) and the M-domain of Ffh (PDB ID 2ffh).

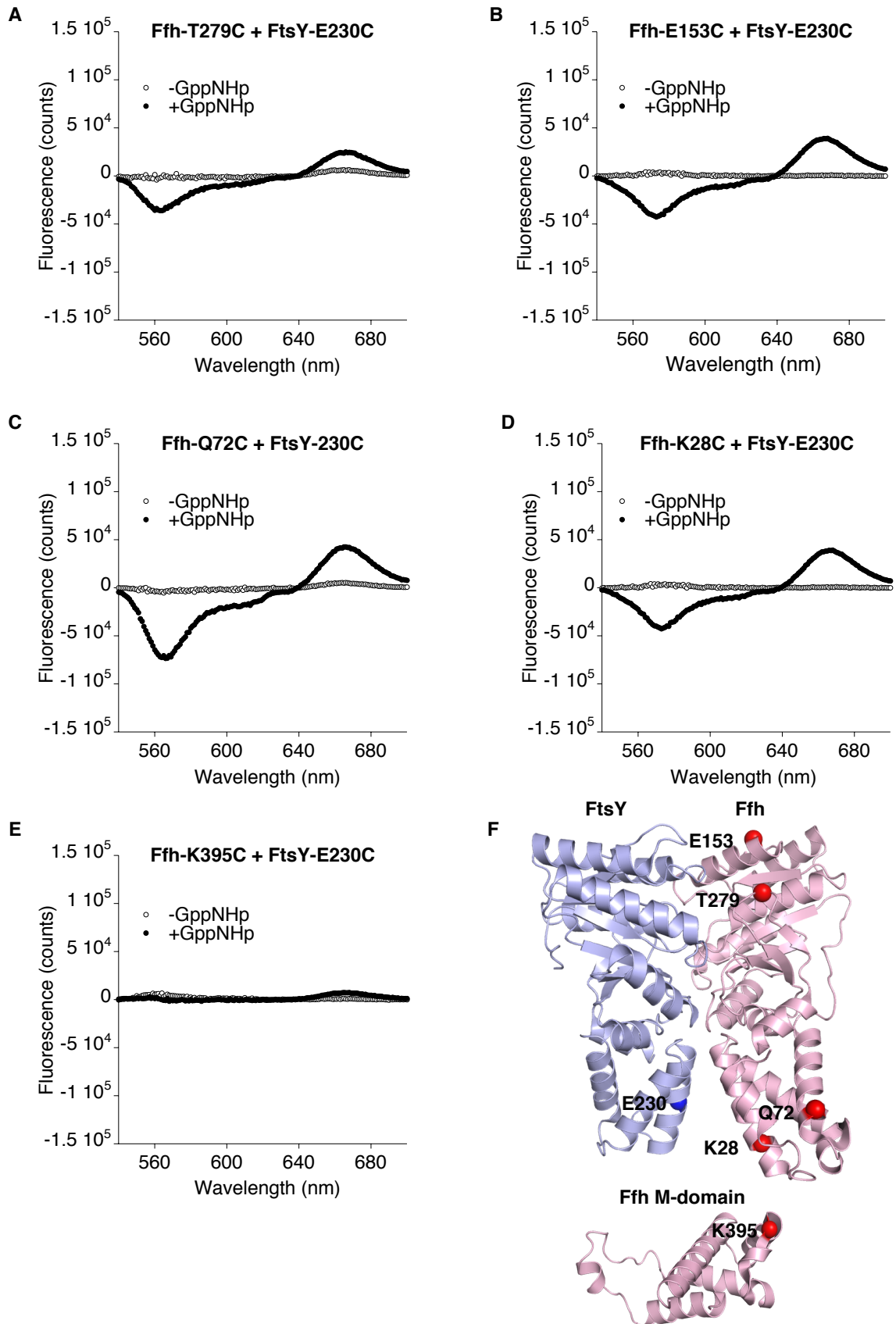


Figure A-3

FRET accurately measures Ffh-FtsY association in the presence of 4.5S RNA. 0.2 μ M FtsY labeled with cy 5 at position 225 was mixed with Ffh labeled at position 72 (A) or 395 (B) in the presence of a 1.5 molar excess of 4.5S RNA, 100 μ M GppNHp, and 0.01% nikkol. Observed association rates were measured at varying Ffh-4.5S RNA concentrations, by exciting at 515nm and observing fluorescence at 670nm. Observed rates are plotted as a function of Ffh concentration. Red lines are fits of the data to the equation $k_{\text{obs}} = k_{\text{on}} * [\text{Ffh}] + k_{\text{off}}$. C and D show measurements of the dissociation rate constants for Ffh-FtsY complexes measured by FRET. Complexes of FtsY labeled with cy5 at position 225 and Ffh labeled at position 72 (C) or 395 (D) were formed in the presence of 4.5S RNA, 50 μ M GppNHp and 0.01% nikkol. These samples were then rapidly mixed with 2mM GDP to trap complexes as they fell apart, and disassembly was monitored by exciting at 515nm and observing fluorescence at 670nm. Red lines represent fits of the data to a single exponential equation.

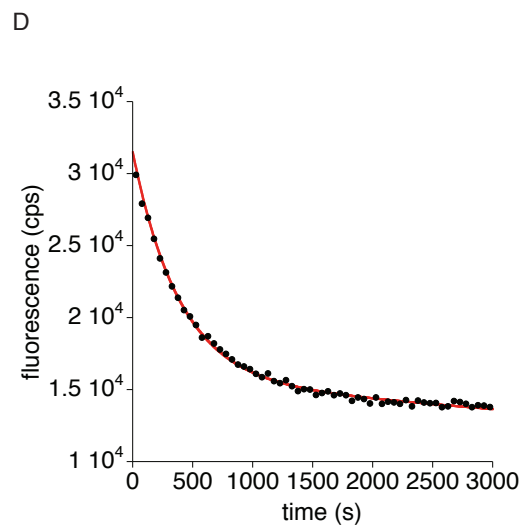
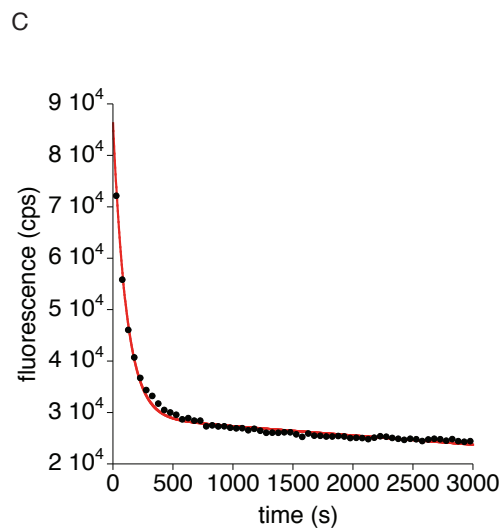
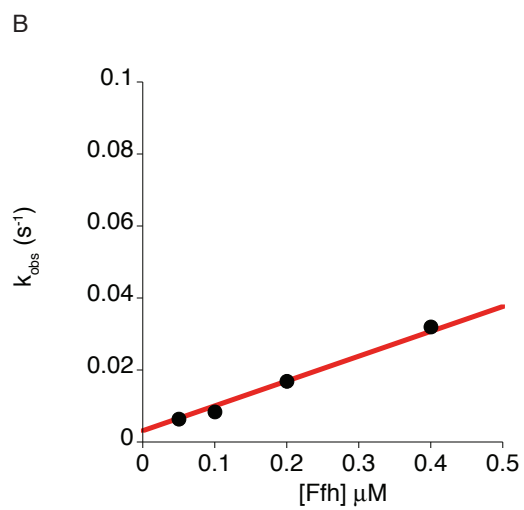
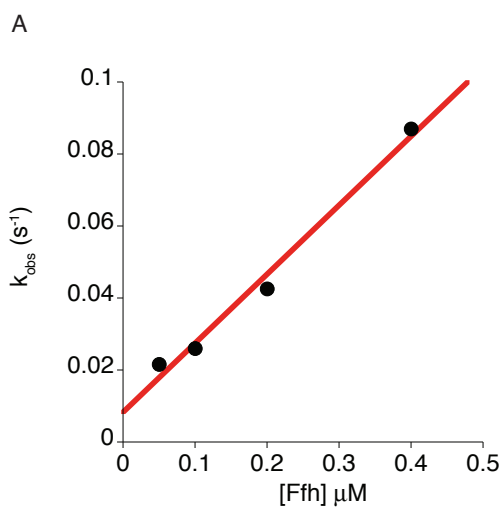
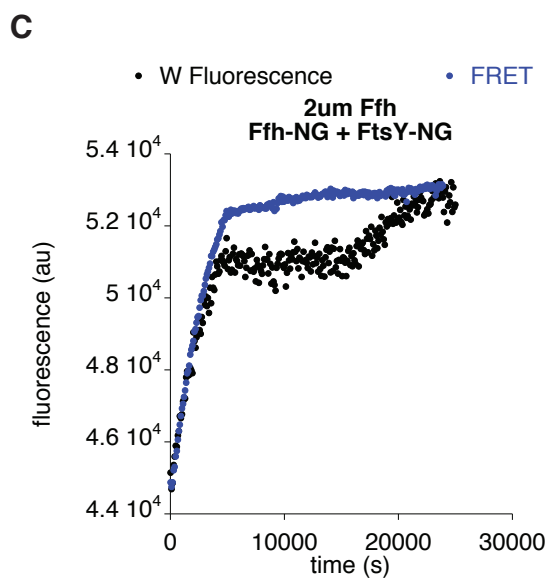
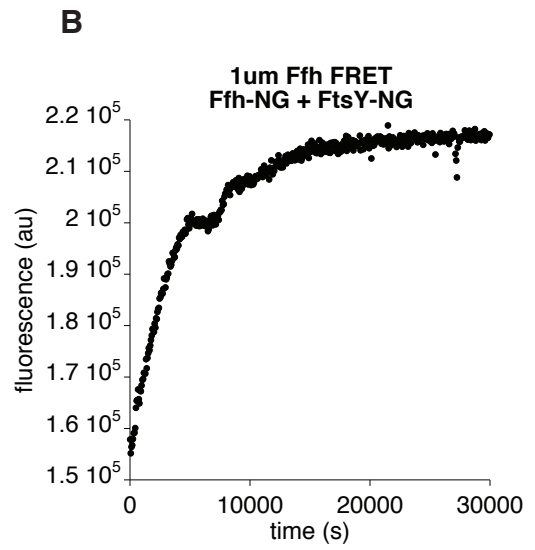
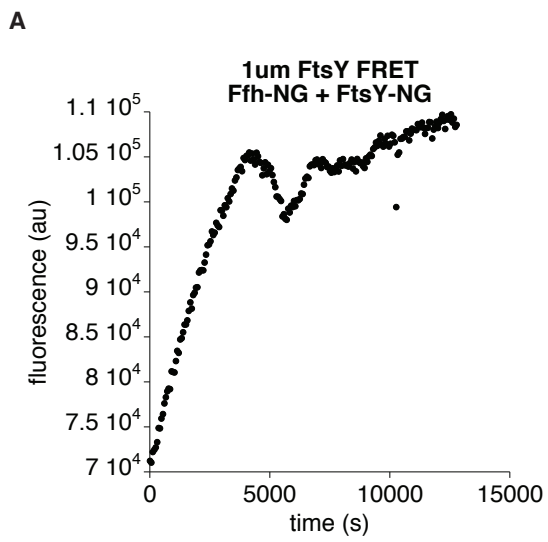


Figure A-4

Abnormalities in association rates for Ffh-FtsY association measured by FRET in the absence of 4.5S RNA. 0.2 μ M FtsY labeled with cy 5 at position 225 was mixed with Ffh labeled at position 72, 100 μ M GppNHP, and 0.01% nikkol. Observed association rates were measured at varying Ffh-4.5S RNA concentrations, by exciting at 515nm and observing fluorescence at 670nm. A and B show separate measurements of Ffh-FtsY association reactions with 1 μ M Ffh. C shows simultaneous measurements of Ffh-FtsY association by FRET and tryptophan fluorescence.



Appendix B

One of the major unanswered questions about cotranslational protein is how signal sequences are recognized by SRP. Due to the fact that signal sequence binding activates SRP to bind SR more rapidly, how signal sequences bind SRP is even more interesting. This section describes several experiments directed at gaining further insight into the signal recognition step of the targeting reaction. First, I describe the kinetic characterization of the SRP-signal peptide interaction. And second, I describe a system to disulfide bond signal peptides to Ffh that could be useful for further biochemical or structural characterization.

Methods

FRET assay for signal peptide SRP binding

FAM-labeled EspP (described in chapter 2) was incubated with Ffh labeled with cy3 at position 395 (described in Appendix A). Fluorescence measurements were made on an SLM fluorimeter. Equilibrium K_d measurements were made with excitation wavelength 470nm and emission wavelength 522nm. 0.1 μ M FAM-EspP was mixed incubated with varying concentrations of cy3-Ffh (and a 2 fold molar excess of 4.5S RNA) for at least 20 minutes before fluorescence measurements were taken. For all samples, the fluorescence signal was corrected by subtracting the fluorescence of cy3-Ffh (+RNA) alone and EspP-FAM alone. The relative fluorescence change for each sample was plotted as a function of cy3-Ffh concentration and the data were fit to a quadratic equation. The affinity of Ffh binding to signal peptide was also measured by competition with unlabeled Ffh. Ffh-peptide complexes were formed with 0.5 μ M cy3-Ffh (+ 4.5S RNA) and 0.1 μ M FAM-

EspP. Unlabeled Ffh (+4.5S RNA) was then added at varying concentrations. Data were fit to the equation: Fraction bound = $K_i * [cy3\text{-Ffh}] / (K_d * (K_i + [Ffh]) + K_i * [cy3\text{-Ffh}])$.

Kinetic measurements were made on a kintec stopped flow fluorimeter with excitation wavelength 490 and a 10nm band pass filter centered at 530nm. All experiments were performed at room temperature in 50mM KHEPES pH 7.5, 150mM KOAc, 2mM MgOAc₂, 2mM DTT, and 10% glycerol.

Signal peptide crosslinking

Crosslinking experiments were performed by buffer exchanging Ffh with various cysteine substitutions into 50mM KHEPES pH 7.5, 150mM KOAc, 2mM MgOAc₂, and 10% glycerol. Proteins were then immediately mixed with 5μM Ffh with 7.5 μM 4.5S RNA was mixed with 1μM FAM-EspP and 50μM Cu²⁺ phenanthroline. (Phenanthroline was dissolved in ethanol to 50mM and diluted to a 1mM stock in buffer. CuSO₄ was added to equimolar concentration.) Samples were then incubated at room temperature for 10 minutes and quenched with 10mM NEM. Samples were then run on a non-reducing gel and scanned on a typhoon.

Results

The kinetics of signal peptide binding to SRP

Signal peptide binding to SRP regulates the rate of SRP interaction with SR. However, we previously knew very little about the kinetics of the interaction of SRP with the signal peptide. This could be quite significant, both for understanding the mechanism by which

signal peptides activate SRP to bind SR, and for understanding subsequent steps in targeting such as transfer of the ribosome to the translocon and disassembly of the SRP-SR complex. There are several potential advantages for the targeting system if SRP binding to signal peptide is in much faster equilibrium than SRP binding to SR. First, proteins must be targeted to the membrane early during their translation, thus, rapid recognition of signal peptides by SRP would insure that signal peptides are recognized early in their translation. Second, rapid SRP-signal peptide equilibrium might provide a mechanism for handoff of the signal peptide from SRP to the translocon. Additionally, rapid signal peptide exchange might allow for kinetic proofreading to enhance the fidelity of targeting.

Therefore, we measured the rate of signal peptide binding to SRP, using the Δ EspP signal peptide described previously. To enhance the signal of our assay, we measured signal peptide binding to SRP by FRET using the FAM-EspP peptide as the donor, and Cy3 labeled Ffh, with the label at position 395 on the M-domain, as the acceptor. Using this assay we were able to measure binding of SRP to the signal peptide. The K_d measured by this assay was slightly tighter than that measured by anisotropy ($0.280 \pm 0.025 \mu\text{M}$ Fig. B-1A compared to $1.5 \pm 0.4 \mu\text{M}$ measured by anisotropy). Competition with unlabeled SRP yielded a K_d of $1.15 \pm 0.57 \mu\text{M}$ (Fig. B-1B), which agrees nicely with the value determined by anisotropy measurements and suggests that the label on Ffh slightly enhances the affinity of peptide binding. Nonetheless, this provides a reasonable assay for monitoring peptide association with SRP.

We next measured the kinetics of SRP signal peptide binding on the stopped flow. The association rate constant was $4.9 \times 10^7 \text{ M}^{-1} \text{ s}^{-1}$ (Fig. B-2A), and the dissociation rate constant was 12.4 s^{-1} (Fig. B-2B). The binding rate is over 100 fold faster than the rate of SRP-SR association, even when stimulated by signal peptide and SRP RNA. Perhaps more importantly, the dissociation rate is also very rapid—over 10 fold faster than the maximal rate of GTP hydrolysis driven disassembly of the SRP-SR complex, suggesting that signal peptide binding to SRP is at steady state before SRP binds SR (this is consistent with experiments measuring the rate of SRP-SR association as a function of peptide concentration). It should be noted that these rates do not take into account any contribution to binding from the ribosome.

Crosslinking signal peptides to SRP

One of the major outstanding questions in cotranslational protein targeting is to understand how SRP binds signal peptides. The soluble EspP signal peptide could provide an important tool for future biochemical and structural studies to determine how this occurs. Initial crystallization trials did not yield a structure of SRP bound to a signal peptide. One reason for this might be the high rate of exchange and the possibility for heterogeneity in how the peptide binds SRP.

To learn more about how SRP binds signal peptides while overcoming these difficulties, we decided to monitor how signal peptides bind to SRP using disulfide crosslinking. The EspP signal peptide has a single cysteine residue in the middle at position 11. By

introducing single cysteines into Ffh, we could then monitor the efficiency with which Ffh and the signal peptide were disulfide crosslinked. We monitored crosslinking of 9 variants of Ffh with the EspP peptide. The cysteine of 5 Ffh variants was in the predicted signal peptide binding groove, while 2 variants had cysteines in other positions of the M-domain, and the final two variants had a cysteine on the N and G domains respectively (Fig. B-3).

We observed crosslinking efficiencies of greater than 25% for four of the cysteine variants of Ffh (Fig. B-3). Three variants had the cysteine positioned in the predicted signal peptide binding groove on the side opposite the 4.5S RNA binding site, while the other variant had the cysteine on the N-domain at position 72. 3 other variants with cysteines in the M-domain had crosslinking efficiencies between 10% and 15%, while the final two variants showed crosslinking that was only slightly elevated above the background observed for Ffh that lacks cysteines entirely. Thus, our results from this assay suggest that the middle of the EspP signal peptide preferentially binds to the predicted signal peptide binding groove opposite the binding site for 4.5S RNA and also contacts the N-domain. Future studies investigating if crosslinking to the N-domain depended on 4.5S RNA or the M-domain of Ffh would be necessary to determine the relevance of the interaction of signal peptides with the N-domain. However, there is previous evidence suggesting that signal peptides contact the N-domain of Ffh¹. In order to establish the relevance of these crosslinking studies, it will be necessary to purify the crosslinked SRP-signal peptide complexes and assay their activity in binding to FtsY.

1. Cleverley, R.M. & Gierasch, L.M. Mapping the signal sequence-binding site on SRP reveals a significant role for the NG domain. *J Biol Chem* **277**, 46763-8 (2002).

Figure B-1

FRET assay for monitoring signal peptide association with SRP. A. Steady state measurements of SRP-signal peptide association by FRET. Ffh labeled with cy3 at position 395 was mixed with EspP-FAM and 4.5S RNA. FAM emission was measured as a function of Ffh-cy3 concentration. Curve represents a fit to a quadratic equation. B. The K_d of Ffh binding to signal peptide was measured by competition with unlabeled Ffh. Data were fit to the equation: Fraction bound = $K_i * [cy3\text{-Ffh}] / (K_d * (K_i + [Ffh]) + K_i * [cy3\text{-Ffh}])$.

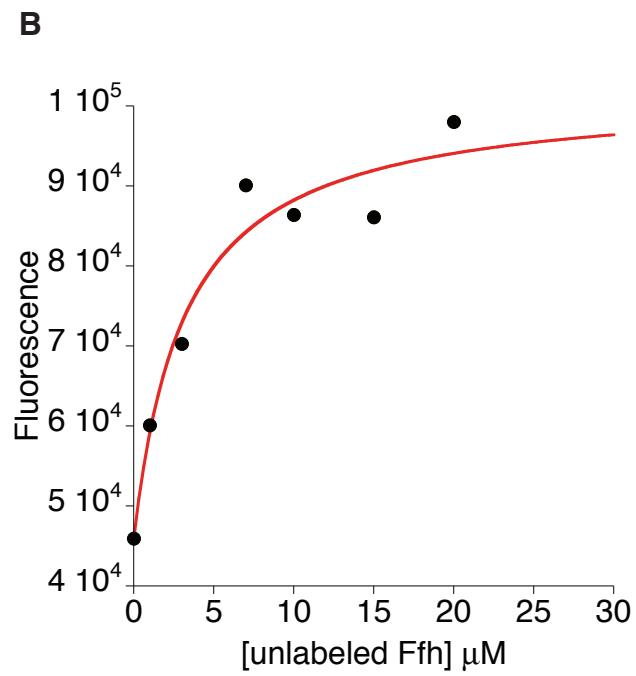
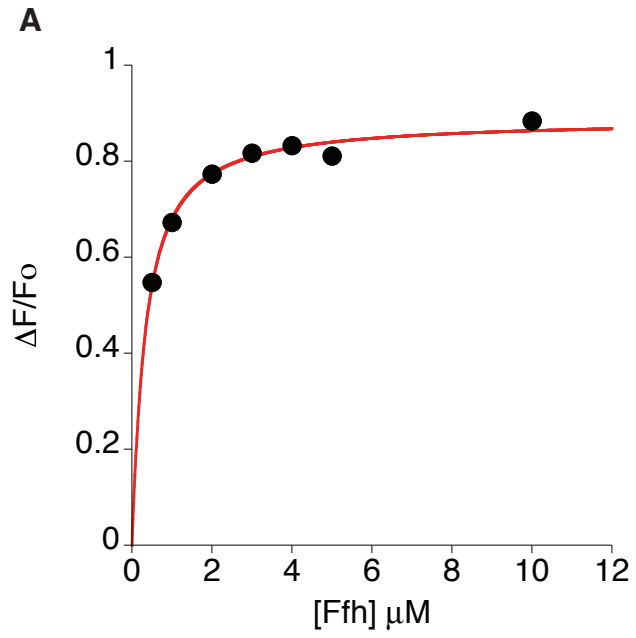


Figure B-2

Kinetics of signal peptide exchange with SRP. A. Association of cy3-SRP with EspP-FAM was measured by FRET using a stopped flow fluorimeter. Binding was monitored by observing quenching of FAM emission when EspP-FAM binds cy3-SRP. Observed association rates of EspP-FAM binding to cy3-SRP are plotted as a function of [cy3-SRP]. The data were fit to the equation $k_{\text{obs}} = k_{\text{on}} * [\text{cy3-SRP}] + k_{\text{off}}$. B. Dissociation of EspP-FAM from cy3-SRP was initiated by rapidly mixing preformed EspP-FAM•cy3-SRP complexes with an excess of unlabeled SRP the increase in FAM emission was monitored. Data were fit to a single exponential equation.

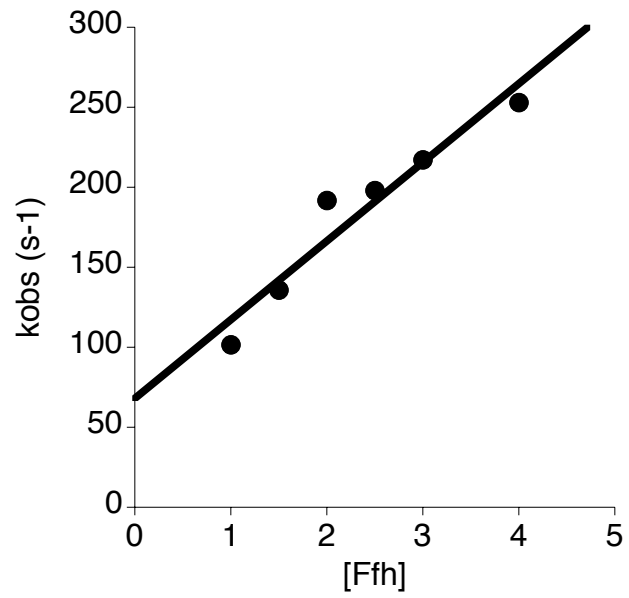
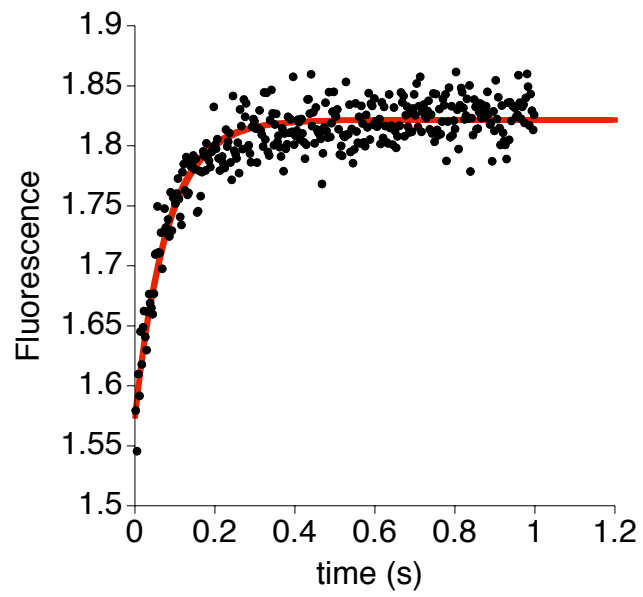
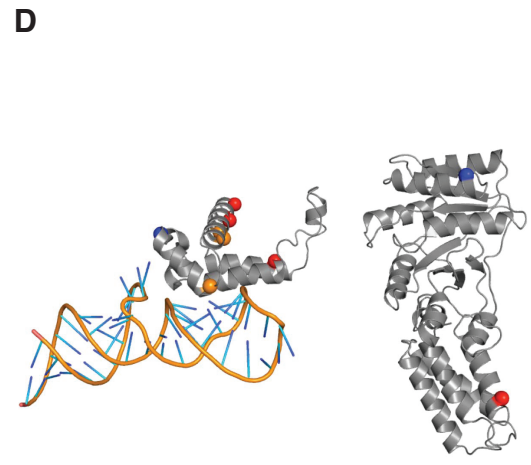
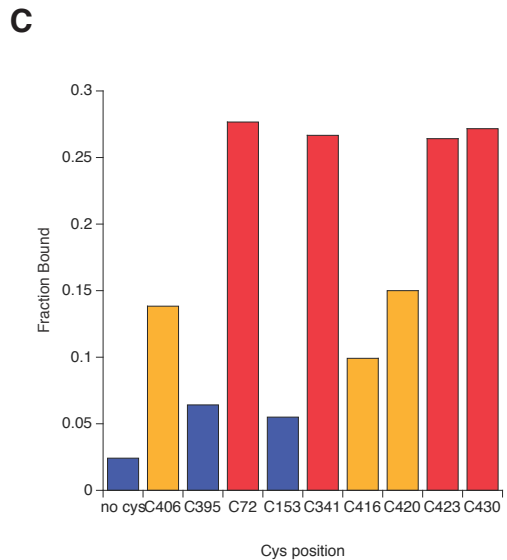
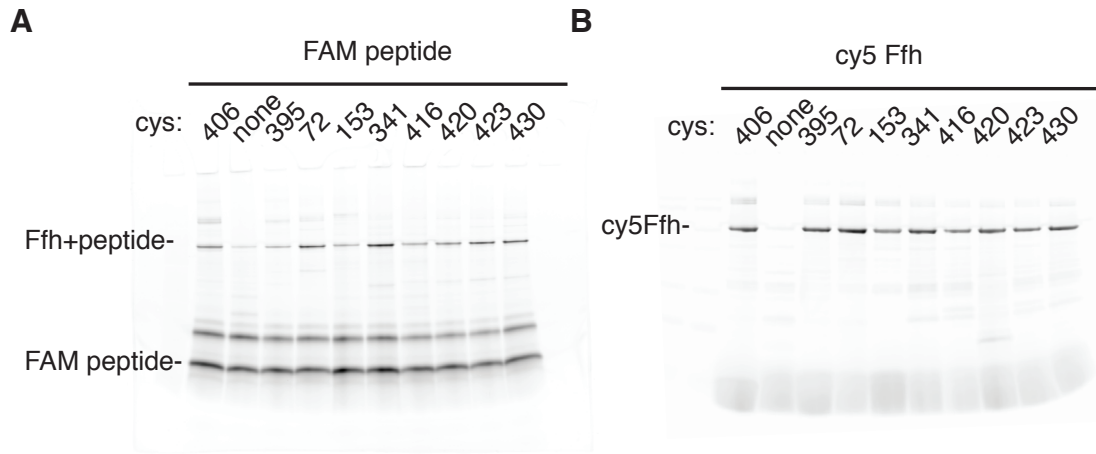
A**B**

Figure B-3

Disulfide crosslinking of EspP-FAM to single cysteine bearing variants of Ffh. A. EspP-FAM was mixed with Ffh bearing single cysteine residues at the indicated positions and Cu^{2+} phenanthroline. Disulfide crosslinking was monitored by running samples on a non-reducing gel. Gels were imaged by monitoring FAM fluorescence on a Typhoon scanner and crosslinked Ffh-EspP complexes were visualized as a higher molecular weight species. B. Ffh cysteine variants were labeled with a 2 fold molar excess of cy5 maleimide to confirm that cysteines were reactive. Samples were run on a gel and imaged on a Typhoon scanner. C. Crosslinking efficiency of cysteine variants of Ffh from A is plotted. Variants that with greater than 25% crosslinking efficiency are colored red, variants with crosslinking efficiency between 10% and 25% are colored orange, and variants with crosslinking efficiency less than 10% are colored blue. D. Structure of Ffh with positions of cysteine substitutions colored as in C.



Appendix C

Previously we showed that signal peptide binding by SRP accelerates the interaction of SRP with SR using synthetic signal peptides that bind SRP (chapter 2). However, during a targeting reaction SRP binds signal peptides as they emerge from the ribosome. How SRP interacts with ribosomes translating nascent secretory proteins is therefore critical to understanding the targeting reaction. This section describes our efforts to develop a method to site specifically label ribosomes with a fluorophore near the exit channel (where the signal sequence emerges), and preliminary results studying the interaction of SRP with ribosomes.

Methods

Purification of labeled ribosomes.

MRE5000 (wt) or AM111(Δ RPL29) cells were grown to OD 0.4 in LB. Cells were rapidly chilled by pouring over ice and were washed and pelleted in cold 50mM Hepes 7.5, 50mM KOAc, 5mM MgOAc₂, 2mM DTT. Cells were then lysed using a microfluidizer and spun for 30 minutes at 30,000Xg. The supernatant was collected and spun for 15hrs at 40,000 in the Ti 50.2 over a 5ml 40% sucrose cushion. The ribosome pellet was separated from the membrane layer, and resuspended in buffer. The ribosomes were then spun for 3.5 hours at 55,000 in the TLS 55 with a 40% sucrose cushion. The pellet was then resuspended as above in buffer with 150mM salt. Ribosomes were then either frozen in aliquots with 10% glycerol or mixed with a 2 molar excess of recently

spun cy3 labeled L29. Incorporation of L29 was measured by comparing the OD260 and OD550 of the resuspended ribosome pellet.

6-his tagged RPL29 was expressed in BL21 cells and purified by nickel affinity chromatography followed by gel filtration on a superdex 75 column. L29 was labeled as described previously for other proteins and frozen at -80 in buffer containing 10% glycerol. RPL29 could not be concentrated effectively on spin concentrators and was therefore dialyzed against sucrose to concentrate.

FRET assay for ribosome-Ffh interaction.

FRET between cy3 labeled ribosomes and cy5 labeled Ffh was measured by mixing 1 μ M Ffh labeled with cy5 with 0.1 μ M ribosomes labeled with cy3 on L29. Emission spectra were recorded for each sample exciting at 550nm (the excitation maximum for cy3). The affinity of the Ffh-ribosome interaction was measured by FRET by mixing 0.02 μ M cy3 labeled ribosomes with varying concentrations of cy 5 labeled.

Fluorescence measurements were made for each sample exciting with 514nm light and recording emission at 550nm, to monitor quenching of cy3. Curves were fit with a quadratic equation. The affinity of the Ffh-ribosome interaction was also measured by competition with unlabeled ribosomes by incubating 0.1 μ M cy5 labeled Ffh with 0.5 μ M cy3 labeled ribosomes and monitoring the loss in cy5 emission as a function of increasing unlabeled ribosome addition. Data were fit to the equation: Fraction bound = $K_i \cdot [\text{cy3-ribosome}] / (K_d \cdot (K_i + [\text{ribosome}]) + K_i \cdot [\text{cy3-ribosome}])$. Similarly, the affinity of the Ffh-ribosome interaction was also measured by competition with unlabeled Ffh by incubating

0.5 μ M cy5 labeled Ffh with 0.1 μ M cy3 labeled ribosomes and monitoring the increase in cy3 emission as a function of increasing unlabeled Ffh addition. Data were fit to the equation: Fraction bound = $K_i \cdot [\text{cy5-Ffh}] / (K_d \cdot (K_i + [\text{Ffh}]) + K_i \cdot [\text{cy5-Ffh}])$.

The association rate of the Ffh-ribosome interaction was measured by rapidly mixing cy5 labeled Ffh with cy3 labeled ribosomes. Observed association rates are measured at varying Ffh concentrations. The data were fit to the equation $k_{\text{obs}} = k_{\text{on}} \cdot [\text{cy5-Ffh}] + k_{\text{off}}$. The dissociation rate of the Ffh-ribosome interaction was measured by rapidly mixing preformed cy5-Ffh•cy3-ribosome complexes with an excess of unlabeled Ffh. The increase in cy3 emission that occurred when cy5-Ffh dissociated was monitored. Data were fit to a single exponential equation.

Results

One of the major challenges to studying how SRP interacts with ribosomes is the large size and complexity of ribosomes. This has previously made it difficult to modify ribosomes with fluorescent dyes or other probes. In order to overcome this obstacle, we took advantage of the fact that the ribosomal protein L29, which sits near the exit channel near the SRP binding site, is nonessential in *E. coli* (Fig. C-1A)¹. We purified ribosomes lacking L29 and then reincorporated L29 that had been modified with a single fluorophore at either position 10 or 38 into the ribosomes. Incorporation of labeled L29 into the ribosome was verified by separating the ribosomes on sucrose gradients (Fig. C-1B). L29 was stably associated with the ribosomes even in 0.5M salt, and labeling efficiencies greater than 90% were achieved.

We then monitored Ffh binding to ribosomes by FRET between Cy3 labeled ribosomes and Cy5 labeled Ffh (Fig. C-2A-D). Using Ffh labeled on both the M and NG domains, robust FRET was observed with the labeled ribosomes. As predicted by the cryo-EM structure of Ffh bound to translating ribosomes, the FRET efficiency was greatest for ribosomes labeled at position Q38 of L29, and was similar for Ffh labeled on the N and M domains². Furthermore, this suggested that this might provide a reliable system for monitoring Ffh association with ribosomes.

We next measured the affinity of Ffh association with ribosomes using this assay. Ffh bound ribosomes labeled at L29 Q38 with a K_d of 0.26 μ M (Fig. C-3A) and ribosomes labeled at L29 S10 with a K_d of 0.45 μ M (Fig. C-3B). These affinities were in good agreement with each other and were similar to previous measurements of SRP binding to ribosomes. To ensure that the dyes did not perturb the binding of Ffh to ribosomes, we performed competition experiments, competing either with unlabeled wildtype ribosomes or Ffh. Unlabeled ribosomes competed with a K_i of 0.36 μ M (Fig. C-3C) while Ffh bound with a K_i of 0.66 μ M (Fig. C3-D), demonstrating that the labels do not influence the binding of Ffh to ribosomes.

Next we measured how 4.5S RNA affects binding of Ffh to ribosomes. Using this assay the K_d for Ffh-4.5S RNA binding to ribosomes was over 10 fold weaker (4.3 μ M) than Ffh binding to ribosomes (Fig. C4). This result is in contrast to the affinities measured by Bornemann et al.³ where binding of Ffh-4.5S RNA to ribosomes was significantly tighter.

One possible explanation for this discrepancy is that the Bornemann study was performed with labeled 4.5S RNA under low salt conditions where the labeled 4.5S RNA is prone to aggregation (Paul Peluso, thesis). Further studies will be necessary to resolve this difference. However, the possibility that SRP binds to non translating ribosomes with significantly lower affinity than was previously supposed could help to explain how SRP is excluded from binding to ribosomes that lack signal peptides. Similarly, if upon binding a signal peptide, SRP RNA no longer inhibits ribosome binding, this could elegantly explain how SRP is selectively recruited to ribosomes with signal peptides.

Kinetics of Ffh binding to ribosomes

Next we determined the kinetics of Ffh binding to ribosomes. Ffh bound ribosomes with an association rate constant of $2.65 \times 10^8 \text{M}^{-1} \text{s}^{-1}$, a rate that approaches the diffusion limit (Fig. C-5A). The Ffh-ribosome association rate constant is therefore approximately 4 orders of magnitude faster than that for 4.5S RNA stimulated binding of Ffh and FtsY and 4 fold faster than that for signal peptide-SRP binding and approaches the theoretical limit of diffusion. The dissociation rate was measured to be 102s^{-1} (Fig. C-5B). The rate constants give a K_d of $0.38 \mu\text{M}$, consistent with the affinity measured by equilibrium techniques (Fig. C-3A). Unfortunately, it was not possible to determine the kinetics of the Ffh-4.5S RNA interaction with the ribosome due to the low affinity of that interaction. However, this suggests that SRP rapidly samples ribosomes that do not display a signal peptide as was previously predicted⁴.

1. Dabbs, E.R. Selection for *Escherichia coli* mutants with proteins missing from the ribosome. *J Bacteriol* **140**, 734-7 (1979).
2. Halic, M. et al. Following the signal sequence from ribosomal tunnel exit to signal recognition particle. *Nature* **444**, 507-11 (2006).
3. Bornemann, T., Jockel, J., Rodnina, M.V. & Wintermeyer, W. Signal sequence-independent membrane targeting of ribosomes containing short nascent peptides within the exit tunnel. *Nat Struct Mol Biol* **15**, 494-9 (2008).
4. Ogg, S.C. & Walter, P. SRP samples nascent chains for the presence of signal sequences by interacting with ribosomes at a discrete step during translation elongation. *Cell* **81**, 1075-84 (1995).

Figure C-1

Incorporation of cy3-labeled L29 into ribosomes. A. Cryo-EM model of *E. coli* SRP bound to a translating ribosome. The ribosome is shown in grey, SRP is shown in blue, the signal peptide is shown in green, and L29 is shown in red. Positions S10 and Q38 of L29 are shown as spheres. B. Same as A, but zoomed in to highlight the proximity of SRP to L29. C. Recombinant L29 incorporates into ribosomes lacking L29. A five fold excess of recombinant L29 labeled with cy3 at position Q38 was mixed with ribosomes purified from a strain that lacks L29. Samples were then pelleted by spinning 100,000XG for 20 minutes. The supernatant (S) and pellet (P) fractions were then run on SDS gels and were scanned on a Typhoon to visualize cy3-L29. D. Same as C. but samples were spun on a 10%-40% sucrose gradient. In addition to cy3-L29, ribosomal RNA was visualized.

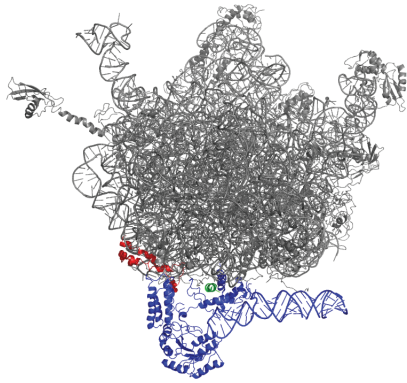
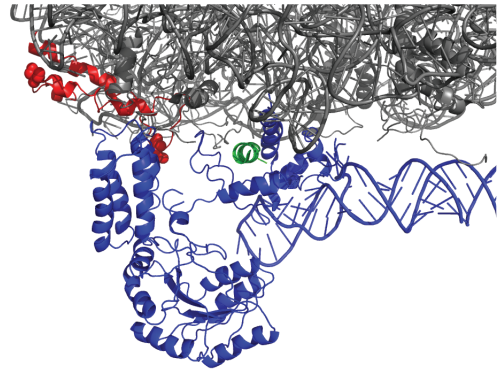
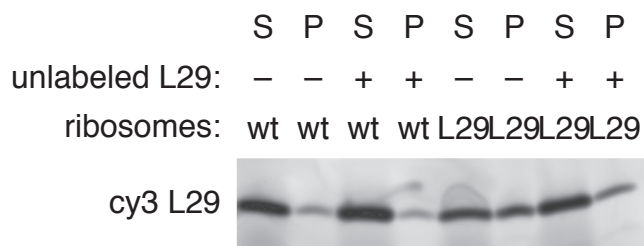
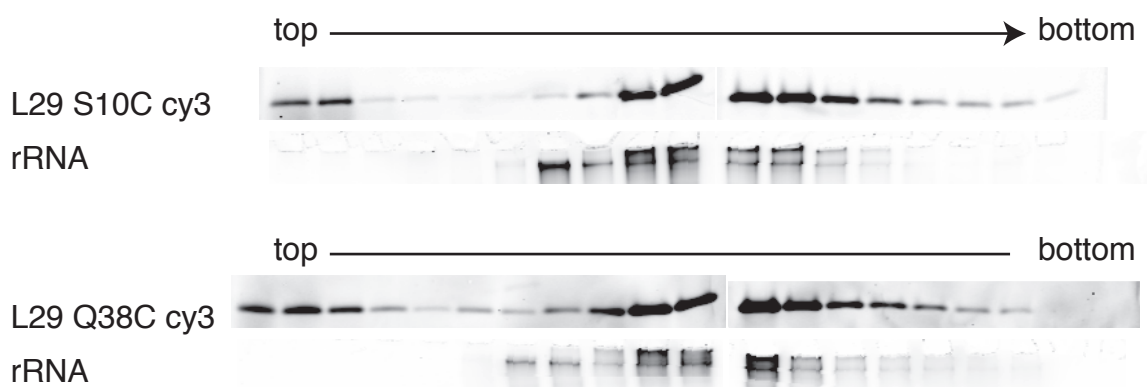
A**B****C****D**

Figure C-2

FRET between cy3 labeled ribosomes and cy5 labeled FFh. 1 μ M FFH labeled with cy5 at position 395 (M-domain, A and B) or 72 (N-domain, C and D) was incubated with 0.1 μ M ribosomes labeled with cy3 on L29 at position 10 (A and C) or 38 (B and D). An emission spectrum was recorded for each sample exciting at 550nm (the excitation maximum for cy3). Spectra were also recorded of each protein alone (green for ribosomes alone, red for Ffh alone) and were subtracted from the spectrum taken for the complex (black). In the difference spectra (shown in blue) negative fluorescence peaking at 570nm (the emission maximum for cy3) represents quenching, while positive fluorescence peaking at 670nm represents energy transfer to cy5.

- Ribosome+Ffh
- Ffh alone
- Ribosome alone
- Difference

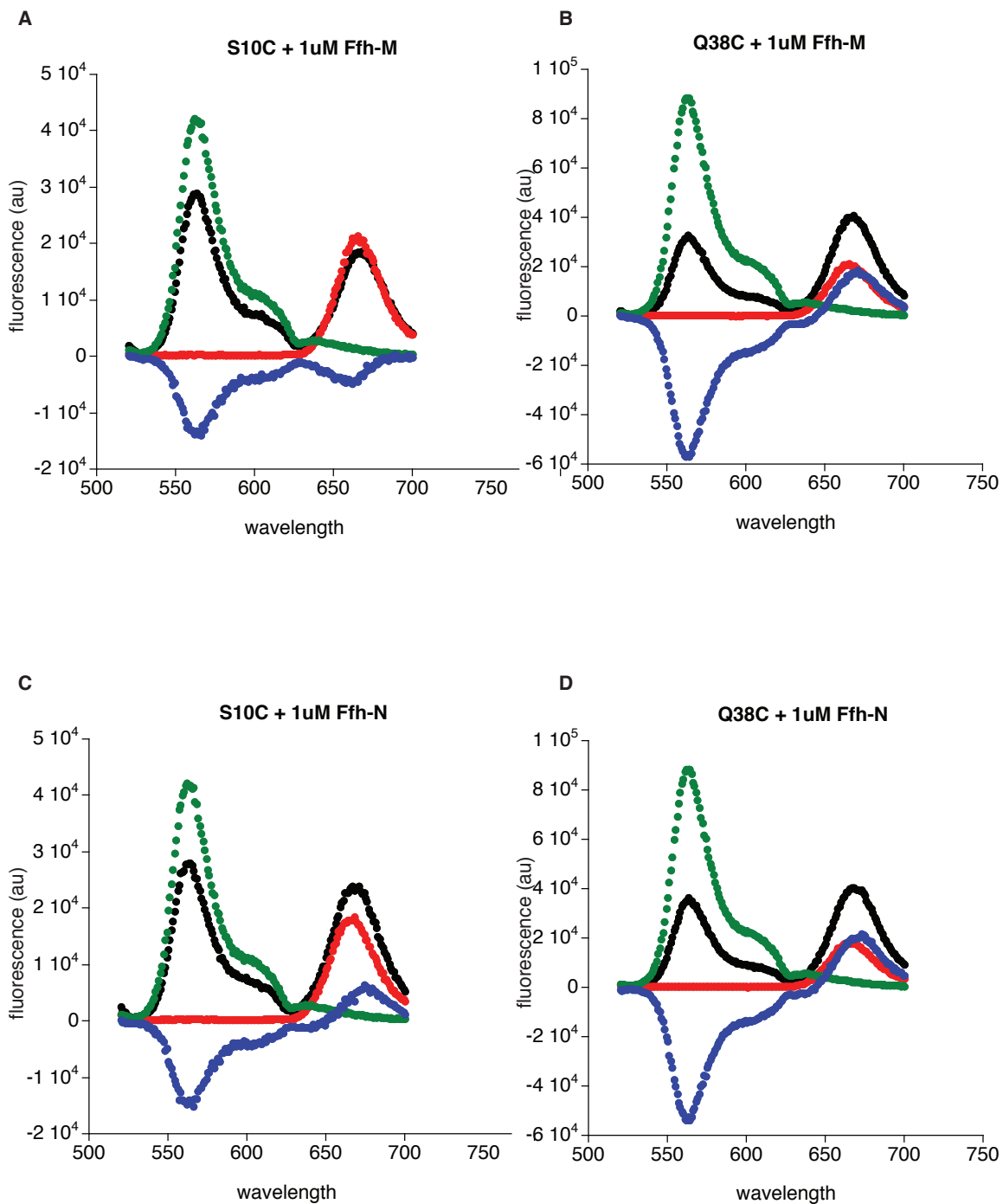


Figure C-3

Affinity of ribosome Ffh complexes measured by FRET. The affinity of the Ffh-ribosome interaction was measured by FRET using the system described in Figure C-2. 0.02 μ M cy3 labeled ribosomes (L29 position 10 A, and L29 position 38 B) were mixed with varying concentrations of cy 5 labeled Ffh (position 72). Fluorescence measurements were made for each sample exciting with 514nm light and recording emission at 550, to monitor quenching of cy3. Curves were fit with a quadratic equation $[Ffh\text{-ribosome complex}] = M2 * (([ribosomes] + [cy5\text{-Ffh}] + K_d) - (([ribosomes] + [cy5\text{-Ffh}] + K_d)^2 - 4 * [ribosomes] * [cy5\text{-Ffh}])^{1/2}) / 2$. The affinity of the Ffh-ribosome interaction was also measured by competition with unlabeled ribosomes (C) or unlabeled Ffh (D).

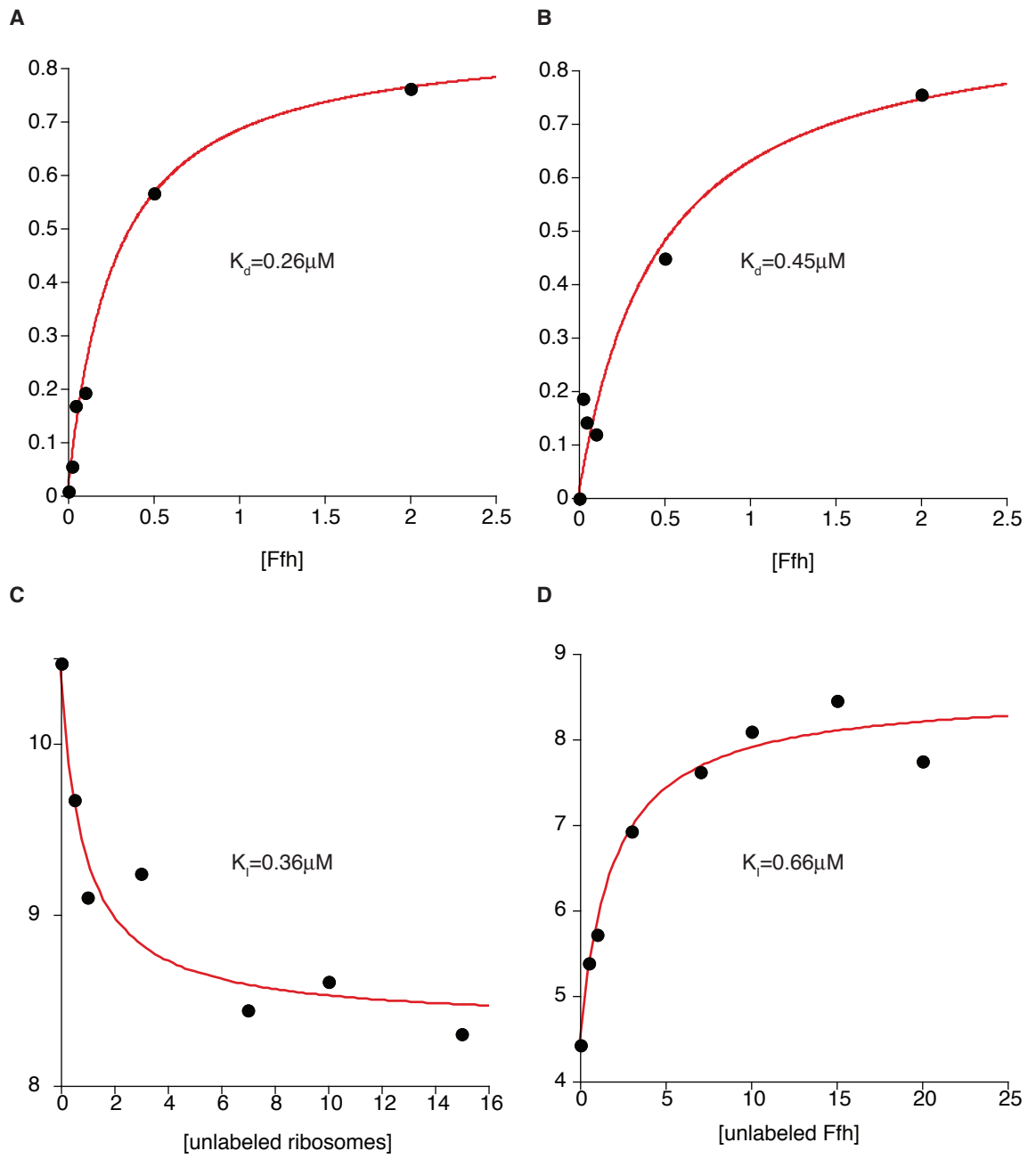


Figure C-4

Affinity of ribosome SRP complexes measured by FRET. The affinity of the SRP-ribosome interaction was measured by FRET using the system described in Figure C-2 with the addition of a 2 molar excess of 4.5S RNA. 0.02 μ M cy3 labeled ribosomes (L29 position 38) were mixed with varying concentrations of cy 5 labeled Ffh and 4.5S RNA(position 72). Fluorescence measurements were made for each sample exciting with 514nm light and recording emission at 550, to monitor quenching of cy3. Curves were fit with a quadratic equation as in C-3.

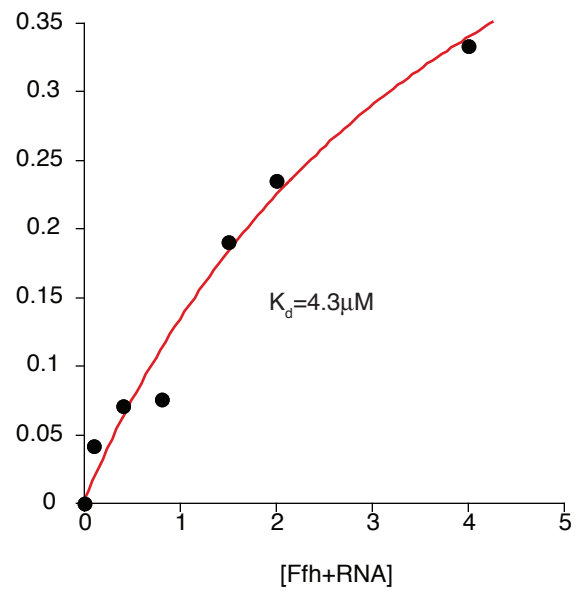
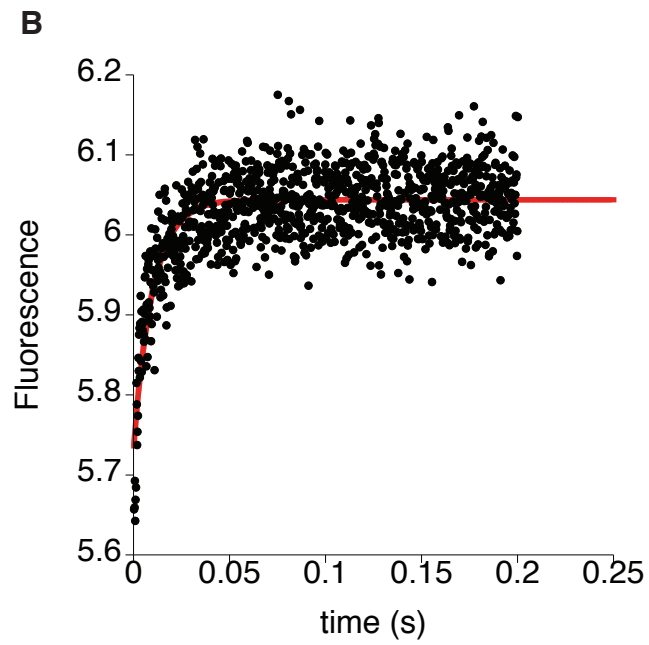
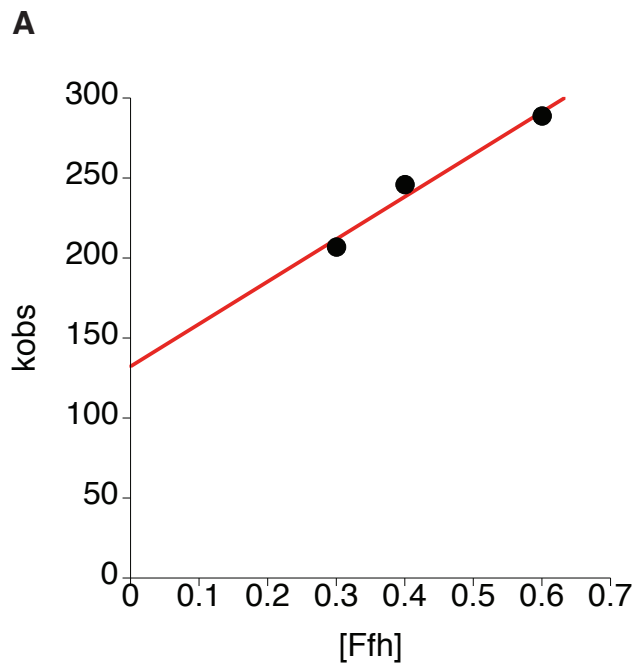


Figure C-5

Association and dissociation rate constants for the Ffh-ribosome interaction. A. The association rate of the Ffh-ribosome interaction was measured by FRET. cy5 labeled Ffh was rapidly mixed with cy3 labeled ribosomes. Observed association rates are plotted at varying Ffh concentrations. The data were fit to the equation $k_{\text{obs}} = k_{\text{on}} * [\text{cy5-Ffh}] + k_{\text{off}}$. B. Dissociation of cy5-Ffh from cy3-ribosomes was initiated by rapidly mixing preformed cy5-Ffh•cy3-ribosome complexes with an excess of unlabeled Ffh. The increase in cy3 emission that occurred when cy5-Ffh dissociated was monitored. Data were fit to a single exponential equation $\text{Fraction bound} = e^{(-k_{\text{off}} * \text{time})}$

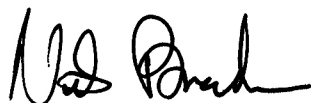


Publishing Agreement

It is the policy of the University to encourage the distribution of all theses, dissertations, and manuscripts. Copies of all UCSF theses, dissertations, and manuscripts will be routed to the library via the Graduate Division. The library will make all theses, dissertations, and manuscripts accessible to the public and will preserve these to the best of their abilities, in perpetuity.

Please sign the following statement:

I hereby grant permission to the Graduate Division of the University of California, San Francisco to release copies of my thesis, dissertation, or manuscript to the Campus Library to provide access and preservation, in whole or in part, in perpetuity.



Author Signature

6/12/2009

Date